NTNU
Norwegian University of
Science and Technology

Reduction of MnO and SiO_2 from Assmang and Comilog based Slags

Trine Asklund Larssen

Chemical Engineering and Biotechnology
Submission date: June 2017
Supervisor: Merete Tangstad, IMA

Norwegian University of Science and Technology
Department of Materials Science and Engineering

Declaration

I hereby declare that the work has been carried out independently and in compliance with the examination regulations of the Norwegian University of Science and Technology, NTNU.

Trondheim, June 2017

Trine Asklund Larssen

Preface

This report presents an investigation of kinetics and mechanisms in silicomanganese production, where the focus has been on how different raw materials affect the reduction of MnO and SiO_2. It is the author's master's thesis and serves as the evaluation basis for the course TMT4900 at the Norwegian University of Science and Technology, NTNU. The majority of the work was executed at the Department of Materials Science and Engineering at NTNU, whereas a small part was performed at Mintek in Johannesburg, South-Africa.

The work performed at Mintek will not be presented as a part of the thesis as it is not directly in line with what was done in Trondheim and due to experimental difficulties few results were obtained. This thesis will hence focus on the work performed in Trondheim before and after the stay in South-Africa.

I would like to thank my supervisor Professor Merete Tangstad for being very encouraging and a great inspiration during the last year. Her interest in the field is very contagious, and her availability for questions and discussions is highly appreciated. I would also like to thank my supervisor at Mintek, Dr. Joalet Steenkamp, for welcoming me with open arms during my stay at Mintek and providing me with a very educational experience. In addition, I want to thank Senior Engineer Morten Raanes for help with the EPMA analyses.

The work was funded by the research centre SFI Metal Production and is a part of Research Domain 2(RD2): Primary Metal Production, lead by Professor Merete Tangstad.

Trondheim, June 2017

Trine Asklund Larssen

Summary

Silicomanganese(SiMn) and ferromanganese (FeMn) represent essential ingredients for the steel producing industries due to enhancing effects on steel quality. While extensive efforts have been made in investigating the kinetics of ferromanganese production, kinetic information on the silicomanganese process is rather scarce.

The goal of this work was to investigate how different raw materials/charge compositions affect the reduction rate of MnO and SiO_2 in SiMn production. The experimental work was carried out in a thermogravimetric furnace in CO-gas at ambient pressure with coke as reducing agent. Investigated charge compositions contained ore (Comilog or Assmang) and HC FeMn slag in a 1:1 ratio, quartz and coke. Melting behaviour was investigated for the mentioned Comilog charge at temperatures 1200-1400°C and compared to charge based on Comilog and quartz at corresponding temperatures. Both mixing and layering of raw materials in crucible were evaluated.

The slag formation temperature was determined to be in the range of 1250-1300°C for all investigated charges. All materials had formed a slag phase at 1250°C when materials were prepared by mixing in the crucible, whereas the quartz particles remained undissolved until 1300°C when prepared by layering.

Assmang and Comilog in combination with HC FeMn slag and quartz show highly similar reduction behaviour, however the rapid reduction stage was initiated at a lower temperature for Assmang, i.e 1535°C vs 1545°C for Comilog.

Charges based on Comilog ore, HC FeMn slag and quartz start to reduce at approximately 50°C lower temperature compared to charges based on Comilog, quartz and coke (and limestone), in spite of lower sulphur content, lower basicity and lower driving force.

There was no observed correlation between the total basicity/viscosity and the reduction rate. However, it was shown that the rate constant increases with the sulphur content.

Foaming was observed at 1550°C for Assmang charges, whereas the first occurrence was at approximately 1560°C for Comilog. It was concluded that the foaming phenomena is a result of initiation of the rapid reduction stage.

Sammendrag/Summary in Norwegian

Silicomangan (SiMn) og ferromangan (FeMn) er essensielle ingredienser i stålindutrien på grunn av forsterkende effekt på stålets egenskaper. Mens kinetikken i produksjon av ferromangan er undersøkt i stor grad er kinetisk informasjon om silicomanganprosessen fortsatt mangelfull.

Målet med dette arbeidet var å undersøke kinetikken i høy-temperatursonen i SiMn prosessen. Hovedfokuset var på hvordan ulike råmaterialer/charge-sammensetninger påvirker reduksjonsraten til MnO og SiO_2. Det eksperimentelle arbeidet ble utført i en termogravimetrisk ovn med CO-gass ved atmosfærisk trykk og koks som reduseringsagent. To ulike blandinger ble undersøkt, hvorav begge inneholdt malm (Comilog eller Assmang) og HC FeMn slagg i 1:1 ratio, kvarts og koks. Det undersøkt ved hvilken temperatur råmaterialene danner en slaggfase i den forenevnte Comilog blandingen, som deretter ble sammenlignet med blanding basert på Comilog og kvarts. Både lagvis og mixet preparering av råmaterialer ble evaluert.

Smeltetemperaturen var i temperaturområdet 1250-1300°C for alle blandinger. Alle materialer hadde dannet slaggfase ved 1250°C ved mixet preparering, mens kvartspartiklene forble usmeltet til 1300°C ved lagvis plassering.

Assmang og Comilog i kombinasjon med HC FeMn slagg og kvarts viser svært lik reduksjonsoppførsel, hvorav den eneste forskjellen er at det hurtige reduksjonsintervallet initieres ved en lavere temperatur i Assmang (1535°C vs 1545°C).

Det var ingen observert sammenheng mellom total basisitet/viskositet og reduksjonsrate. Derimot er svovelinnhold den viktigste faktoren med hensyn til reduksjonsraten og det ble funnet at ratekonstanten øker med økende svovelinnhold.

Blandinger basert på Comilog-malm, HC FeMn slagg og kvarts reduseres ved temperatur tilnærmet 50°C lavere enn blandinger basert på Comilog og kvarts (og kalkstein), til tross for lavere svovelinnhold, lavere basisitet og lavere drivkraft.

Skumming ble observert i Assmang blandingen ved 1550°C, mens det første tilfellet var ved tilnærmet 1560°C for Comilog. Det ble konkludert at skummingen er et resultat av en allerede høy reduksjonsrate.

Contents

1 | Introduction

1.1 The silicomanganese process

Silicomanganese (SiMn) is one of the two main manganese alloys, the other being ferromanganese, which is used as an ingredient in the steelmaking industry. Both silicon and manganese can work as a deoxidizer due to the higher affinity towards oxygen compared to iron and have shown to increase both strength, hardness and ductility when used as an alloying element. In addition, manganese has the ability of working as a desulphurizer by forming manganese sulphide (MnS) with any potential sulphur in the metal[1]. Figure 1.1 shows the annual SiMn alloy production over the last nine years. The output of SiMn alloys is a reflection of the global production of high quality steel products, which is not expected to decrease in the foreseen future.

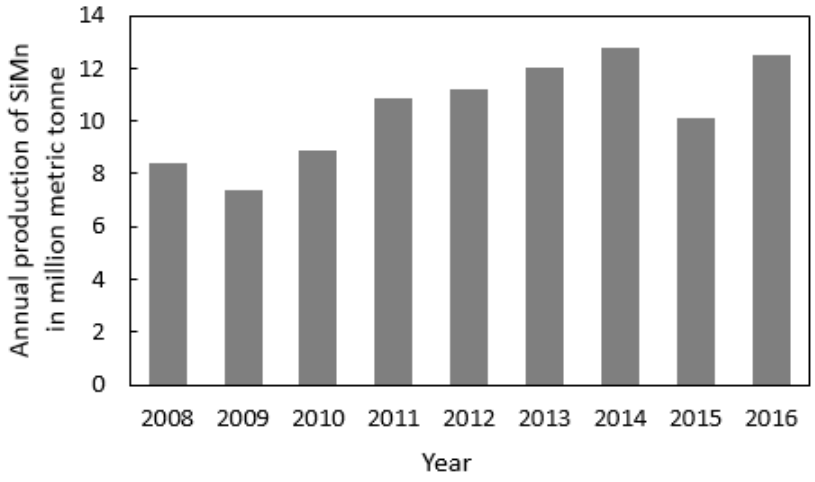

Figure 1.1: SiMn alloy production in million metric tonne[2].

Standard produced SiMn-alloys contain 18-20 wt pct silicon and 68-70 wt pct manganese. In addition, the alloy contains 1.5-2 wt pct carbon (saturated), iron and various trace elements. The industrial production process involves simultaneous carbothermic reduction of MnO and SiO_2 in a blend of manganese ore, quartz, coke and fluxes (usually dolomite or limestone). Norwegian producers also uses Mn-rich slag from the FeMn-process as a source of manganese. The mix of raw materials, called charge, is fed into an electrical submerged arc furnace (SAF), where three Soderberg electrodes are located in a triangle orientation inside the furnace, each connected to a separate electrical phase. The size of SiMn furnaces are usually in the range of 15-40 MW, giving 80-220 tons of alloy per day[3]. The charge passes through the furnace from initial temperature 200-500°C at the top to a temperature of 1600-1650°C when being tapped from the lower parts of the furnace.

Figure 1.2 shows an example of a SAF (48 MVA) used for SiMn production. The raw materials are added at the top where they will start to descend down the furnace. *Burden* is where the materials are still in solid form, often called the prereduction zone. *Coke bed* denotes the area where the materials are in liquid form and the metal producing reactions are occurring.

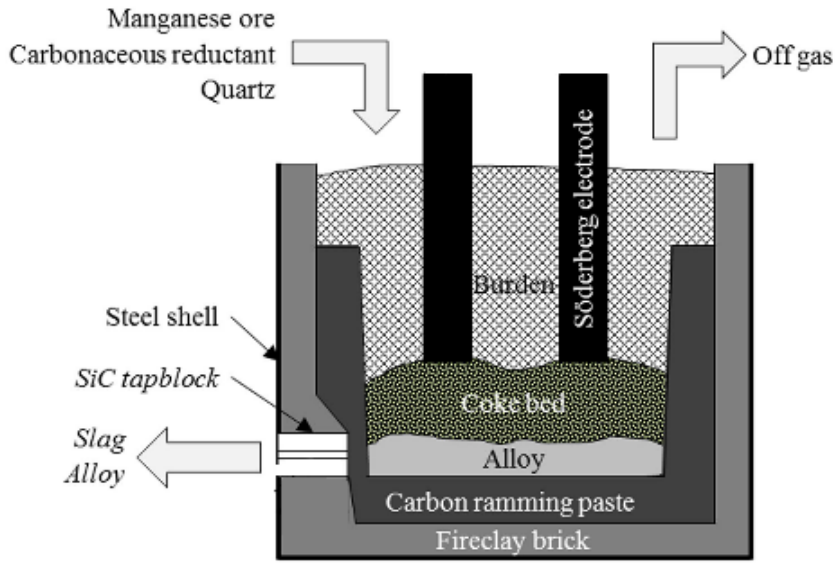

Figure 1.2: Layout of a submerged arc furnace (48 MVA) producing silicomanganese, modified from Steenkamp[4].

1.1.1 Reaction overview

The furnace can be divided into two regions according to temperature range, namely prereduction zone(low temperature) and coke bed zone(high temperature). Following is an overview of the reactions occuring in the different furnace regions.

Prereduction zone

The charge mixture enters the furnace in the prereduction zone. The temperature at the top of the charge will be between 200°C and 500°C. As a result, evaporation of water takes place.

$$H_2O\,(l) = H_2O\,(g) \qquad \Delta H^{\circ}_{298^{\circ}C} = 44.0\,kJ \tag{1.1}$$

Fluxes may be added to the charge to alter the slag properties and optimize metal recovery. Common fluxes are limestone and dolomite. These will decompose in temperature range 300°C to 900°C and increase the amount of basic oxides MgO and CaO[1].

$$MgCO_3 = MgO + CO_2 \qquad \Delta H^{\circ}_{298^{\circ}C} = 101.1\,kJ \tag{1.2}$$

$$CaCO_3 = CaO + CO_2 \qquad \Delta H^{\circ}_{298^{\circ}C} = 178.3\,kJ \tag{1.3}$$

$$CaCO_3 \cdot MgCO_3 = CaO + MgO \qquad \Delta H^{\circ}_{298^{\circ}C} = 295.4\,kJ \tag{1.4}$$

The manganese in the Norwegian industrial SiMn-process comes from manganese ores and Mn-rich slag from the HC FeMn-process, which in turn also originates from ores. The manganese content of the ores is dominated by higher oxides MnO_2, Mn_2O_3 and Mn_3O_4. The ores also contains other oxides, where the most important are Al_2O_3, MgO, CaO and SiO_2. In addition, iron is always present in manganese ores. Iron oxides will reduce completely to metallic iron at high temperatures and go completely into the metallic phase[1].

$$\tfrac{1}{2}Fe_2O_3 + \tfrac{3}{2}CO = Fe + \tfrac{3}{2}CO_2 \qquad \Delta H^{\circ}_{298^{\circ}C} = -12.9\,kJ \tag{1.5}$$

The oxides Al_2O_3, MgO and CaO are considered unreducible and will enter the slag phase. They

do however have an impact on the thermodynamics of the process. This will be covered later on.

The higher oxides of manganese will easily be reduced to MnO in the prereduction zone by CO gas ascending from the coke bed zone according to equations 1.6-1.8. These reactions are highly exothermic and will hence heat the charge material. The extent of the gas reductions will be reflected by the off-gas CO_2/CO ratio[1].

$$MnO_2 + \tfrac{1}{2}CO = \tfrac{1}{2}Mn_2O_3 + \tfrac{1}{2}CO_2 \qquad \Delta H^\circ_{298^\circ C} = -99.9\,kJ \tag{1.6}$$

$$\tfrac{1}{2}Mn_2O_3 + \tfrac{1}{6}CO = \tfrac{1}{3}Mn_3O_4 + \tfrac{1}{6}CO_2 \qquad \Delta H^\circ_{298^\circ C} = -31.3\,kJ \tag{1.7}$$

$$\tfrac{1}{3}Mn_3O_4 + \tfrac{1}{3}CO = MnO + \tfrac{1}{3}CO_2 \qquad \Delta H^\circ_{298^\circ C} = -16.9\,kJ \tag{1.8}$$

The reduction degree of reaction 1.8 depends on the reactivity of the ore. If the reactivity is low, reduction of Mn_3O_4 will continue simultaneously as the Boudouard reaction when the oxides reach the surface of the coke bed. The Boudouard reaction, equation 1.9, is the formation of CO gas from solid carbon in the coke bed reacting with the CO_2 gas produced in the Mn_3O_4 reduction. As a result, Mn_3O_4 is reduced by solid carbon.

$$\tfrac{1}{3}C + \tfrac{1}{3}CO_2 = \tfrac{2}{3}CO \qquad \Delta H^\circ_{298^\circ C} = 57.5\,kJ \tag{1.9}$$

$$\tfrac{1}{3}Mn_3O_4 + \tfrac{1}{3}C = MnO + \tfrac{1}{3}CO \qquad \Delta H^\circ_{298^\circ C} = 40.5\,kJ \tag{1.10}$$

The Boudouard reaction is highly endothermic, which in turn makes reaction 1.10 endothermic. Hence, the reduction degree has large impact on the energy consumption.

High temperature zone

The prereduced oxide blend will start melting at approximately 1150-1300°C, depending on the specific composition, and fuse together with the Mn-rich FeMn-slag. The dominating components of the SiMn slags are MnO, SiO_2, Al_2O_3, CaO and MgO. The metal phase will at this temperature be composed of approximately 95% Fe and 5% C.

The thermodynamic temperature for reduction of MnO to liquid manganese is 1370°C, however research suggests that the reduction takes place in temperature range 1500 - 1600°C[5]. The reduction of MnO is highy endothermic and will consume about one third of the supplied electric energy for SiMn production[1].

$$MnO\,(l) + C = Mn\,(l) + CO\,(g) \qquad \Delta H^{\circ}_{298^{\circ}C} = 252.3\,kJ \tag{1.11}$$

At temperatures approximately 1600°C, the MnO content in the slag phase will be up to 10% according to equilibrium relations, depending on the amounts of other oxides in the slag[1]. Silica is assumed to reduce to silicon metal at temperatures in the range 1550 to 1650°C according to reaction 1.12[3]:

$$SiO_2\,(l) + 2\,C = Si\,(l) + 2\,CO \qquad \Delta H^{\circ}_{298^{\circ}C} = 754.9\,kJ \tag{1.12}$$

Silicon carbide is the stable carbon phase at higher Si-contents, meaning that silicon metal is formed according to reaction 1.13. This occurs when the Si content exceeds about 17% in Mn-Si-Fe-C_{sat} alloys[1].

$$SiO_2\,(l) + 2\,SiC = 3\,Si\,(l) + 2\,CO\,(g) \tag{1.13}$$

Even though reaction 1.12 is used to express the silicon transfer, it is established that the reduction path from SiO_2 in slag to Si in metal involves the formation and reduction of SiO gas through reactions 1.14-1.15[1].

$$SiO_2 + CO\,(g) = SiO\,(g) + CO_2\,(g) \tag{1.14}$$

$$SiO\,(g) + C = Si + CO\,(g) \tag{1.15}$$

The driving force and kinetics for reaction 1.15 are determined by the SiO pressure generated in reaction 1.14, which is assumed small. The reaction is therefore normally neglected in kinetic considerations. The gas pressure is further mentioned in the theory chapter covering thermodynamic relations.

The slag/metal equilibrium of the simultaneous reductions of MnO and SiO_2 needs to be taken

into account and is presented in equation 1.16.

$$SiO_2\,(l) + 2\,Mn\,(l) = Si\,(l) + 2\,MnO\,(l) \tag{1.16}$$

Some of the manganese metal will evaporate according to reaction 1.17. In addition to iron, silicon and manganese, carbon will dissolve in the metal up to carbon saturation.

$$Mn\,(l) = Mn\,(g) \tag{1.17}$$

$$C\,(s) = C\,(l) \tag{1.18}$$

The metal phase will be a Fe-Mn-Si-C_{sat} system, where the specific composition is determined by reaction temperature and slag chemistry.

1.2 Objectives

This thesis presents work that is a part of a larger ongoing project at the research centre SFI that aims to investigate how different charge compositions/raw materials affect the reduction rate of MnO and SiO_2 in production of silicomanganese.

The investigations will be executed by examining three different sources of manganese, i.e. Comilog and Assmang ore and waste slag from the high-carbon ferromanganese process. Experiments will be carried out in a thermogravimetric graphite tube furnace (TGA) in a CO(g) atmosphere at temperatures 1530-1650°C. Results will be discussed in terms of weight loss curves retrieved from the TGA and compositions analysed by EPMA. Kinetic parameters such as rate constants and activation energies for reaction 1.10 and 1.11 will be presented and discussed. In addition, the specific temperature at which the slag is homogeneous will be found for two different charges based on Comilog ore at different positions of raw materials (layering vs mixing).

2 | Theory

The silicomanganese process does normally not reach equilibrium, making information about kinetics very important. Kinetics is partly determined by the distance the system has towards equilibrium, hence it is also essential to know the thermodynamics of the system. The following chapter presents the thermodynamics for SiMn production, as well as existing relevant research on kinetics.

2.1 Thermodynamics

The main oxides represented in SiMn production are MnO, SiO_2, CaO, Al_2O_3 and MgO. The oxides CaO, Al_2O_3 and MgO are considered unreducible during this process and will go to the slag phase. Manganese and silicon are the only two components that will be distributed between slag and Mn-Si-Fe-C_{sat} alloy.

The distribution of manganese between slag and alloy in equilibrium with CO gas is defined by the equilibrium constant at temperature T:

$$K_T = \frac{a_{Mn} \cdot P_{CO}}{a_{MnO} \cdot a_C} \tag{2.1}$$

At high temperatures the pressure of CO is approximately 1 atm. With the activity of solid carbon equal to unity, equation 2.1 takes the form of 2.2:

$$K_T = \frac{a_{Mn}}{a_{MnO}} = \frac{\gamma_{Mn}\%Mn}{\gamma_{MnO}\%MnO} \tag{2.2}$$

In a similar manner as for manganese, the equilibrium distribution of silicon is given by the equilibrium contant at temperature T for reduction of silica according to reaction 1.12, and can be expressed as:

$$K_T = \frac{a_{Si} \cdot P_{CO}^2}{a_{SiO_2} \cdot a_C^2} = \frac{\gamma_{Si}\%Si}{\gamma_{SiO_2}\%SiO_2} \tag{2.3}$$

Hence, the equilibrium amounts of manganese and silicon is dependent on temperature through the equilibrium constant, the partial pressure of CO and the slag composition influencing the activity coefficients of MnO and SiO_2.

The CO pressure will mainly be determined by the amount of CO_2 gas produced by the Boudouard reaction. The left image in figure 2.1 shows that the gas will be approximately 100% CO at temperatures exceeding 900°C. However, as mentioned in the introduction, formation of SiO(g) and Mn(g) can occur at higher temperatures.

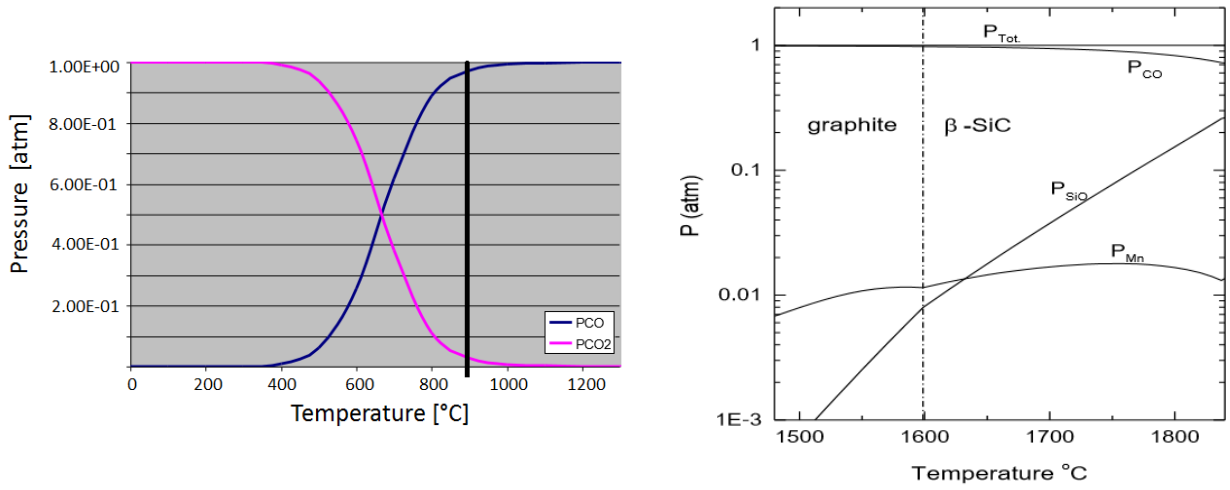

Figure 2.1: Left graph shows pressure relations according to the Boudouard reaction: $p_{tot} = p_{CO} + p_{CO_2} = 1$ atm. Graph on the right shows equilibrium pressure relations above a Mn-Si-C_{sat} alloy and slag phase where $a_{SiO_2} = 0.2$.[6]

The graph to the right in figure 2.1 shows the equilibrium pressures of CO(g), SiO(g) and Mn(g) above a Mn-Si-C_{sat} alloy and slag phase where $a_{SiO_2} = 0.2$ at increasing temperatures. Normal process temperature for SiMn production is between 1600 and 1650°C, where it is seen that the partial pressure of SiO(g) is lower than 2% and P_{Mn} ~= 1%. This implies that it is reasonable to neglect these gas components at normal process temperatures. While the partial pressure of

Mn(g) only increases slightly at increasing temperature, a larger temperature effect is seen for SiO(g). At 1750°C, the partial pressure of SiO(g) is approximately 8%.

The slag is of ionic nature and the oxide components can be categorized as basic (forming cations) or acidic (forming anions). MnO, CaO and MgO are basic oxides, whereas SiO_2 is the most important acidic oxide. Al_2O_3 is an amphoteric oxide, which means that it behaves like a basic oxide in an acidic environment and vice versa. Slag characteristics (such as viscosity) are determined by the ratio between the two types of oxides. For ferromanganese(FeMn) the basicity can be expressed according to equation 2.4.

$$B = \frac{CaO + MgO}{SiO_2 + Al_2O_3} \tag{2.4}$$

For calculations of basicity for SiMn production a ratio R is used. This is omitted the value for SiO_2, as it is reduced during the process.

$$R = \frac{CaO + MgO}{Al_2O_3} \tag{2.5}$$

Similar oxides will enhance each other by increasing the chemical activity, whereas different oxides will weaken each other by decreasing the chemical activity and lowering the melting point.

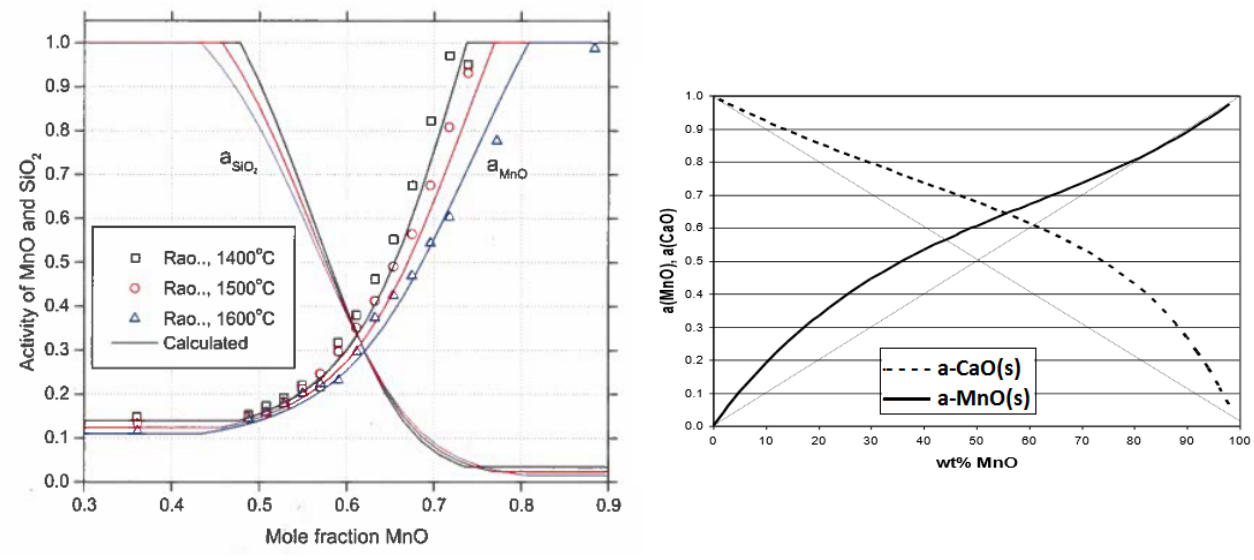

Figure 2.2: Left: Activity of MnO and SiO_2 in the MnO-SiO_2 system at 1400-1600°C[1].
Right: Activity of MnO and CaO in the MnO-CaO system at 1600°C[6].

The activity of MnO and SiO_2 in the MnO-SiO_2 system is seen in the left part of figure 2.2, whereas the right part show the activities of MnO and CaO in the MnO-CaO system. This shows that increasing the basicity would imply an increase in the activity of MnO. However, it would also cause a decrease in the relative amount of MnO. An increase in basicity will theoretically retard the reduction of SiO_2 by reducing the activity of SiO_2. When only considering metal yield, an optimal value for basicity at 1.8 has been suggested[7].

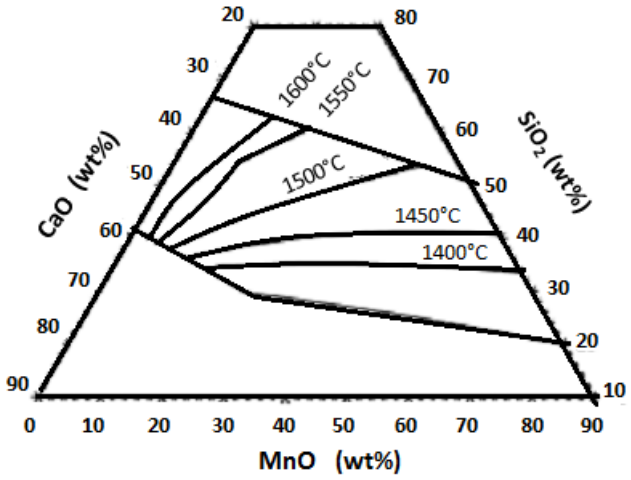

Figure 2.3: Complete equilibrium relations for ternary MnO-SiO_2-CaO slags with Mn-Si-C_{sat} alloys at p_{CO} = 1 atm[3].

Figure 2.3 shows the effect of temperature and slag composition on MnO reduction in ternary MnO-SiO_2-CaO slags where p_{CO} = 1 atm[3]. The MnO content in the slag decreases with increasing temperature and increasing CaO content in the slag.

The amount of silicon in the metal is dependent on the temperature and the activity of SiO_2. The relationship between the amount of silica in the slag and the produced silicon is displayed in figure 2.4. Initially, the amount of silicon in the metal increases linearly with the amount of SiO_2 in the slag. The change of slope at approximately 17-18 wt% Si is due to silicon carbide replacing graphite as the stable phase, where a lower amount of Si at a specific amount of SiO_2 in the slag is observed. In addition, the temperature effect on the amount of silicon in the metal phase is shown in the same figure. At 40 wt% SiO_2 in the slag, approximately 19 wt% Si is observed at 1600°C, whereas 27 wt% is observed at 1700°C. The presented relations are valid for the Mn-Fe-Si-C_{sat} alloy in equilibrium with a MnO-SiO_2-CaO-MgO-Al_2O_3 slag with characteristics Mn/Fe =

7, CaO/MgO = 2.5 and an R-ratio of 1.0.

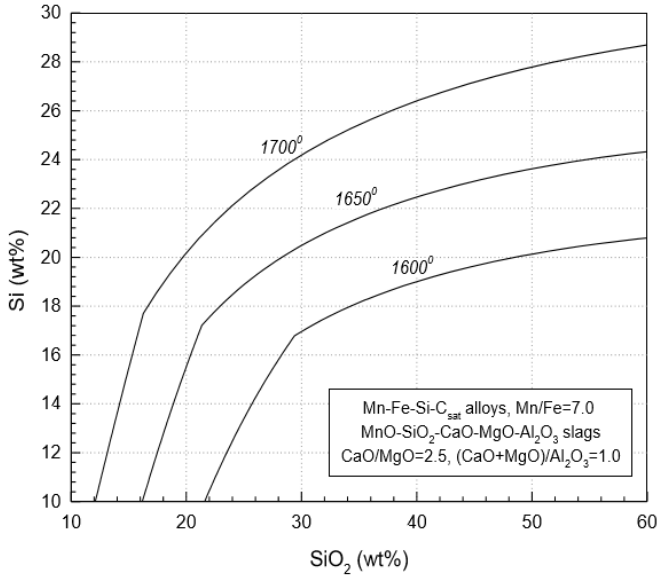

Figure 2.4: Calculated distribution of Si between slag and Mn-Fe-Si-C_{sat} [1]

Figure 2.5 shows how the amount of Si in the metal phase varies with the R-ratio. It is clear that the amount of Si decreases with increasing R-ratio, which is due to the increasing content of basic oxides.

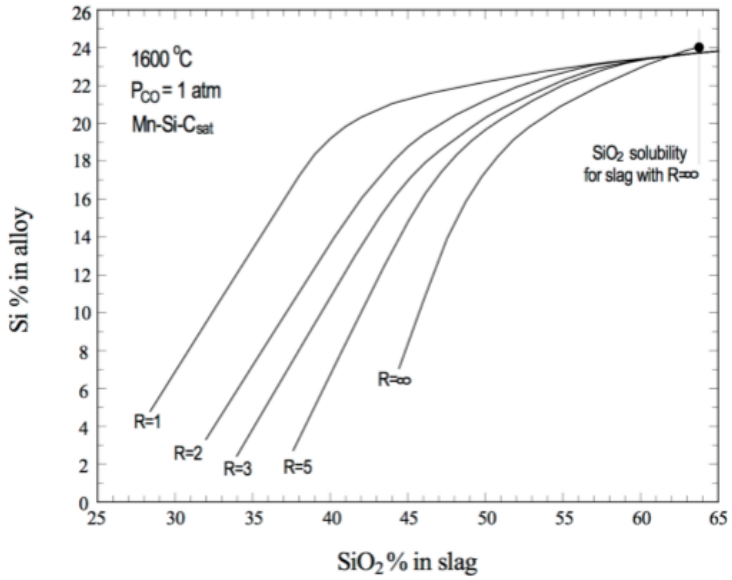

Figure 2.5: Distribution of Si in metal phase as a function of SiO_2 in slag phase for different R-ratios[1].

2.1.1 Slag Phase Relations

The slag phase will consist of components MnO-SiO_2-CaO-Al_2O_3-MgO. The ternary phase diagrams for the systems MnO-SiO_2-Al_2O_3 and MnO-SiO_2-CaO and the quaternary phase diagram for the system MnO-CaO-SiO_2-Al_2O_3 are presented in figure 2.6, 2.7 and 2.8, respectively.

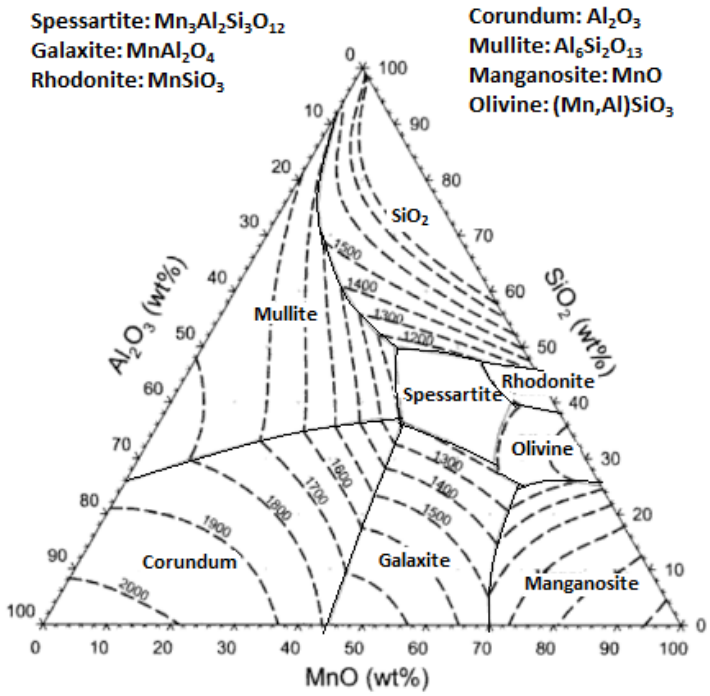

Figure 2.6: Calculated phase and liquidus relations for the MnO – SiO_2 – Al_2O_3 system [1]

Comilog is considered an acidic ore due to its high content of SiO_2 and Al_2O_3. Industrial SiMn charges based on Comilog ore and quartz will have a typical composition inside the $MnSiO_3$ area (Rhodonite) or the Mn_2SiO_4 area (Olivine) in phase diagram 2.6. These relations will also apply for Assmang charges. The liquidus lines show that these compositions will be partially melted at temperatures 1200-1300°C, where the amount of melted phase and melting temperature will depend on the specific composition.

Figure 2.7 shows the calculated phase and liquidus relations for the MnO-SiO_2-CaO system. Charges for SiMn production could typically contain 50-70%MnO and ~30%SiO_2, which means that the total composition would lie in the lower part of the phase diagram, shifted to the right.

These compositions are inside the 1300°C isothermal area and is fully liquid at temperatures above 1300°C.

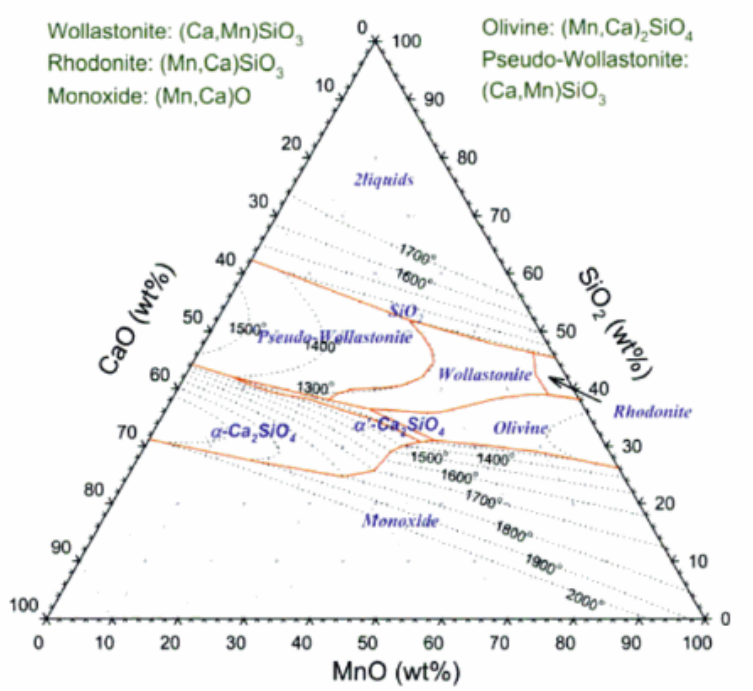

Figure 2.7: Calculated phase and liquidus relations for the $MnO-SiO_2-CaO$ system [1]

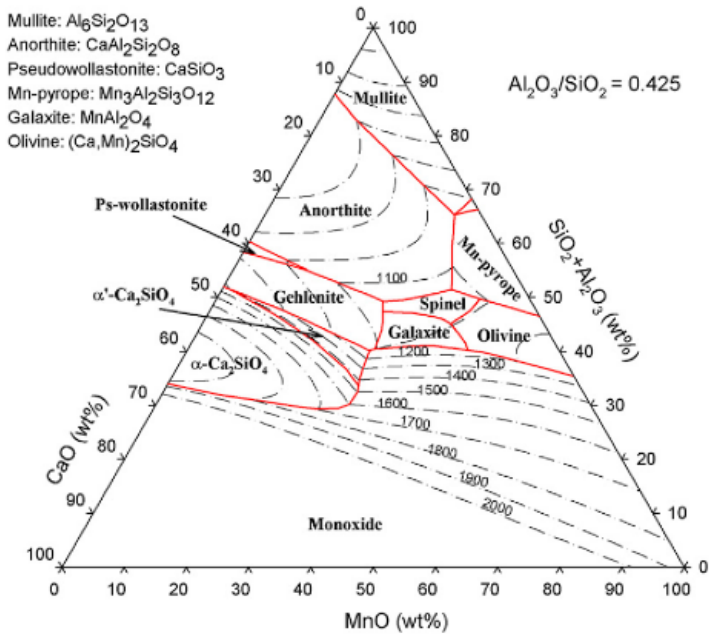

Figure 2.8: Calculated phase and liquidus relations for the $MnO-SiO_2-CaO-Al_2O_3$ system (weight ratio $Al_2O_3/SiO_2 = 0.425$ [8]

Generally, manganese ores have a relatively low content of MgO (applies for both Comilog and Assmang ore), which means that the quaternary system MnO-SiO_2-CaO-Al_2O_3 presented in figure 2.8 gives a good representation of the phase and liquidus relations in the system. Mn and Ca have great solubility in each other, which results in the large monoxide (Ca,Mn)O area at the lower part of the phase diagram. Typical compositions will be in the area close to Olivine, Galaxite, Monoxide and Mn-pyrope, which lies inside the isothermal areas of 1200-1400°C.

2.1.2 The Mn-Fe-Si-C system

Commercially important silicomanganese alloys are described by the Mn-Fe-Si-C_{sat} system. Isothermal phase relations for a Mn-Fe-Si-C_{sat} with Mn/Fe = 7 at 1550°C are shown in figure 2.9. For this alloy, SiC replaces graphite as the stable phase when the silicon content exceeds approximately 16.4% .

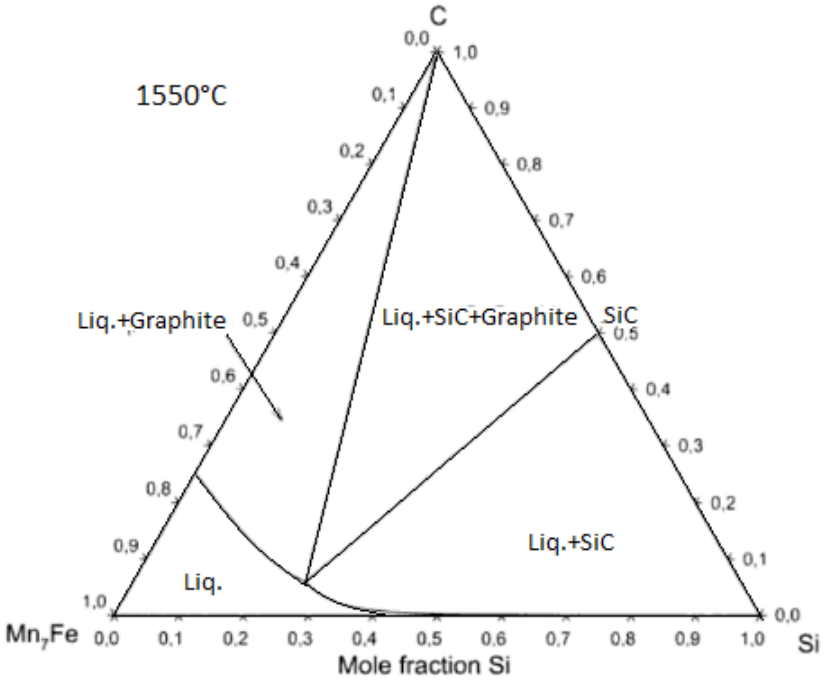

Figure 2.9: Calculated phase diagram showing an isothermal section of the Mn7Fe-Si-C system at T = 1550°C[1].

The solubility of carbon in silicomanganese has previously been calculated at temperatures between 1500 and 1650°C. Results are printed by Olsen et. al[1] and reprinted here in figure 2.10.

The separation line illustrates the shift from carbon as graphite to carbide. In addition, measurements of carbon solubility by Tuset and Sandvik[9] at temperatures 1530 and 1630°C are illustrated in the same figure. Tuset and Sandvik found that the carbon content increases with temperature and increasing Mn/Fe ratio. Further, it was found that the carbon content decreases rapidly from 7% to 1.5% when the silicon content increases from 0% to 20%.

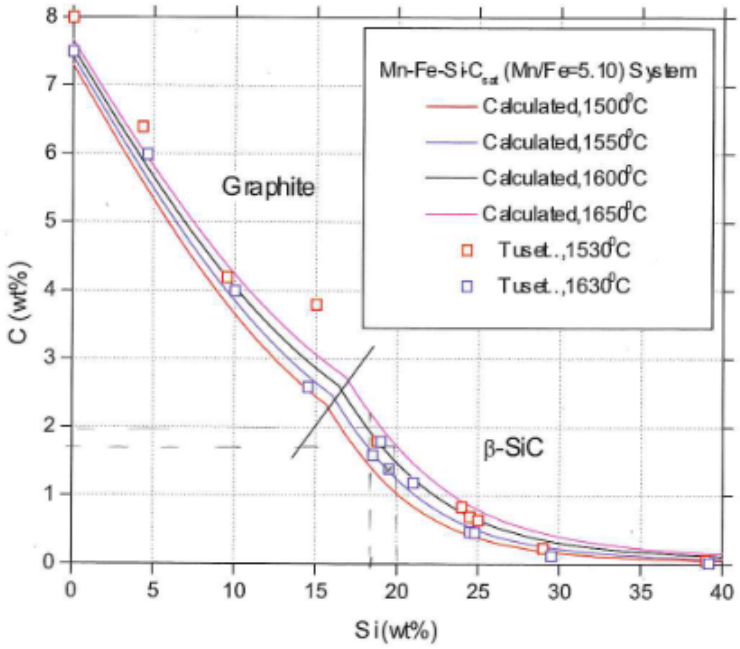

Figure 2.10: Calculated carbon solubility in Mn-Fe-Si-C alloys with fixed Mn/Fe weight ratio = 5.1 at 1500-1650°C. Measured carbon solubility by Tuset and Sandvik(1970). Reprinted from Olsen et al.[1].

2.2 Kinetics

A system that is not at equilibrium will move towards equilibrium at a rate given by a driving force. The driving force can be defined as the distance the system has to equilibrium state in terms of activity. Extensive research has been made on kinetics in the ferromanganese process, however information on silicomanganese is rather scarce. In the FeMn process, the reduction rate of MnO will be rapid when MnO is present in solid state, due to the high and constant activity. The activity decreases rapidly when the liquidus composition is reached, causing the reduction rate to slow down drastically. For SiMn, the reductions will occur when all raw mate-

rials are in liquid state, implying that the activity of MnO and SiO_2 will already be relatively low. Furthermore, SiMn has a higher content of silicon compared to FeMn, which leads to additional considerations. Nonetheless, the two processes are highly similar and it is reasonable to assume that the mechanisms will be as well.

Chinese investigators Xu et. al[10] studied the reduction of MnO from molten slag with carbon saturated iron where the contents of both %MnO and %Mn were high. They found the reduction of MnO to be limited by an interfacial reaction, and not MnO diffusion, as the variation of the surface active agent sulphur affected the reaction rate. Their results are presented in figure 2.11 and it should be noted that the results show that the reduction ratio for MnO increases with decreasing sulphur content in metal. The slag/metal interface was proven to be the essential site for the formation of the reduction product CO(g).

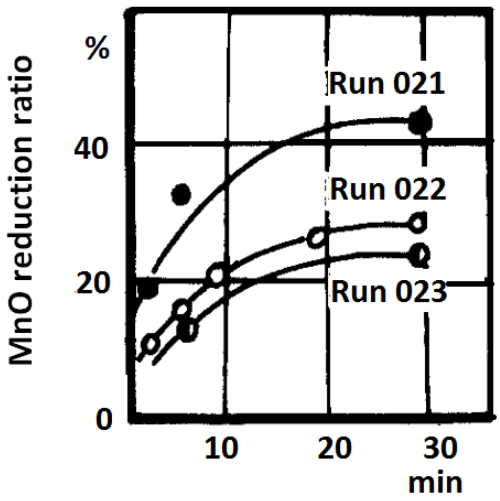

Figure 2.11: Effect of initial %S on the reduction ratio of MnO[10]. Initial sulphur contents in metal were 0.027, 0.048 and 0.079 wt% for run 21, 22 and 23, respectively.

The reduction rate of MnO being controlled by the chemical reaction at the interface has been concluded by many other researchers. Daines and Pehlke[11] investigated MnO reduction from basic slags by carbon dissolved in iron where it was observed that stirring had no effect on the rate. Skjervheim and Olsen[12] investigated the reduction of MnO from silicate slags by varying different experimental parameters as composition, temperature and stirring rate. Both solid

carbon and carbon saturated manganese were used as reducing agents. Based on the lack of impact of stirring and the rates sensitivity to temperature, they concluded that the rate of reduction is controlled by chemical reactions, and thereby not diffusion. The effect of temperature found by Skjervheim and Olsen can be seen in figure 2.12a.

Skjervheim and Olsen further reported the effect of sulphur on the reduction of MnO from silicate slags by comparing synthetic and industrial slags. They found that the industrial slags reduces much faster compared to the synthetic, which can be seen in figure 2.12b. A similar reduction rate with synthetic slag was obtained when sulphur was added to the Mn-C_{sat} alloy.

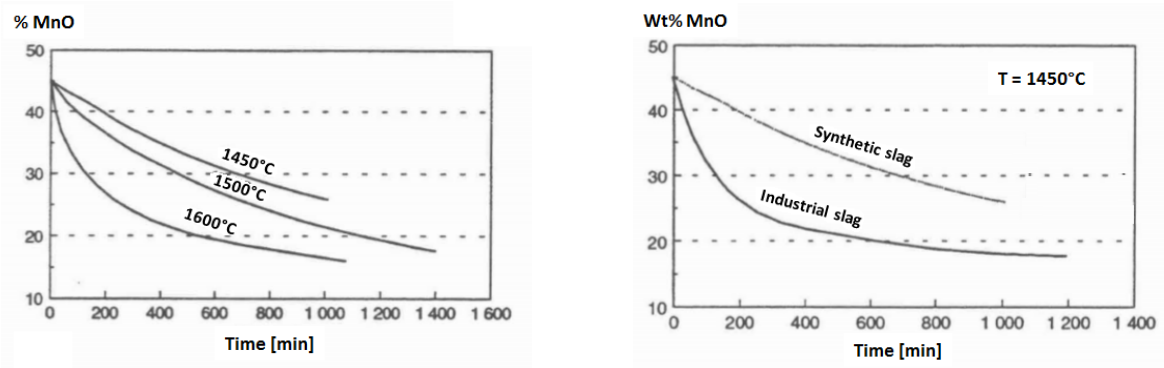

(a) Effect of temperature

(b) Industrial vs synthetic slag

Figure 2.12: Left: Effect of temperature on reduction of MnO from FeMn slag (27.5%SiO_2-45%MnO-27.5%CaO). Exp. at 1450°C and 1500°C without initial metal, exp. at 1600°C with 1:1 ratio of slag and metal. Right: wt% MnO as a function of process time in synthetic and industrial FeMn slag.[12]

Information on silica reduction from ferromanganese slags is rather scarce, whereas several investigations are performed in relation with iron making. Sun et al.[13] studied the reduction of SiO_2 from CaO-SiO_2-Al_2O_3 and CaO-SiO_2-Al_2O_3-TiO_2 slags by carbon saturated iron. Their results are presented in figure 2.13, where a) shows that the reduction of SiO_2 is strongly dependent on temperature, which indicates that the chemical reaction at the slag-metal interface is the rate-limiting step. In addition, it was found that the reaction rate decreased with increasing basicity (CaO/SiO_2), as shown in figure b).

SiO_2 reduction being controlled by a chemical reaction was supported by Futon and Chipman[14] from the investigation of silica reduction by carbon saturated iron from SiO_2-CaO-Al_2O_3 slag.

They found that the reduction was nearly independent of stirring, which implies that a chemical reaction is rate determining, rather than diffusion.

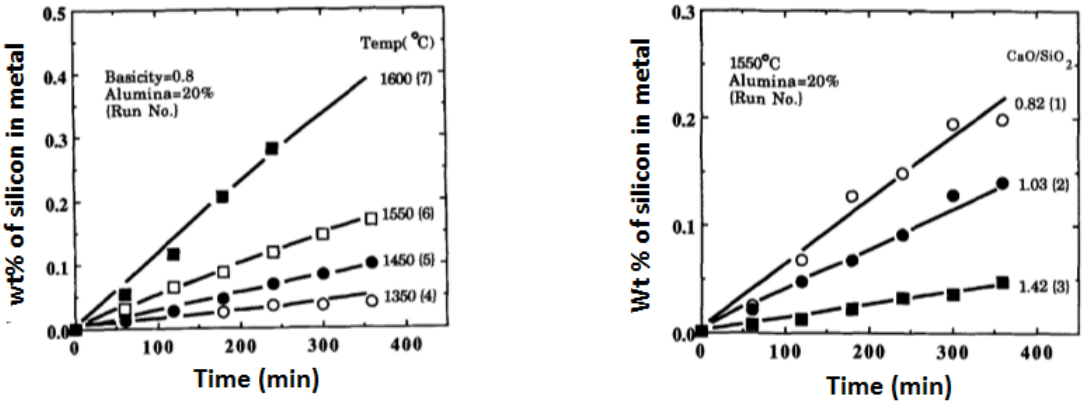

(a) Effect of temperature

(b) Effect of basicity

Figure 2.13: Experimental results presented by Sun et al[13]: reduction of SiO_2 increases with temperature and decreasing ratio of CaO/SiO_2.

Previous studies have shown that the reduction rate of MnO by solid carbon can be described by equation 2.6[1, 15]. Assuming that the reduction of SiO_2 is also controlled by a chemical reaction, a similar kinetic model for SiO_2 can be considered as equation 2.7.

$$r_{MnO} = \frac{gMnO}{min} = k_{Mn} \cdot A(a_{MnO} - a_{MnO,eq}) = k_{Mn} \cdot A(a_{MnO} - \frac{a_{Mn,eq}}{K_T}) \tag{2.6}$$

$$r_{SiO_2} = \frac{gSiO_2}{min} = k_{Si} \cdot A(a_{SiO_2} - a_{SiO_2,eq}) = k_{Si} \cdot A(a_{SiO_2} - \frac{a_{Si,eq}}{K_T}) \tag{2.7}$$

Where r is the reduction rate (g/min), A is the interfacial area (cm^2), a_{MnO} and a_{SiO2} are the activities of MnO and SiO_2 in the slag phase, a_{Mn} and a_{Si} are the activities of Mn and Si in the metal and K_T is the equilibrium constant at temperature T. k is the rate constant ($g/min \cdot cm^2$) described by equation 2.8.

$$k = k_0 \cdot e^{\frac{-E_a}{RT}} \tag{2.8}$$

Where k_0 is the frequency factor, E_a is the activation energy of species MnO or SiO_2 (kJ/mol), R is the ideal gas constant (J/K· mol) and T is the temperature (K).

The activities defining the driving force in 2.6 and 2.7 were modelled during a recent study and

expressed as equations 2.9-2.12[16]. Fitted temperatures were in the range 1500-1600°C

$$\begin{aligned} a_{MnO} = \; & C_{\mathrm{MnO}} \cdot \exp(0.0007576T - 123.7C_{MnO} + 30.14C_{\mathrm{SiO_2}} + 47.84C_{\mathrm{MgO}} + 49.54C_{\mathrm{CaO}} \\ & - 47.96C_{\mathrm{Al_2O_3}} + 122.8C^2_{\mathrm{MnO}} - 67.78C^2_{\mathrm{SiO_2}} - 46.32C^2_{\mathrm{MgO}} - 47.68C^2_{\mathrm{CaO}} \\ & + 22.51C^2_{\mathrm{Al_2O_3}} + 78.32C_{\mathrm{MnO}}C_{\mathrm{CaO}} + 77.56C_{\mathrm{MnO}}C_{\mathrm{MgO}} + 176.6C_{\mathrm{MnO}}C_{\mathrm{Al_2O_3}} \\ & + 101.2C_{\mathrm{MnO}}C_{\mathrm{SiO_2}} - 71.52C_{\mathrm{SiO_2}}C_{\mathrm{CaO}} - 70.58C_{\mathrm{SiO_2}}C_{\mathrm{MgO}} + 27.35C_{\mathrm{SiO_2}}C_{\mathrm{Al_2O_3}} \\ & + 46C^3_{\mathrm{SiO_2}} - 92.97C_{\mathrm{CaO}}C_{\mathrm{MgO}} + 2.44C^3_{\mathrm{CaO}}) \end{aligned} \tag{2.9}$$

$$\begin{aligned} a_{\mathrm{SiO_2}} = \; & C_{\mathrm{SiO_2}} \cdot \exp(-0.0003408T + 113.8C_{MnO} - 22.79C_{\mathrm{SiO_2}} - 51.36C_{MgO} - 52.44C_{CaO} \\ & + 36.3C_{\mathrm{Al_2O_3}} - 119.3C^2_{\mathrm{MnO}} + 42.56C^2_{\mathrm{SiO_2}} + 32.25C^2_{\mathrm{MgO}} + 30.12C^2_{\mathrm{CaO}} \\ & - 26.26C^2_{\mathrm{Al_2O_3}} - 82.725C_{\mathrm{MnO}}C_{\mathrm{CaO}} - 82.9C_{\mathrm{MnO}}C_{\mathrm{MgO}} - 155.2C_{\mathrm{MnO}}C_{\mathrm{Al_2O_3}} \\ & - 86.98C_{\mathrm{MnO}}C_{\mathrm{SiO_2}} + 86.21C_{\mathrm{SiO_2}}C_{\mathrm{CaO}} + 86.19C_{\mathrm{SiO_2}}C_{\mathrm{MgO}} - 23.06C_{\mathrm{SiO_2}}C_{\mathrm{Al_2O_3}} \\ & - 31.26C^3_{\mathrm{SiO_2}} + 69.45C_{\mathrm{CaO}}C_{\mathrm{MgO}} + 2.44C^3_{\mathrm{CaO}}) \end{aligned} \tag{2.10}$$

$$\begin{aligned} a_{Mn} = \; & C_{Mn} \cdot \exp(0.0005382T - 37.41C_{Mn} - 2.966C_{Si} - 0.6835C_{Fe} + 39.52C^2_{Mn} \\ & - 1.453C^2_{\mathrm{Si}} - 0.556C^2_{\mathrm{Fe}} + 27.48C_{Mn}C_{Si} + 38.69C_{Mn}C_{Fe} + 0.214C_{Si}C_{Fe}) \end{aligned} \tag{2.11}$$

$$\begin{aligned} a_{Si} = \; & C_{Si} \cdot exp(0.002464T + 10.3C_{Mn} - 1.081C_{Si} + 27.52C_{Fe} - 15.49C^2_{Mn} - 3.713C^2_{Si} \\ & - 34.66C^2_{Fe} + 1.324C_{Mn}C_{Si} - 47.01C_{Mn}C_{Fe} - 9.127C_{Si}C_{Fe}) \end{aligned} \tag{2.12}$$

The activation energy of MnO has been reported to be 350-370 kJ/mol in the two-phase area of synthetic ferromanganese slags of components MnO-SiO_2-CaO-Al_2O_3, where experiments were conducted within temperatures 1450-1550°C[15, 17]. A few studies have recently been carried out to find the kinetic parameters of the metal producing reactions in SiMn production[18, 19]. Activation energy of MnO in Assmang based charges were found to be 920 kJ/mol, whereas 304 kJ/mol for Comilog charges and 975 kJ/mol for synthetic slag. As for SiO_2 reduction, values of

870 kJ/mol, 796 kJ/mol and 2313 kJ/mol were reported for the same charges, respectively. This shows that the current studies are highly inconsistent.

Larssen [19, 20] recently investigated the reduction of MnO and SiO_2 from Comilog based charges at temperatures in the range of 1500 to 1725°C. Two different charges of basicities 0.05 and 2.09 were heated in CO(g) atmosphere. The reduction of MnO (and SiO_2) was relatively low in both charges in spite of high driving forces, however a higher reduction was obtained in charge with the lower basicity. Similar low reductions from SiMn slags where ore was the only source of manganese has previously been observed. Holtan[21] investigated charges based on Comilog ore, where the amount of MnO in the slag remained in range 30-50% at all investigated temperatures (up to 1700°C). No explanation for the lack of reduction was presented. From personal communication with P. Kim, PhD student at the Department of Materials Science and Engineering at NTNU, similar low reduction was obtained from SiMn slags based on Assmang ore. An increased reduction rate was observed when MnO-rich slag from the high-carbon FeMn process was used as an additional source of manganese. A possible explanation is that when HC FeMn slag is used as a partial source of manganese, one also obtaines a higher content of trace elements, such as sulphur, which has a large impact on the reduction rates. This was also observed by Larssen[19] and the results are reprinted in figure 2.14. The graph shows four different charges, where charge Com.+Q and Com.+Q+S has the exact same composition, except for additional sulphur in the latter. The same applies for charge Com.+Q+Lime and Com.+Q+Lime+S.

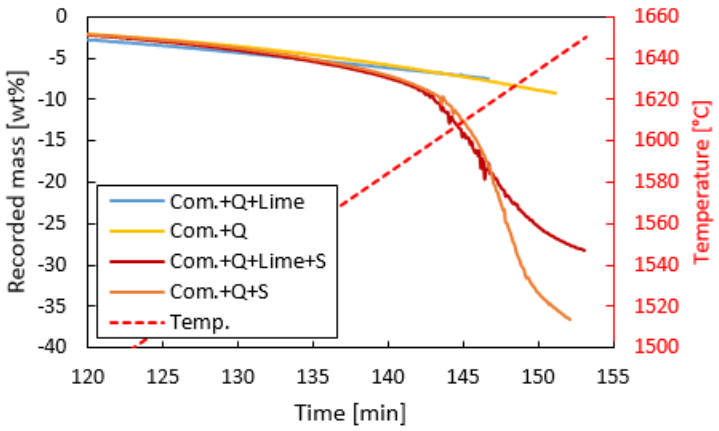

Figure 2.14: Effect of additional sulphur in charge based on Comilog ore, with or without limestone[19]. (Q=quartz, S = sulphur)

Kim et al.[18] published an investigation of reduction of MnO and SiO_2 from industrial slags A and B and synthetic SiMn slag under CO atmospheric pressure. The synthetic charge was prepared according to the industrial slag A by adding the different oxide components in powder form. It was shown that MnO was reduced faster from the corresponding industrial slag. As the synthetic slag was not added any trace elements, this supports the fact that the lack of sulphur abates the reduction. However, the lowest reduction rate was observed in industrial slag B. The amount of sulphur in the two industrial charges were not presented, but as slag A was added equal amounts of manganese ore and high-carbon FeMn slag, whereas slag B was only based on ore, it would be reasonable to assume that slag A had a higher sulphur content. The synthetic slag also showed a higher reduction of MnO compared to industrial slag B. This can not be explained by trace elements, as this would favor the industrial slag. However, the synthetic slag was prepared by mixing of powder compared to the industrial slag which was prepared by layering of the raw materials. Previous research has shown that mixing can increase the interfacial reaction area with a factor of 1.6, which implies that the rate is increased accordingly[17].

Another possible explanation for the increased reduction rate when adding slag from the FeMn process is that the melting point of the slag is lowered and a homogeneous slag is formed at a lower temperature. Brynjulfsen[22] found a clear relation between the melting temperature of the slag and the reduction rate, where a lower melting point of the slag correlated to a lower reduction temperature for MnO. The materials that melt at a lower temperature will also be reduced at a lower temperature due to the availability of of liquid phase.

2.2.1 Viscosity

Viscosity represents an important parameter regarding the mass transfer phenomena in metallurgical processes. Viscosity is a physical property of the system that is defined as a measure of the ability of one layer of molecules to move over an adjacent layer of molecules. The viscosity is a temperature and composition dependent property, where the composition is determined by the amount of the different species in the slag. For manganese slags it is shown that the

temperature dependency of viscosity can be represented by an Arrhenius-type relationship[23]:

$$\eta = \eta_0 \cdot \exp(\frac{G^*}{RT}) \tag{2.13}$$

where η_0 is the pre-exponential factor, G^* is the viscous activation energy, R is the ideal gas constant (J/K·mol) and T is the thermodynamic temperature (K).

It was previously mentioned that the slag contains individual oxides, such as MnO and SiO_2. However, electrical conductivity studies has shown that the liquid slag must be of ionic nature[1]. The slag can be divided into *network breaking* oxides (also known as basic oxides) forming cations:

$$MnO = Mn^{2+} + O^{2-} \tag{2.14}$$

$$CaO = Ca^{2+} + O^{2-} \tag{2.15}$$

$$MgO = Mg^{2+} + O^{2-} \tag{2.16}$$

SiO_2 is the strongest *network forming* oxide producing anions in manganese silicate slags:

$$SiO_2 + 2\,O^{2-} = SiO^{4-} \tag{2.17}$$

Al_2O_3 is an amphoteric oxide, which means that is behaves basic in an acidic system and vice versa.

$$Al_2O_3 + 3\,O^{2-} = 2\,AlO_3{}^{3-} \tag{2.18}$$

$$Al_2O_3 = 2\,Al^{3+} + 3\,O^{2-} \tag{2.19}$$

If a network breaking oxide (MeO) is added to a silica network, the added oxygen anions will connect with the silicate anion and break up the network, as shown in figure 2.15.

Basicity can provide an indication regarding the viscosity as it gives the ratio between the basic and acidic oxides, where reducible oxides are omitted. Hence, for SiMn the ratio is R = [CaO + MgO]/Al_2O_3. The viscosity decreases with increasing basicity at a constant MnO and SiO_2

content.

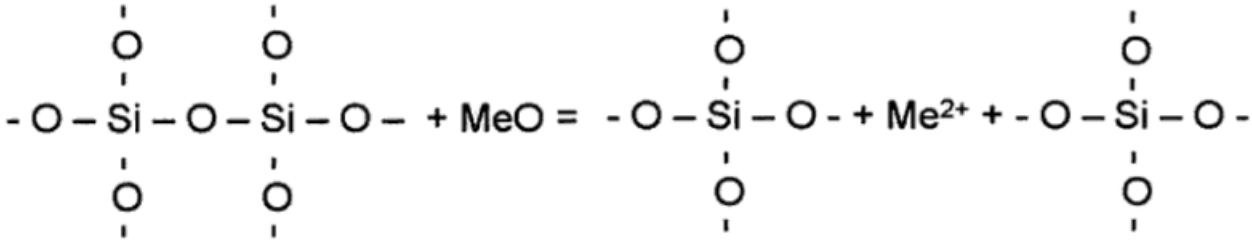

Figure 2.15: Illustration of interaction between silica network and network breaking oxide MeO[1].

Calculated iso-viscosity contours and experimental results for MnO-SiO_2-CaO slags are shown in figure 2.16 at 1500°C[23]. From this it appears that increased content of network forming oxides, here SiO_2, increases the slag viscosity. It is also seen that substitution of CaO with MnO will not change the viscosity considerably.

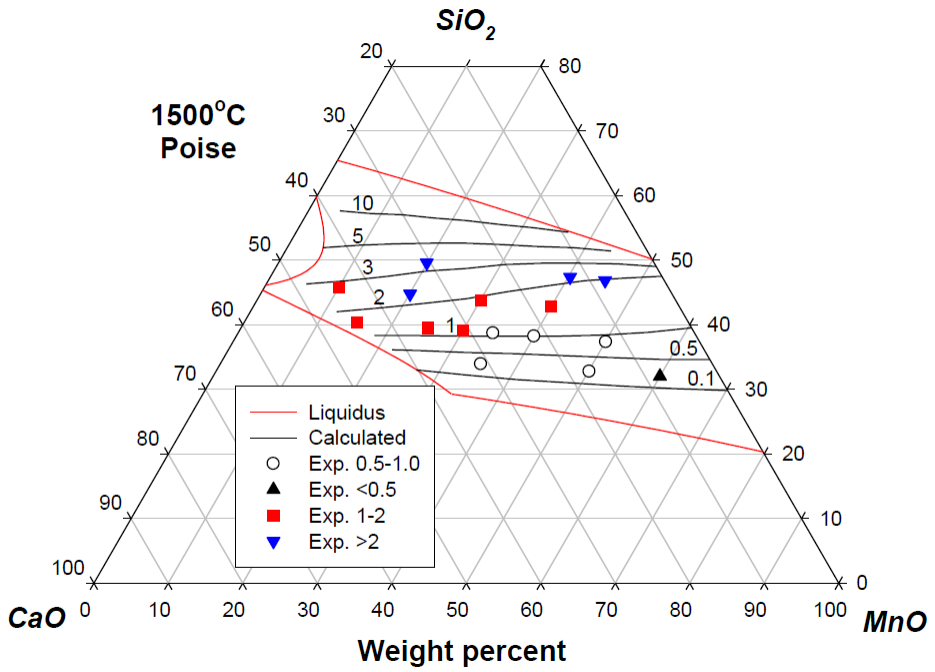

Figure 2.16: Calculated iso-viscosity curves for the MnO-SiO_2-Al_2O_3 system at 1500°C. Measured experimental data at same temperature[6]

The slag viscosity has shown to affect the production of manganese alloys in many ways. For ex-

ample, the slag and metal separation at given temperature will be better at lower viscosities and the slag viscosity has a great impact on the flow pattern in the furnace. At constant composition, the rates of mass transfer and thermal transfer by diffusion and convection are related inversely to the viscosity of the melt.

Slag foaming is a physical phenomenon that is a result of gas evolution at the slag and coke interface caused by chemical reaction and a viscous slag that may entrap these bubbles of gas[24]. The phenomenon is caused by two principial factors; (1) the rate of the gas evolution from chemical reactions and (2) the stability of the foam[25]. The stability of the foam is controlled by the viscosity and the movements of the gas bubbles through the slag. A review in relation with steel-making processes showed that foaming slags are highly viscous and that the extent of foaming increases with increasing silica content[26, 27]. Foaming in silicomanganese slags were reported by Holtan[21] that observed foaming in charges based on Comilog ore, quartz and coke (and limestone). The temperatures were 1650°C for charge with Comilog ore and quartz, and 1600°C with addition of limestone. It is not concluded on whether foaming occurs due to a fast reduction rate or if the reduction rate increases due to foaming.

3 | Experimental

The reduction of MnO and SiO_2 by solid carbon as reducing agent was studied by evaluating Comilog and Assmang ore in combination with HC FeMn slag and quartz. This chapter provides the chemical compositions of utilized raw materials, equipment, procedure and calculations.

3.1 Raw materials

The analyses of the raw materials presented in this section were executed by SINTEF Molab AS. The manganese ores used in the experiments are Comilog and Assmang. All elements were determined by X-ray fluorescence (XRF), except for MnO_2 which was determined by titrimetric analysis. A water content of 5% was assumed for the ores for calculations of weight loss. In addition, all Mn which is not MnO_2 is assumed to be MnO and all reported iron was assumed to be Fe_2O_3.

The quartz composition was determined by inductively coupled plasma optical emission spectroscopy (ICP-OES), where the amount of SiO_2 was determined by subtracting all other elements from 100%.

The composition of the polish coke is presented in table 3.2 and 3.3. Amount of volatiles, ash and fixed carbon content were determined on dry basis according to procedures specified according to the International Organization of Standardization (ISO). More specific, amount of volatiles by ISO-562: 1998, amount of ash by ISO-1171: 1997 and amount of fixed carbon by ISO-17246: 2005. The composition of ash was determined by X-ray fluorescence (XRF).

Table 3.1: Chemical composition of Comilog ore and quartz.

	Comilog ore [wt%]	Assmang ore [wt%]	HC FeMn slag	Quartz [wt%]
MnO	3.03	32.69	35.23	0.006
MnO_2	72.40	33.22	-	-
SiO_2	4.60	5.77	25.45	97.70
Fe_2O_3	6.73	15.06	-	0.17
CaO	0.07	6.26	18.45	0.068
MgO	0.05	1.10	7.53	0.038
Al_2O_3	5.60	0.26	12.30	1.40
CO_2	0.10	3.52	-	-
P	0.13	0.03	0.0095	-
S	<0.004	0.16	0.46	0.0070
TiO_2	0.14	-	-	0.040
K_2O	0.97	0.01	-	0.47
BaO	0.26	0.33	-	-
Na_2O	-	-	-	0.082

Table 3.2: Chemical composition of polish coke.

	wt%
Ash	9.80
Vol	1.20
Fix. C	89.00

Table 3.3: Chemical composition of ash in polish coke.

	SiO_2	Fe_2O_3	Al_2O_3	P_2O_5	MnO	CaO	K_2O	MgO	Na_2O	TiO_2	S
wt%	46.00	8.63	30.40	1.30	1.50	5.00	2.10	1.70	1.50	1.20	0.44

3.2 Equipment

3.2.1 Furnace

The furnace is a thermogravimetric graphite tube furnace that can handle temperatures up to 1700°C and which continuously measures the weight of the sample during the process. The furnace is attached to two different types of thermocouples. The software that controls the power supply to the furnace uses the S-type thermocouple that is located at the outer wall. At temperatures in the range of 1000 to 1600°C, the temperature at the B-type thermocouple located inside the furnace will be approximately 400°C higher than the S-type. A schematic of the furnace is displayed in figure 3.1.

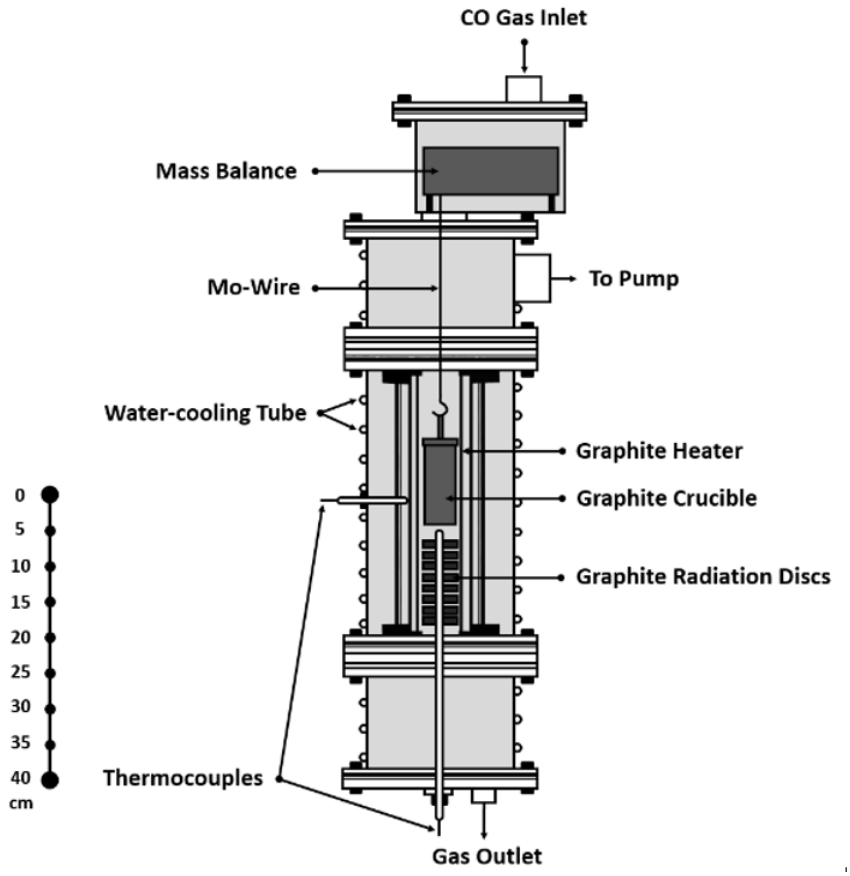

Figure 3.1: Schematic of furnace setup[5]. Crucible is located 0.5-1 cm above thermocouple to ensure no contact.

The temperature gradient of the furnace is presented in figure 3.2. Previous experiments has shown that a set point temperature of 1167°C for the S-type thermocouple corresponds to a temperature of 1600°C inside the furnace. This set point temperature was therefore chosen to evaluate the temperature profile. The furnace was kept constant at set point temperature and the temperature inside the furnace was evaluated at every cm by moving the thermocouple. This showed that the highest temperature observed in the furnace was when the thermocouple was located at approximately 50-51 cm. The figure shows the placing of the crucible respective of the thermocouple, at a separation of 0.5-1 cm to ensure that there is no contact between the crucible and the thermocouple. The temperature variance over the charge will be less than 1 K.

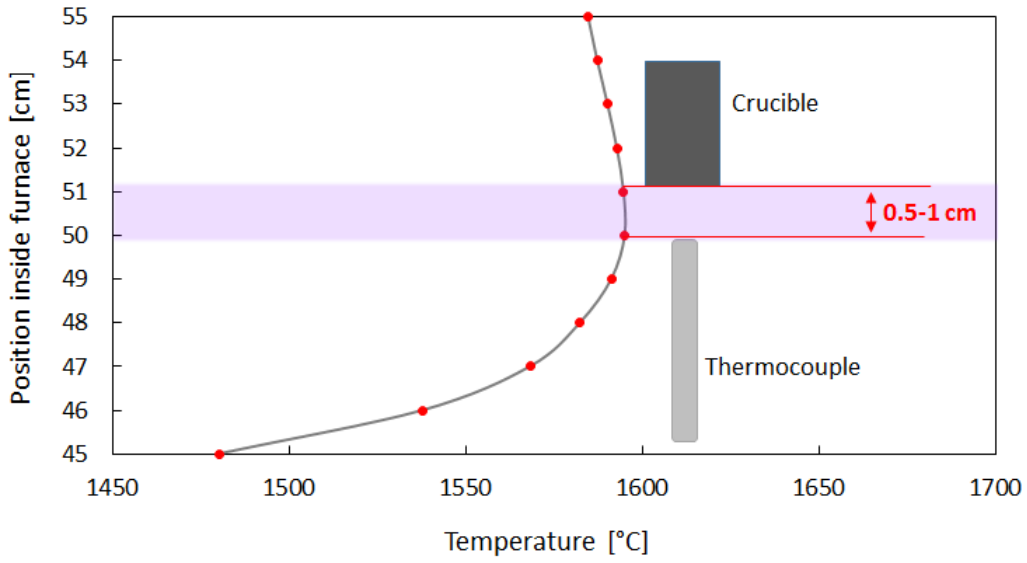

Figure 3.2: Temperature gradient of the TGA furnace found by evaluating the temperature at a specific set point temperature by moving the thermocouple.

The furnace is heated by an electric power supply which can result in a fluctuating temperature at certain temperature intervals. In order to show a clear representative curve for the recorded weight loss as a function of temperature, the temperature is fitted to linearity at average at these specific intervals. Figure 3.3 shows the original temperature as a function of time retrieved from the furnace mass log (blue curve). It is seen that the temperature mainly fluctuates between 850 and 1200°C and slightly during dwell at 1200°C. At temperatures exceeding the dwell period, the original curve show a relatively linear trend. The red curve shows the new temperature as

a function of time, which has been corrected to average for temperatures 850 to 1200°C and during dwell period.

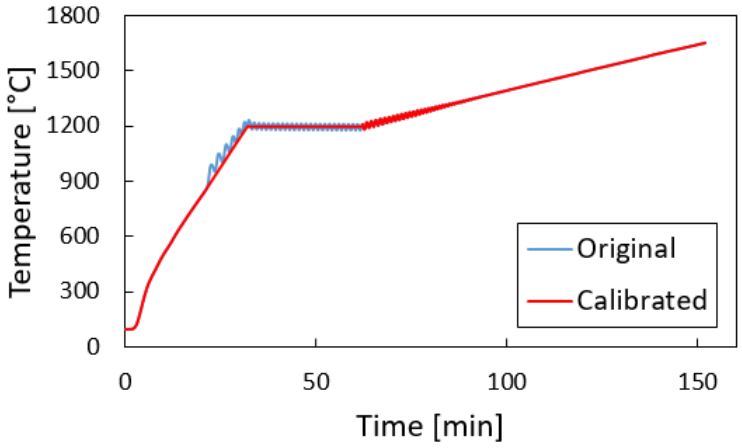

Figure 3.3: Temperature as a function of time retrieved from the mass log (blue curve) and temperature calibrated for fluctuations at temperature range 850-1200°C (orange curve).

3.2.2 Crucibles

Graphite crucibles are used to contain the samples during the experiments. The crucibles are of dimensions 36 mm outer diameter, 30 mm inner diameter, 70 mm high and 61 mm deep. They have three holes in the lid that enables transportation of gas in and out of the crucible.

Holtan[21] tested the crucibles for weight loss during heating to ensure that any recorded weight loss is from the raw materials and not the crucible itself. This was executed by heating an empty crucible up to 1600°C. Recorded weight loss during heating was 0.02 g, which is insignificant compared to loss of raw materials.

3.3 Procedure

Three different charge compositions were prepared, where two contained ore(Assmang or Comilog), HC FeMn slag and quartz and the last one contained Comilog and quartz. In addition, coke was added to all the charges. The composition(amounts of raw materials) for the mixtures were cal-

culated to obtain 18% Si in the metal phase at 1600°C. In addition, 10% MnO and 40% SiO_2 in the slag phase were assumed, which is expected according to thermodynamics at 1600°C.

Table 3.4: Amounts of raw materials in investigated charge mixtures. (C = Comilog, HC = HC FeMn slag, Q = quartz, A = Assmang)

	Comilog	Assmang	HC FeMn slag	Coke	Quartz	Total
C+HC+Q	4.00 g	-	4.00 g	2.30 g	1.59 g	11.89 g
C+Q	6 g	-	-	2.00 g	1.40 g	9.40 g
A+HC+Q	-	4.00 g	4.00 g	2.50 g	1.69 g	12.19 g

The raw materials are added layerwise in the crucible according to their respective melting temperature for the majority of the experiments. Coke was added first, following quartz, Mn ore and lastly HC FeMn slag. This was done to ensure a complete smelting, as previous experiments with mixing of raw materials showed unmelted lumps of material after finished experiments. Some experiments were also executed where the raw materials were thoroughly mixed before heating to see if this had an impact on the smelting temperature of the slag.

3.3.1 Furnace operation

The raw materials are weighed and added separately into the crucible before being placed in the furnace. The crucible hangs in a molybdenum wire and is not in contact with the furnace walls. The thermocouple is located under the crucible at a separation distance of 0.5-1 cm, where no contact is ensured.

The furnace is evacuated in three repeating steps to ensure that all air is removed. After evacuation the furnace is filled with argon gas up to 1050 mbar. When the temperature reaches 500°C the argon gas is replaced by a constant flow of CO gas at 0.5 l/min. Reverse procedure is executed at cooling of the furnace. CO gas is not introduced at low temperatures as it could initiate a reverse Boudouard reaction, equation 1.9 in introduction, meaning that CO-gas could precipitate into solid carbon and interfere with the weight balance.

The temperature profile is shown in figure 3.4. The heating to 1200°C is fast at rate 25°C/min, as

the interest is in the high temperature zone. The temperature is held at 1200°C for 30 minutes to ensure a complete prereduction. The heating rate is 4.5°C/min at higher temperatures. To simulate the industrial process, an increased temperature was used in the experiments rather than the more common high-temperature isothermal setups. As the reduction of MnO is highly endothermic, an increasing temperature is beneficial in terms of obtaining the desired extent of SiO_2 reduction.

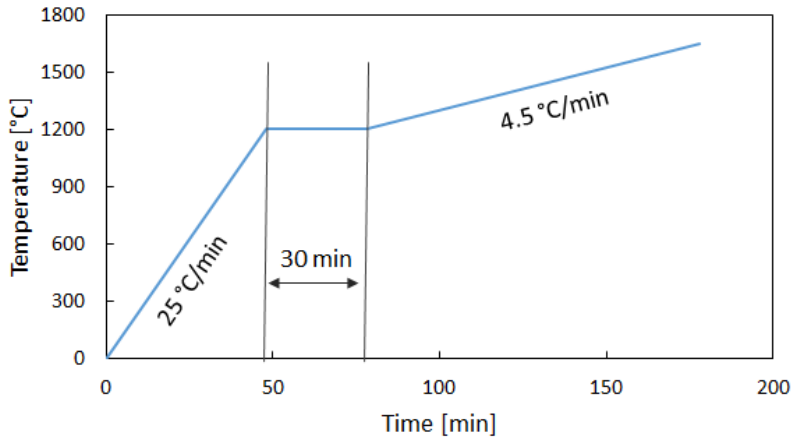

Figure 3.4: Temperature profile during experiments. Rate is 25°C/min up to 1200°C where the temperature is dwelled for 30 minutes. Rate of 4.5°C/min is executed up to aimed temperature.

3.3.2 Overview of experiments

Table 3.5 shows an overview of the experiments conducted for investigation of the reduction rate of MnO and SiO_2. Five different temperatures in the range of 1530-1650°C were evaluated for the same charge composition containing Assmang ore, HC FeMn slag, quartz and coke. Similarly, the charge containing Comilog ore, HC FeMn slag, quartz and coke were evaluated at five temperatures in the range 1550-1650°C.

Table 3.6 shows the experiments conducted for investigation of slag formation temperature. It can be seen that the first evaluated charge is identical to the Comilog charge in table 3.5. The second charge (without HC FeMn slag) is identical to charge investigated by Larssen[19]. Four different temperatures were evaluated when the raw materials were layered in the crucible, whereas two temperatures were evaluated when mixed. The aimed amount of the different raw

materials have been presented, however potential deviations in order of ±0.1 g may have been observed.

Table 3.5: Overview of experiments conducted for investigation of kinetics.

Temperature	Assmang	Comilog	HC FeMn slag	Quartz	Coke	Total
1530°C	4.00 g	-	4.00 g	1.69 g	2.5 g	12.19 g
1550°C	4.00 g	-	4.00 g	1.69 g	2.5 g	12.19 g
1570°C	4.00 g	-	4.00 g	1.69 g	2.5 g	12.19 g
1600°C	4.00 g	-	4.00 g	1.69 g	2.5 g	12.19 g
1650°C	4.00 g	-	4.00 g	1.69 g	2.5 g	12.19 g
1550°C	-	4.00 g	4.00 g	1.59 g	2.3 g	11.89 g
1580°C	-	4.00 g	4.00 g	1.59 g	2.3 g	11.89 g
1600°C	-	4.00 g	4.00 g	1.59 g	2.3 g	11.89 g
1630°C	-	4.00 g	4.00 g	1.59 g	2.3 g	11.89 g
1650°C	-	4.00 g	4.00 g	1.59 g	2.3 g	11.89 g

Table 3.6: Overview of experiments conducted for investigation of slag formation temperature.

Temperature	Preparation	Comilog	HC FeMn slag	Quartz	Coke	Total
1200°C	Layered	4.00 g	4.00 g	1.59 g	2.30 g	11.89
1250°C	Layered	4.00 g	4.00 g	1.59 g	2.30 g	11.89
1300°C	Layered	4.00 g	4.00 g	1.59 g	2.30 g	11.89
1400°C	Layered	4.00 g	4.00 g	1.59 g	2.30 g	11.89
1200°C	Mixed	4.00 g	4.00 g	1.59 g	2.30 g	11.89
1250°C	Mixed	4.00 g	4.00 g	1.59 g	2.30 g	11.89
1200°C	Layered	6.00 g	-	1.59 g	2.00 g	9.40 g
1250°C	Layered	6.00 g	-	1.59 g	2.00 g	9.40 g
1300°C	Layered	6.00 g	-	1.59 g	2.00 g	9.40 g
1400°C	Layered	6.00 g	-	1.59 g	2.00 g	9.40 g
1200°C	Mixed	6.00 g	-	1.59 g	2.00 g	9.40 g
1250°C	Mixed	6.00 g	-	1.59 g	2.00 g	9.40 g

3.3.3 Subsequent treatment of samples

After the crucibles are collected from the furnace, they are filled with epoxy. The crucibles are cut with a diamond saw to expose the area of interest after solidification. The desired area is mounted in epoxy and thereafter ground with SiC paper in repeating steps. The grinding papers are numbered according to coarseness, where a higher number indicates a finer ground product. The first paper is coarse (500 paper) and the last is 4000 paper. After this, the samples are polished with diamond paste on a polishing apparatus. The last step is performed with 1 μm diamond particles. The sample is then coated with carbon to increase the conductivity before EPMA analysis.

3.3.4 Analysis method

A JEOL JXA-8500F Electron Probe Micro Analyzer(EPMA) was used to execute the analyses. This is a high performance thermal field emission electron probe micro analyzer which combines high SEM resolution with high quality X-ray analysis of submicron areas.

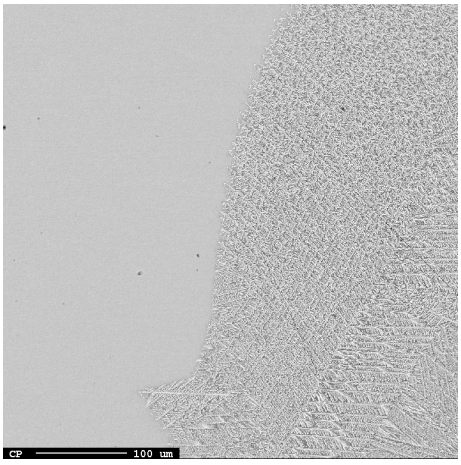

(a) Glassy and fine crystalline slag. (Scale = 100 um)

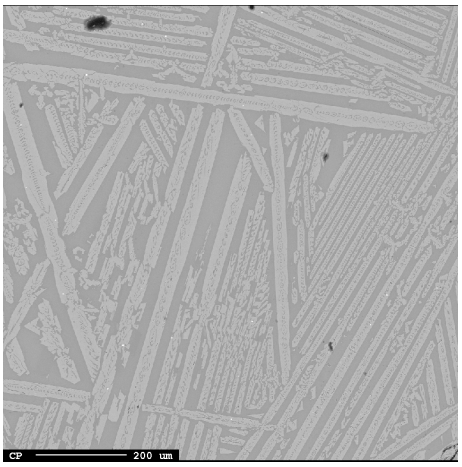

(b) Coarse crystalline slag. (Scale = 200 um)

Figure 3.5: Different types of slag structures that can be found in the analysed samples.

The slag phases will either be a homogeneous glassy structure or be a two-phase slag, as can be seen in figure 3.5. 3.5a shows a glassy structure to the left and a fine crystalline structure to the right, whereas 3.5b shows a more coarse crystalline structure. At least three separated areas,

preferably far from each other, will be analysed in order to confirm that the slag is homogeneous. The composition can either be given by spot-analysis or by defocused area analyses, which gives the average composition within the selected area (usually 1 mm^2). Glassy and fine crystalline slag is analysed with defocused area analysis, whereas the different phases are analysed separately in more coarse structures. An estimation of the distribution between the different phases by visual observation of the structure is performed in order to determine the composition.

3.3.5 Calculations

Equation 3.1 shows how the initial mass of the different compounds are calculated, here by MnO as example. The calculations are based on the chemical analyses of the raw materials executed by SINTEF Molab AS presented in tables 3.1 and 3.2. Amounts of other chemical compounds are calculated in similar manner.

$$m_{MnO} = m_{Ore} \cdot \frac{MnO_{Ore}}{Ore_{tot}} + m_{coke} \cdot \frac{MnO_{Coke}}{Coke_{tot}} + m_{Quartz} \cdot \frac{MnO_{Quartz}}{Quartz_{tot}} \tag{3.1}$$

Where m_{Ore} is feed of Comilog or Assmang ore (g), MnO_{Ore} is the weight percent of MnO in the ore and Ore_{tot} is the total weight percent of the ore given by the chemical analysis.

After calculating the amounts of the chemical components in the raw materials, the composition after prereduction can be found. To do this, the following assumptions are made:

- All MnO_2 is reduced to MnO
- All water is evaporated
- All iron oxides are reduced to metallic iron
- All CO_2 has gone off from the carbonates
- All volatiles are evaporated from coke

The increase in amount of MnO from reduction of MnO_2 is calculated as follows:

$$m_{MnO} = m_{MnO,in} + \frac{m_{MnO_2,in}}{Mm_{MnO_2}} \cdot Mm_{MnO} \tag{3.2}$$

Primary slag compositions for charge based on Comilog and Assmang, respectively, are presented in table 3.7.

Table 3.7: Calculated primary slag composition for the two different charges.

Charge	MnO	SiO_2	Al_2O_3	CaO	MgO	R-ratio
C+HC+Q	45.53	33.08	9.25	8.62	3.52	1.31
C+Q	63.58	29.13	6.94	0.23	0.11	0.05
A+HC+Q	43.56	34.39	6.71	11.37	3.96	2.29

The expressions used for calculating the mass of MnO and SiO_2 in the end slag are as shown in equation 3.3 and 3.4.

$$mass_{MnO} = \frac{wt\%MnO \cdot (m_{CaO} + m_{MgO} + m_{Al_2O_3})}{100 - wt\%MnO - wt\%SiO_2} \tag{3.3}$$

$$mass_{SiO_2} = \frac{wt\%SiO_2 \cdot (m_{CaO} + m_{MgO} + m_{Al_2O_3})}{100 - wt\%MnO - wt\%SiO_2} \tag{3.4}$$

Where m_{CaO}, m_{MgO} and $m_{Al_2O_3}$ are the initial amounts of the unreducable oxides (g), as their amounts are constant throughout the process. The weight percent of MnO and SiO_2 is from the slag analysis of each sample.

The amount of manganese in the metal is simply calculated as the amount of manganese which is not in the end slag phase. This is calculated by equation 3.5. Similar calculation for amount of Si.

$$m_{Mn} = (n_{MnO,primary} - n_{MnO,end}) \cdot Mm_{Mn} \tag{3.5}$$

Where m_{Mn} is the amount of produced manganese (g), $n_{MnO,\,primary}$ is the amount of MnO from primary slag composition (mol) and $n_{MnO,\,end}$ is the amount of MnO from slag analysis (mol)

and Mm_{Mn} is the molar mass of manganese (g/mol).

The total weight loss due to the reduction of MnO and SiO_2 can be calculated accordingly:

$$Weightloss_{red} = n_{Mn} \cdot M_{CO} + n_{Si} \cdot 2 \cdot M_{CO} \tag{3.6}$$

Where n_{Mn} and n_{Si} is the amount of produced manganese and silicon (mol), respectively and M_{CO} is the molar mass of CO gas (g/mol).

3.3.6 Computational model

A computational model was produced in Excel (2013) in order to simulate the data obtained during the experiments. The model was constructed to calculate the reduction rates according to the existing equations for MnO and SiO_2 reduction that were presented in equation 2.6 and 2.7, respectively. The frequency factor k_0 is the only fitting value. The activities giving the driving force will be calculated by the formulas presented in theory section on kinetics, equations 2.9-2.12, which were modeled by Olsen[16]. Temperature range for the developed model is 1200 to 1650°C in order to use the primary slag compositions at 1200°C as initial composition/starting point.

The reaction area was assumed to be constant for temperatures lower than 1400°C and was at higher temperatures estimated from the consumed amount of carbon correlating to the produced amount of metal. The density of the coke particles was approximated to 1 g/cm^3 and the average coke diameter of 1.1 mm was used for the calculations. MnO and SiO_2 have three available sources of carbon for reduction when graphite crucibles are used for the experiments, i.e coke, carbon in metal and the graphite crucible, however in this case the reaction area was estimated by assuming reduction only by coke. Equation 3.7 shows the relationship between the reaction area and the produced amount of manganese and silicon for Comilog charge, whereas 3.8 show the same relationship for Assmang charge.

$$A[cm^2] = -13.17 \cdot (Mn[g] + Si[g]) + 126.73 \tag{3.7}$$

$$A[cm^2] = -13.77 \cdot (Mn[g] + Si[g]) + 138.75 \tag{3.8}$$

The rate at a given composition was used to determine the new composition at increasing temperature. The error of the fitted curve was estimated by using the standard error of estimate, as presented in equation 3.9.

$$Error_i = \sqrt{\frac{\sum (Y - Y')^2}{N}} \tag{3.9}$$

Where Y is the actual value, Y' is the predicted value and N is the number of paired values. The error was evaluated by comparing the calculated values for wt% MnO and wt% SiO_2 with the experimental values.

The solver function in Excel was used to minimize the error value by adjusting $k_{0,Mn}$ and $k_{0,Si}$.

Example of calculation

The primary slag composition that was calculated in section 3.3.4 was used as the starting point of the model. The composition in wt% was used to calculate the activities of MnO, SiO_2, Mn and Si at 1200°C from Olsen's model. The composition and the corresponding activities for charge containing Comilog, quartz and HC FeMn slag are shown in table 3.8

Table 3.8: Primary slag composition at 1200°C and the corresponding activities in slag and alloy.

MnO	SiO_2	Al_2O_3	CaO	MgO	a(MnO)	a(SiO_2	a(Mn)	a(Si)
45.53	33.08	9.25	8.62	3.52	0.179	0.121	0.00	0.00

The driving force (DF) is given by the distance the system has towards equilibrium in terms of activity. As the system maintains CO at ambient pressure and the activity of carbon is unity (solid state), the driving force of MnO can be calculated as follows when the rate constant is retrieved from HSC Chemistry[28]:

$$DF = a_{MnO} - a_{MnO,eq} = a_{MnO} - \frac{a_{Mn}}{K} \tag{3.10}$$

$$r = \frac{g}{min} = k_{0,MnO} \cdot A \cdot e^{\frac{-Ea}{RT}} \cdot DF \tag{3.11}$$

According to the equation describing the rate of MnO, reprinted here in 3.11, all values are either given or estimated:

- A = 138.75 cm^2 (estimated)
- R = 8.314 J/K·mol (ideal gas constant)
- T = 1200°C + 273.15 = 1473.15 K
- DF = 0.179 - 0.00/2.1 = 0.179
- Ea = activation energy of MnO. Needs to be given to the system. Ex: Ea = 360 kJ/mol as presented by Tangstad[17]

Hence, the mass transfer coefficient is the only fitting value for the model. A qualified guess is made in order to start the model.

If $k_{0,MnO} = 1.8 \cdot 10^8$ g/min·cm^2, the rate becomes:

$$\begin{aligned} r = \frac{g}{min} &= 1.8 \cdot 10^8 g/min \cdot cm^2 \cdot 138.75 cm^2 \cdot 0.179 \\ &\cdot e(-360 kJ mol^{-1}/(8.314 JK^{-1} mol^{-1} \cdot 1473.15 K)) \\ &= 7.7 \cdot 10^{-4} g/min \cdot cm^2 \end{aligned} \tag{3.12}$$

Then the new composition (in grams as the rate was expressed in g/min), is calculated accordingly:

$$g(MnO, 1210^\circ C) = g(MnO, 1200^\circ C) - 7.7 \cdot 10^- 4 \cdot dt = 3.776g - 0.002g = 3.774g \tag{3.13}$$

Similar calculations are performed on the amount of SiO_2, whereas the amounts of CaO, MgO and Al_2O_3 are assumed constant throughout the process.

4 | Results

4.1 Comilog based charges

Five experiments were conducted with the specific charge composition based on Comilog ore, HC FeMn slag, quartz and coke. The R-ratio for all experiments in this section is 1.31 and the investigated temperature range was 1550-1650°C. The raw materials were added in a specific order of layers according to melting temperature, as mentioned in experimental.

The obtained weight loss at maximum temperatures is presented in table 4.1, in both grams and mass percent. The values show an increasing weight loss at increasing temperature, where the largest difference is between the two first evaluated temperatures, i.e. 1550 and 1580°C. Note that the calculated weight loss at 18% Si in alloy and 6% MnO in slag was 4.18 grams, equal to 35.17 mass%. It is seen that this weight loss is obtained at a temperature in the range of 1630-1650°C.

Table 4.1: Obtained weight loss at maximum temperature for the five different experiments with the same Comilog based charge composition.

	Weight loss [g]	% mass loss
1550°C	1.64	13.50
1580°C	2.71	23.03
1600°C	3.16	26.18
1630°C	3.87	32.52
1650°C	4.29	37.19

4.1.1 Temperature profiles and mass loss curves

The furnace used for the experiments logs temperature, time and weight at a five second interval. The temperature as a function of time is presented in figure 4.1. The program starts heating from room temperature, however it is seen that the software records approximately 95-100°C as starting point. The temperature was calibrated to linearity at average at temperatures 850-1200°C and during dwell period. The temperature profile shows a heating rate of 25°C/min from room temperature up to 1200°C, where the temperature is dwelled for 30 minutes to ensure a complete prereduction. Further, from 1200°C to maximum temperature a heating rate of 4.5°C/min was executed. The graph show that the same temperature program was successfully performed in each of the experiments.

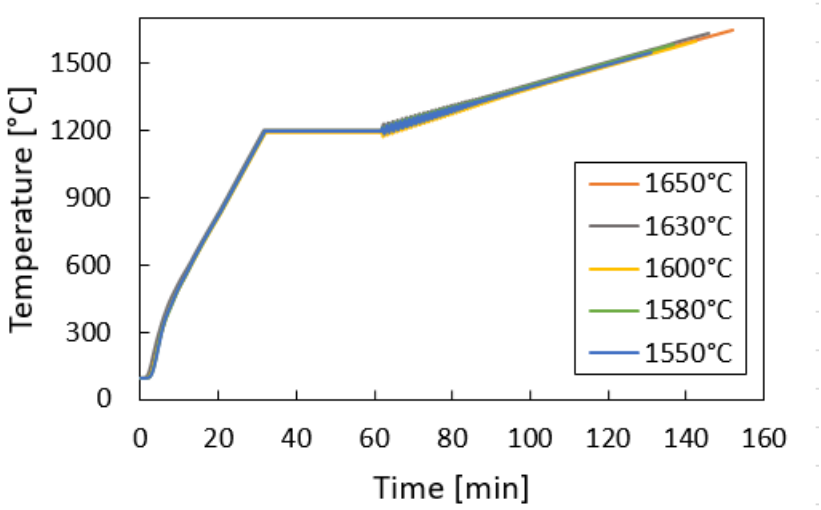

Figure 4.1: Temperature as a function of time logged by the furnace in figure a). Figure b) shows the temperature when the fluctuations at 900-1200°C has been fitted to linearity at average.

Figure 4.2 and 4.3 shows the recorded weight (g) as a function of process time (min) and temperature (°C), respectively, retrieved from the mass log of the TGA furnace. In addition, the theoretical weight losses of complete prereduction and 18% Si in alloy at 1600°C have been marked. All raw materials, including coke, was evaluated when calculating the theoretical weight losses. Red circles shows obtained weight for each of the samples weighed manually subsequent to experiments, confirming that recorded weight from the furnace and physical weight loss is similar.

The curves can be divided into two regions separated by the 30 minute dwell at 1200°C, namely prereduction zone (low temperature zone) and coke bed zone (high temperature zone). During prereduction, the charges will experience a weight loss due to evaporation of water, decomposition of carbonates and reduction of higher manganese oxides to MnO, whereas in the high-temperature zone the weight loss can be assumed to be due to the reduction of MnO and SiO_2.

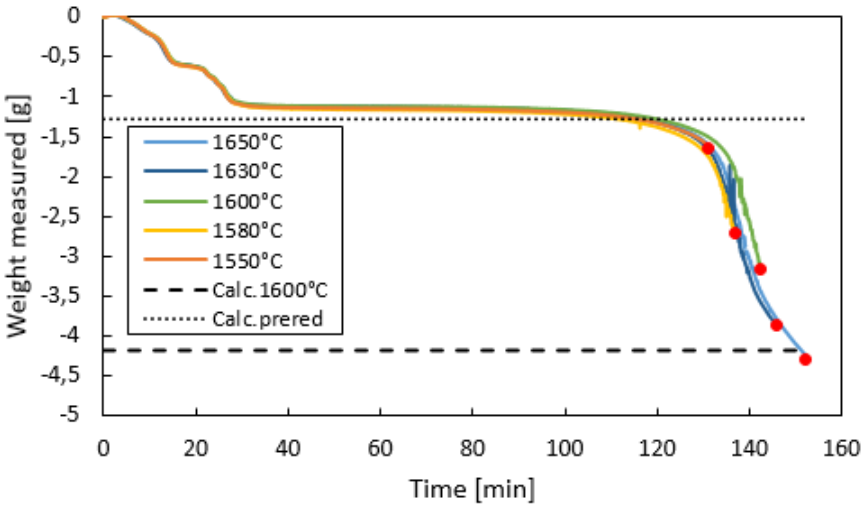

Figure 4.2: Mass loss [g] as a function of time [min] for Comilog based charges.

There is an observed weight loss from room temperature and up to 700°C at approximately 0.59 g for all charges. Evaporation of moisture from the raw materials takes place during this interval starting at 100°C, however evaporation of water that is chemically bonded could require higher temperatures. The theoretical weight loss from evaporation of moisture from all raw materials is 0.60 g, which is highly consistent. It is also expected that MnO_2 could start to reduce to Mn_2O_3 at temperatures lower than 700°C, which could indicate that the moisture content of the raw materials could be somewhat inaccurate.

Between 700 and 1200°C the charges suffers a weight loss of 0.52 g. MnO_2 will be reduced to Mn_2O_3, further to Mn_3O_4 and lastly to MnO. This reaction course will give a combined theoretical weight loss of 0.54 g, which fits quite accurately. After the complete dwell at 1200°C the charges have obtained a total weight loss of 1.12-1.16 grams, whereas the theoretical weight loss is 1.28 g. The deviation could be due to inaccuracy in moisture content. The theoretical weight loss at complete prereduction is obtained at temperatures in the range of 1460-1490°C for the

different experiments.

The calculated weight loss for the charges during the high temperature zone (after 30 minute dwell at 1200°C) to obtain 18% Si in alloy at 1600°C is 2.89 g. This weight loss is only obtained for charge heated to 1650°C, whereas charge heated to 1630°C is fairly close at 2.72 g.

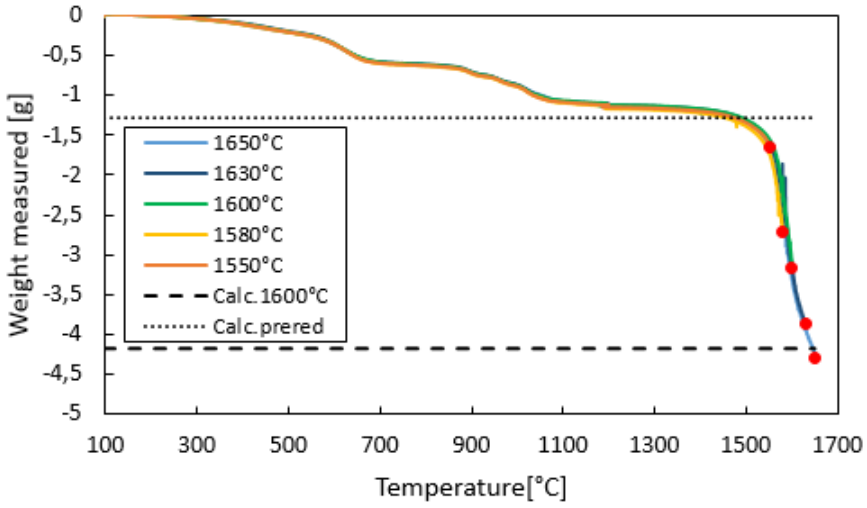

Figure 4.3: Mass loss [g] as a function of temperature [°C] for Comilog based charges.

4.1.2 Analysis of end product

Visual inspection of the crucibles after completed experiments revealed that foaming had occurred for charges heated to temperatures including and exceeding 1580°C. Figure 4.4a shows the interior of crucible heated to 1650°C, where the lower parts of the crucible shows coke (grey) and slag (pale green). The inner surface of the crucible wall is covered in small metal particles as a result of foaming, ranging approximately 2 cm from the bottom and up. The samples were mounted in epoxy and ground to expose the bottom surface of the slag. These pictures are presented in figures 4.4b-4.4f.

(a) 1650°C

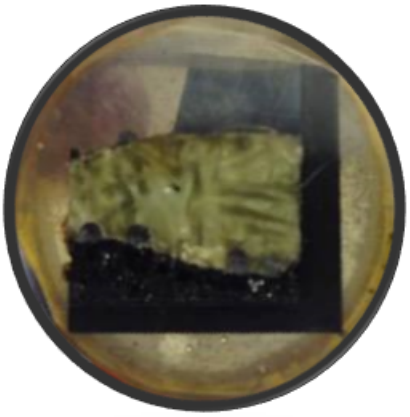

(b) 1550°C

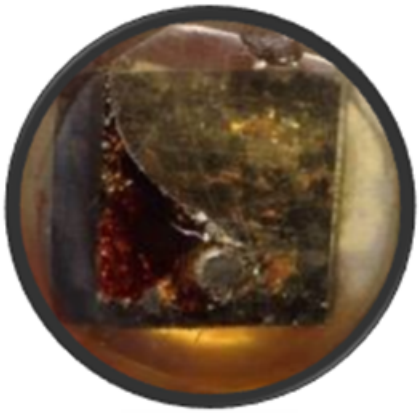

(c) 1580°C

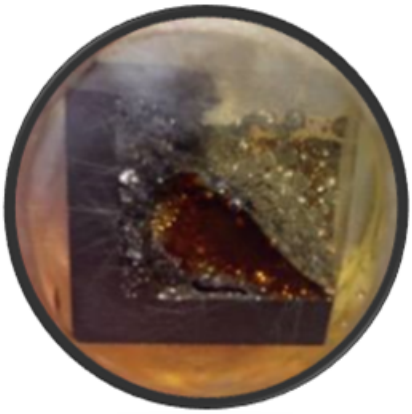

(d) 1600°C

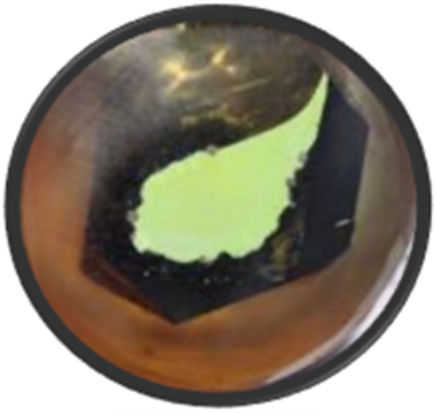

(e) 1630°C

(f) 1650°C

Figure 4.4: Image a) shows the interior of crucible heated to 1650°C where foaming can be confirmed by the small metal particles covering the inside of the crucible surface. Image b)-f) shows samples after mounting in epoxy displaying bottom surface of the slag.

All slag phases were of amorphous/glassy structure, except for sample C.1, heated to 1550°C, which had a fine crystalline structure. This means that the only sample without glassy structure was also the only sample that did not experience foaming. The structure of C.1 is seen in figure 4.5a, whereas 4.5b shows a homogeneous glassy structure.

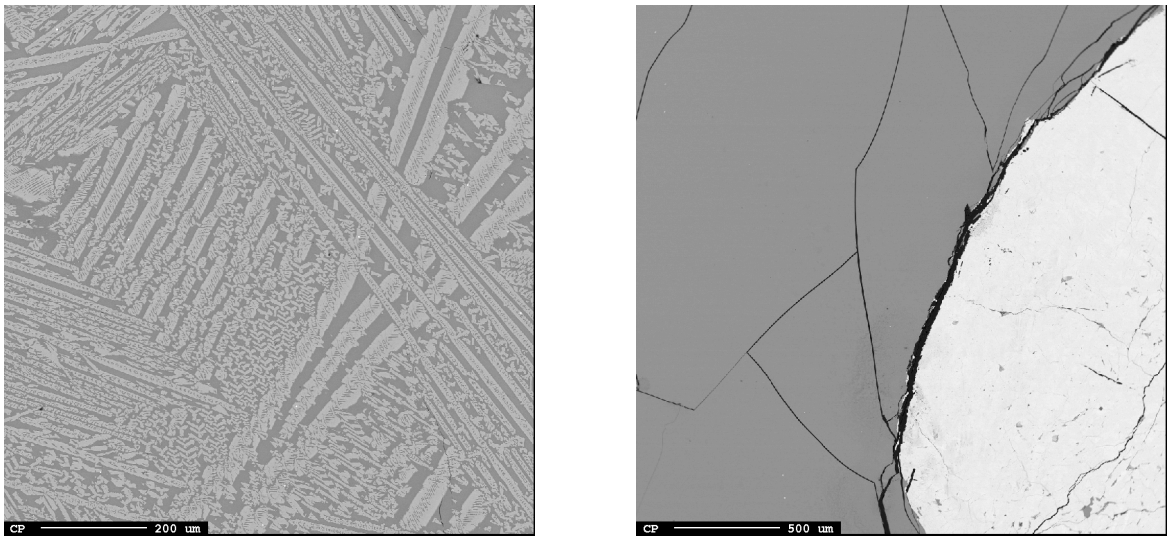

(a) (b)

Figure 4.5: Crystalline structure for sample heated to 1550°C in a) and glassy structure found at all other temperatures in b). Scale bar reads 200 um.

Composition for slags of amorphous structure was determined by defocused area analysis, while the composition for the crystalline sample was determined by analyzing the two phases separately and estimating the distribution of the phases. According to structure shown in 4.5a, 55% bright and 45% dark phase was estimated. Resulting slag compositions are presented in table 4.2. Only the five main oxides represented in the slag are included, hence giving a total of less than 100% for the samples. The components making up the remaining amount of the composition can be seen in the raw data presented in appendix B.

As the oxides CaO, MgO and Al_2O_3 are considered unreducable, their respective amounts should stay constant throughout the process, giving a constant R-ratio. Table 4.3 shows the slag composition where the amounts of MnO and SiO_2 are from the EPMA analyses and the remaining oxides are from their respective initial amounts. This composition is calculated under the assumption that the slag consists only of these five oxides, which can be considered a fair approximation.

Table 4.2: Average analysed composition of slag phases from EPMA for charges based on Comilog ore. All spot analyses are presented in table in appendix A.

Experiment	Temperature	MnO	SiO_2	Al_2O_3	CaO	MgO	Total	R-ratio
C.1	1550°C	43.14	33.87	7.40	8.97	3.62	97.00	1.70
C.2	1580°C	26.16	41.29	11.76	13.03	4.37	96.62	1.48
C.3	1600°C	18.98	42.98	14.17	14.66	5.08	95.88	1.39
C.4	1630°C	10.40	43.33	17.72	18.97	6.52	96.95	1.44
C.5	1650°C	5.70	40.89	20.55	22.18	7.62	96.95	1.45

Table 4.3: Average analysed composition from EPMA for MnO and SiO_2, whereas CaO, MgO and Al_2O_3 are from their initial amounts.

Experiment	Temperature	MnO	SiO_2	Al_2O_3	CaO	MgO	R-ratio
C.1	1550°C	43.14	33.87	9.94	9.26	3.78	1.31
C.2	1580°C	26.16	41.29	14.08	13.12	5.36	1.31
C.3	1600°C	18.98	42.98	16.45	15.33	6.26	1.31
C.4	1630°C	10.40	43.33	20.00	18.64	7.62	1.31
C.5	1650°C	5.71	40.89	23.10	21.52	8.79	1.31

The metal composition will vary according to particle size, implying that metal analyses will not be representative for the amount of metal produced. From the calibrated slag composition, the metal composition can be calculated under the assumption that all MnO/SiO_2 that is not recorded in the slag phase has been reduced to the metal phase. Resulting metal compositions are presented in table 4.4. It is seen that the amounts of Mn and Si increases at increasing temperature, where the largest increase is seen for the manganese content, as expected.

The amounts of MnO/Mn and SiO_2/Si at increasing process time and temperature can be seen in figure 4.6a and 4.6b, respectively. Second order polynomial regression lines are also added for the increasing or decreasing amounts, however the relation for SiO_2/Si is approximately linear.

Table 4.4: Metal composition calculated from analysed slag composition. The initial amounts of the unreducable oxides were used to determine the amounts of MnO and SiO_2 in grams.

Temperature	Mn [g]	Si [g]	Fe [g]	C [g]	Mn [wt%]	Si [wt%]	Fe [wt%]	C [wt%]
1550 °C	0.36	0.06	0.20	0.02	55.66	9.80	31.74	2.81
1580 °C	1.88	0.24	0.20	0.07	78.67	9.98	8.55	2.80
1600°C	2.31	0.36	0.20	0.10	77.69	12.00	6.86	3.44
1630°C	2.70	0.52	0.20	0.11	76.46	14.79	5.78	2.97
1650°C	2.87	0.67	0.20	0.11	74.56	17.39	5.31	2.74

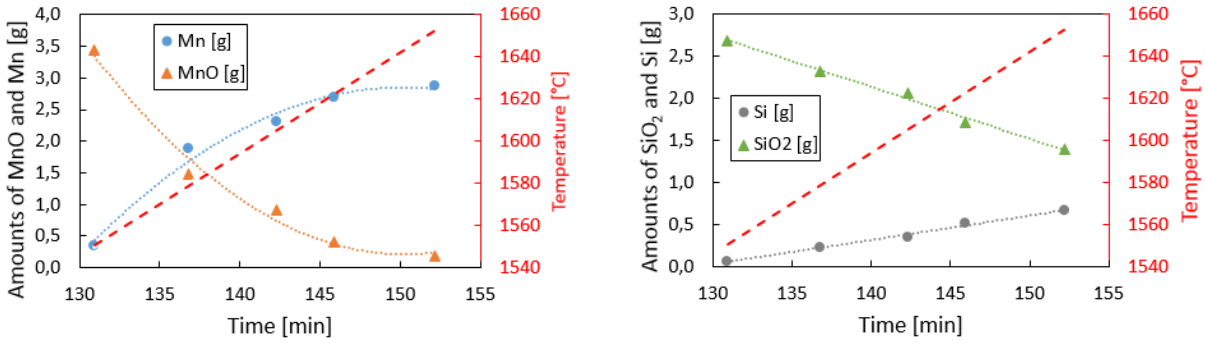

(a) (b)

Figure 4.6: The amounts of MnO/Mn and SiO_2/Si at increasing process time in figure a and b, respectively.

The amount of produced manganese (g) divided by the amount of produced silicon (g) at increasing process time and temperature is presented in figure 4.7. The ratio increases for temperatures up to 1580°C, as the reduction of MnO is more dominant than the reduction of SiO_2. At higher temperatures it can be seen that the ratio decreases, due to that the temperature is in the main reduction area for SiO_2, making the amount of Si more dominant.

As was shown in experimental section 3.3.5, the reaction area at increasing temperature can be evaluated as a function of produced amount of manganese and silicon. Table 4.5 shows the resulting reaction area in the case of Comilog, HC FeMn slag and quartz charge in both cm^2 and as percent of initial area. It is seen that the reaction area is reduced by approximately 35% at 1650°C.

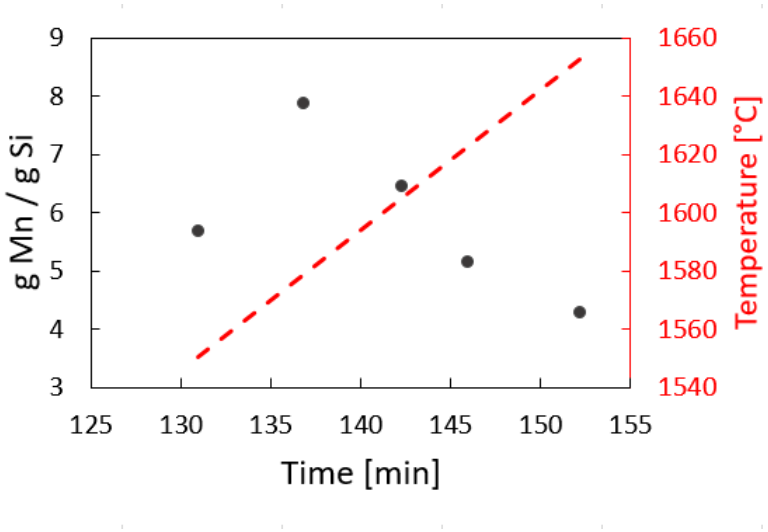

Figure 4.7: Amount of Mn (g) divided by amount of Si (g).

Table 4.5: Reaction area at increasing temperature calculated according to procedure described in experimental section 3.3.5. Column to the right shows reaction area as percent of initial area (prior to any reduction).

Temperature [°C]	Reaction area [cm^2]	Reaction area (%)
1400	126.16	100.00
1550	121.18	96.06
1580	98.85	78.36
1600	91.60	72.61
1630	84.32	66.83
1650	80.18	63.56

The models presented by Olsen (2016)[16] reprinted in equations 2.9 - 2.12 and thermodynamic equilibrium data from HSC Chemistry[28] were used to estimate the driving forces for MnO and SiO_2 reduction at different temperatures. These are presented in table 4.6 and it is seen that the driving force for both MnO and SiO_2 decreases at increasing temperature, due to MnO and SiO_2 content being reduced. The driving force for reduction of SiO_2 was negative at 1550°C, which could indicate that the composition is close to equilibrium at this specific temperature.

Table 4.6: Calculated activities and driving forces at different process times/temperatures.

Temperature [°C]	a(MnO)	a(SiO_2)	a(Mn)/K_T	a(Si)/K_T	DF(MnO)	DF(SiO_2)
1550	0.216	0.116	0.003	0.142	0.213	-
1580	0.074	0.231	0.004	0.061	0.070	0.170
1600	0.043	0.241	0.002	0.071	0.041	0.169
1630	0.012	0.209	0.001	0.067	0.016	0.142
1650	0.008	0.142	0.001	0.074	0.007	0.068

4.2 Slag formation temperature

12 experiments were executed to investigate the formation temperature of the slag for charges based on Comilog ore. Two different charges were evaluated where one had Comilog ore as the source of manganese and the other contained both Comilog ore and waste slag from the HC FeMn process. In addition, both charges contained quartz and coke. The composition for the charge containing FeMn slag is identical to the charge presented in the previous section, whereas the charge based only on Comilog ore is identical to charge investigated by Larssen[19]. The charges were evaluated both for mixing of raw materials and layering at temperatures between 1200 and 1400°C.

4.2.1 Comilog, quartz and HC FeMn slag

The specific charge composition containing Comilog, quartz and HC FeMn slag was evaluated at temperatures, 1200, 1250, 1300 and 1400°C with layered materials and at 1200 and 1250°C with mixed materials. Figure 4.8 shows the recorded weight as a function of temperature retrieved from the TGA mass log. It can be seen that all layered charges show highly similar behaviour at the different experiments, confirming that the experimental procedure is successfully reproduced. Similarly, both charges with mixed materials show similar behaviour to one another. However, the mixed and the layered charge show some dissimilarities. Generally, the mixed charge experiences a faster reduction of the higher manganese oxides than the layered charge.

Nonetheless, they have obtained the same weight loss at 1200°C.

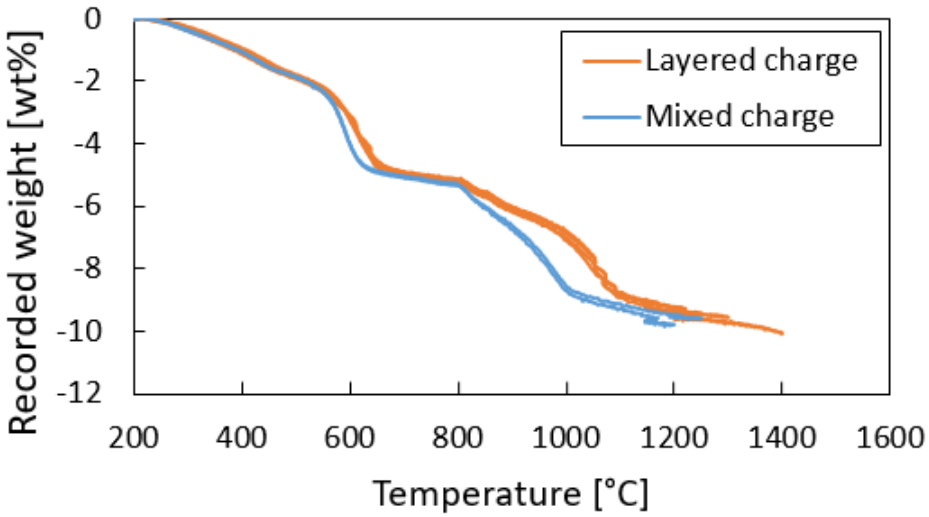

Figure 4.8: Recorded weight [wt%] as a function of process temperature [°C] for layered and mixed charges containing Comilog, quartz and HC FeMn slag.

The crucible contents after finished experiments for charge containing Comilog and HC FeMn slag layerwise can be seen in figure 4.9. It is seen in 4.9a that the raw materials are unmelted at 1200°C. At 1250°C, the ore and HC FeMn slag have melted, whereas white quartz particles are observed unmelted throughout the slag surface. 4.9c shows the bottom surface of the slag at 1250°C, which confirms that the quartz has not melted into the slag. An apparent homogeneous slag is observed at temperatures including and exceeding 1300°C.

(a) Layered at 1200°C

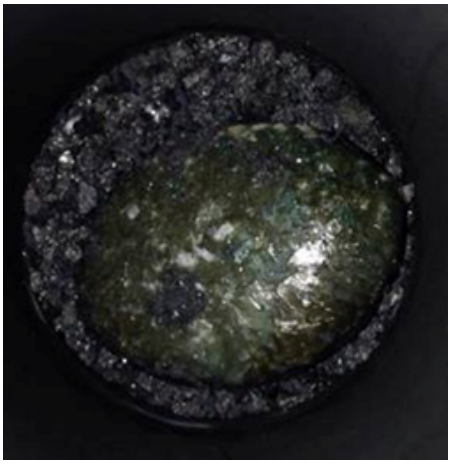

(b) Layered at 1250°C

(c) Bottom surface of layered at 1250°C

(d) Layered at 1300°C

(e) Layered at 1400°C

Figure 4.9: Crucible contents after finished experiments for layered charges. Ore and HC FeMn slag are melted at 1250°C. All materials have fused into the slag at 1300°C.

A cross section of the slag was evaluated by EPMA and the different phases of the structure were analysed. The charge heated to 1200°C was not analysed, as a slag phase had not been formed and none of the raw materials had melted. Figure 4.10 shows the parts of the structure found in the cross section of layered sample heated to 1250°C, where 4.10b shows a cut of the same structure at higher magnification. The slag is not homogeneous and several different structures are observed. The dark particles in the upper part of figure a) are undissolved quartz particles and it was seen in figure 4.9c that the majority of the quartz were unmelted at this temperature. The different phases were analysed and the results are presented in table 4.7. Numbered phases are according to the respective labeling in figure 4.10b.

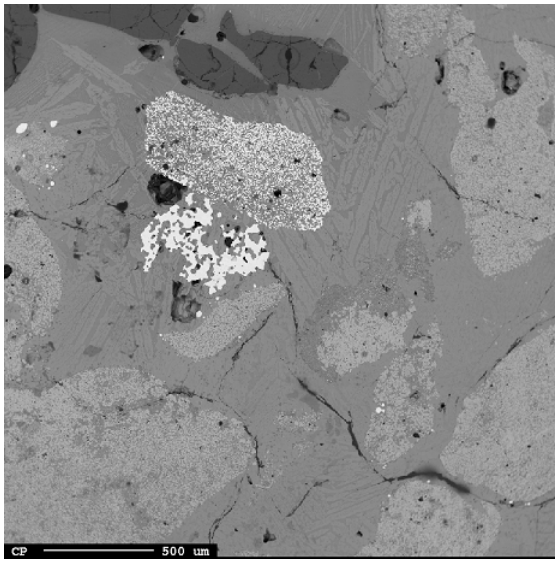

(a) Scalebar reads 500 um

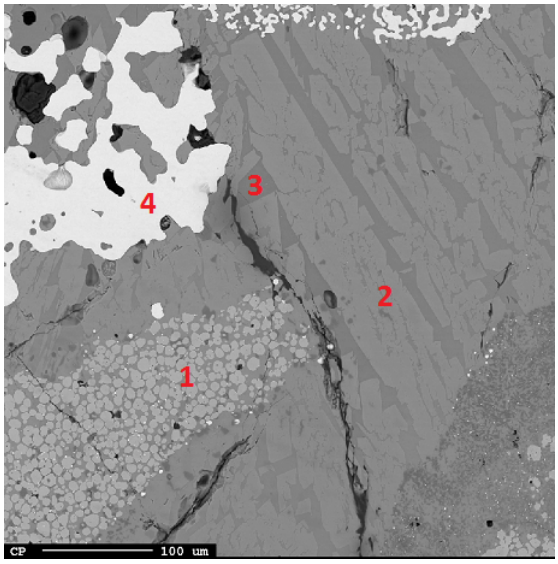

(b) Scalebar reads 100 um

Figure 4.10: Slag structure of layered charge based on Comilog ore and high-carbon ferromanganese slag 1250°C.

The bright grey areas observed throughout the slag at magnification 500 um are clusters of spheres, as confirmed by magnification at 100 um (phase 1). The analysis show that these spheres consist of approximately 95.5 wt% MnO. The matrix surrounding these clusters can be seen to be a two-phase structure. The bright phase has the main components MnO-SiO_2-CaO-MgO, whereas the dark phase is a MnO-SiO_2-CaO-Al_2O_3-compound. The brightest phase(phase 4) is a metal particle and the composition can be seen in table 4.8. An additional observed particle of significantly smaller size was also analysed. The metal consists mainly of iron, however 18% of manganese is recorded in the smallest particle.

Table 4.7: Average analysed composition for different phases found in sample heated to 1250°C. All spot analyses are presented in table in appendix A.

Phase	MnO	SiO_2	Al_2O_3	CaO	MgO	FeO	K_2O	Total	R-ratio
1	95.45	0.35	0.22	0.33	4.02	0.43	0	100.81	19.44
2	53.73	31.63	0.41	8.00	6.67	0.26	0	100.71	35.53
3	27.00	37.24	25.70	12.67	0.51	0.17	2.85	96.13	0.51

Table 4.8: Composition of metal particles (wt%) found in layered Comilog, quartz and HC FeMn slag charge at 1250°C.

	Mn	Si	Fe	C	Total
1	5.87	0.15	96.56	4.44	106.02
2	18.09	0.11	73.80	8.85	100.84

Figure 4.11 shows the slag structure for layered charges at 1300 and 1400°C, respectively. The MnO clusters are now completely dissolved and a relatively homogeneous structure is observed. Table 4.9 shows the composition of the two different phases observed in the slag. The structure at 1300°C was sufficiently fine crystalline so that a defocused area analysis could be executed in order to get the average composition. The two phases were also analysed separately.

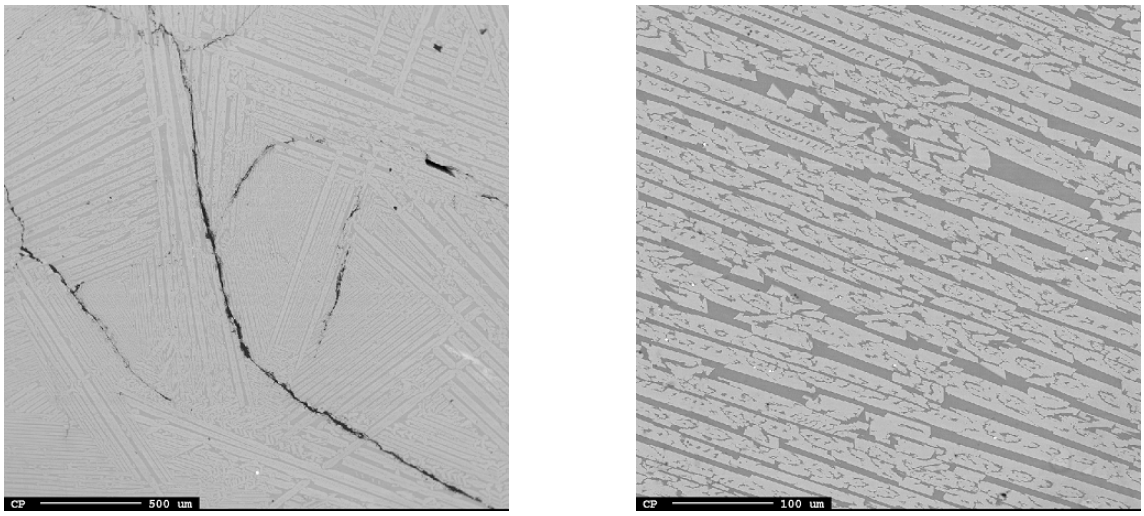

(a) 1300°C. (Scale = 500 um) (b) 1400°C. (Scale = 100 um)

Figure 4.11: Slag structure of layered charge based on Comilog ore and high-carbon ferromanganese slag at 1300°C and 1400°C.

Similarly as to phases at 1250°C, the bright phase at 1300°C has a negligible content of Al_2O_3, whereas the dark phase has a negligible content of MgO. The same phases are observed at 1400°C. The defocused area analysis gives a composition that has a highly similar R-ratio to theoretical, i.e recorded at 0.95 vs theoretical of 0.9. The composition is within 2% deviation of the calculated primary slag composition respective to each oxide.

Table 4.9: Analysed composition of slag structure at 1300 and 1400°C.

Temperature	Phase	MnO	SiO_2	Al_2O_3	CaO	MgO	Total	R-ratio
1300°C	Bright	59.28	32.02	0.63	4.96	4.77	101.66	15.44
	Dark	33.17	28.96	21.40	11.62	0.49	95.64	0.57
	Area est.	47.11	30.73	11.31	8.34	2.36	99.86	0.95
1400°C	Bright	58.77	31.58	0.61	4.98	4.45	100.38	15.42
	Dark	28.65	28.50	24.49	12.57	0.39	94.60	0.53

Metal particles were observed in the cross section in sample heated to 1300°C, whereas none was seen at the exposed area in sample heated to 1400°C. The metal at 1300°C was analysed by EPMA and the composition is given in 4.10. The manganese content was recorded to 23.5%, which is an increase from 18% at 1250°C.

Table 4.10: Composition of metal particle (wt%) found in layered Comilog, quartz and HC FeMn charge at 1300°C.

Mn	Si	Fe	C	Total
23.52	0.01	67.69	6.21	99.78

The charge was evaluated with mixed raw materials at temperatures 1200 and 1250°C. Figure 4.12 shows the crucible contents for these two experiments. It is seen that the materials are unmelted at 1200°C, whereas a slag phase is observed at 1250°C. The charge heated to 1200°C was not analysed, as a slag phase had not been formed. Slag structure at 1250°C can be seen in figure 4.13. Several clusters of MnO spheres, similarly as to layered charge at 1250°C, can be observed, in addition to several small metal particles. The slag matrix is a two-phase structure, as seen in 4.13b. In contrast to the layered charge, the majority of the quartz particles was melted and had fused into the slag phase for the mixed charge at 1250°C.

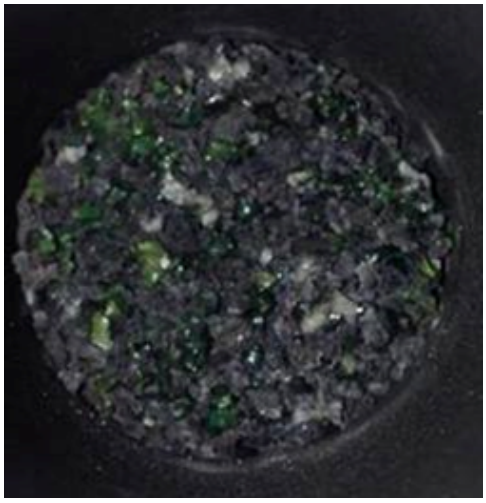

(a) Mixed at 1200°C.

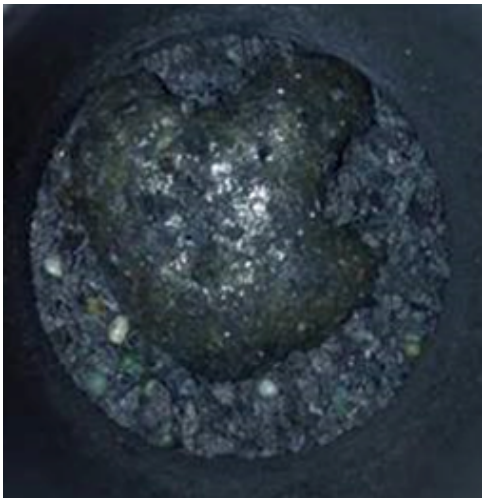

(b) Mixed at 1250°C.

Figure 4.12: Crucible contents after finished experiments for charge with mixed materials.

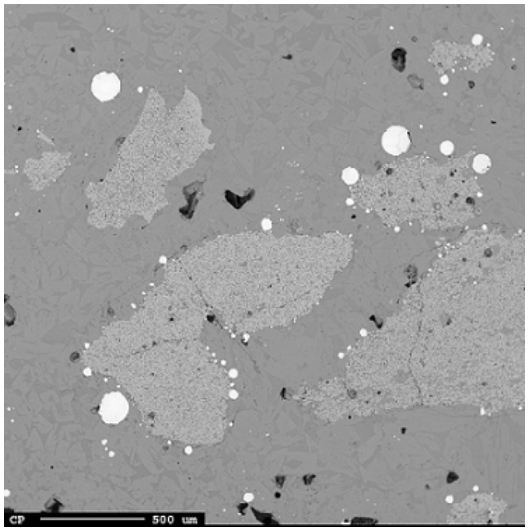

(a) 1250°C. (Scale = 500 um)

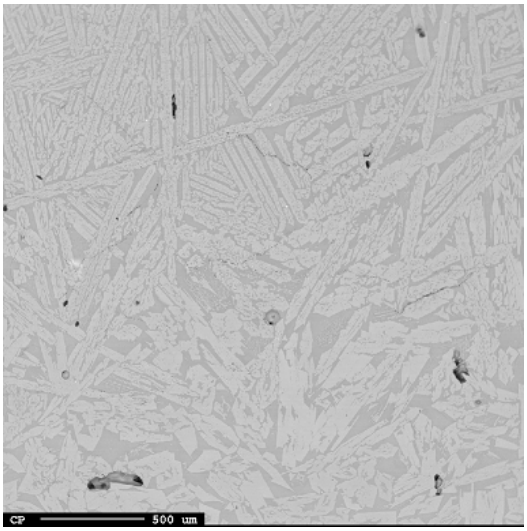

(b) 1250°C. (Scale = 500 um)

Figure 4.13: Slag structure of mixed charge based on Comilog ore and high-carbon ferromanganese slag at 1250°C.

The matrix has a bright phase with a negligible content of Al_2O_3 and a dark phase with a negligible content of MgO, which is consistent with the matrix phases observed in the layered charge. A metal particle was analysed, presented in 4.12, which showed 64.6% of manganese and the remaining iron.

Table 4.11: Analysed composition of slag in charge with mixed raw materials.

Temperature		MnO	SiO_2	Al_2O_3	CaO	MgO	Total	R-ratio
1250°C	Bright	59.70	31.46	0.31	4.86	5.35	101.68	32.94
	Dark	30.94	30.12	21.99	12.32	0.47	95.84	0.58

Table 4.12: Analysed metal composition of mixed charge at 1250°C.

Mn	Si	Fe	C	Total
64.59	0.27	29.75	6.17	100.78

4.2.2 Comilog and quartz

The specific charge with Comilog and quartz was evaluated at temperatures 1200, 1250, 1300 and 1400°C with layered materials and at 1200 and 1250°C with mixed materials. Figure 4.14 shows the recorded weight as a function of time for both charge types.

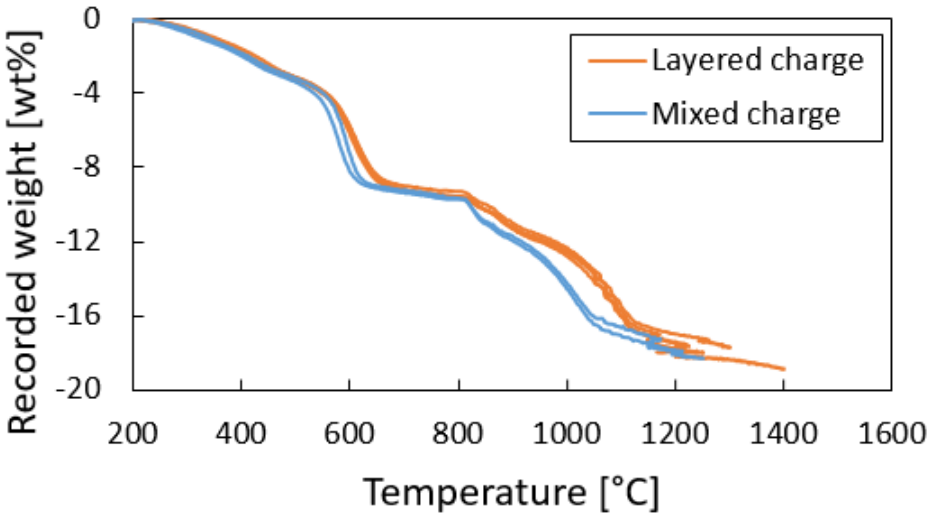

Figure 4.14: Recorded weight [wt%] as a function of process temperature [°C] for layered and mixed charges containing Comilog, quartz and HC FeMn slag.

It is seen that the charges that are prepared in the same manner (layered vs mixed) show the same weight loss behaviour. The reduction of the higher manganese oxides to MnO occurs at an

earlier stage in the mixed charge compared to the layered charge, however both have obtained the same weight loss at 1200°C.

Figure 4.15 shows the crucible contents for the experiments executed with layered raw materials. It is seen that no materials have melted at 1200°C in 4.15a. Upper and bottom surface of charge heated to 1250°C is shown in figure 4.15b and 4.15c, respectively. The ore has melted, however a homogeneous slag is not formed at this temperature. The bottom surface shows that the quartz particles remains unmelted. By visual inspection, the slag appears homogeneous at temperature 1300 and 1400°C.

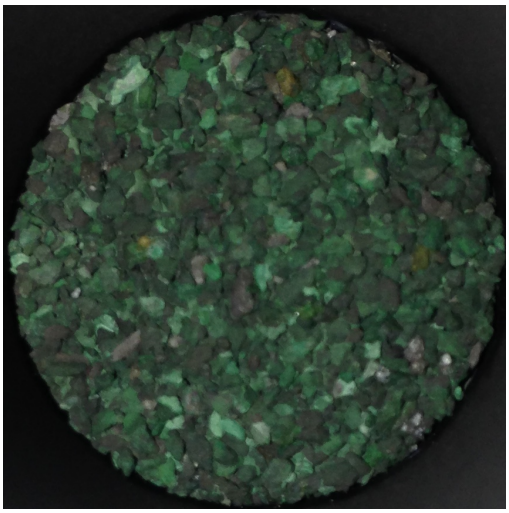

(a) Layered at 1200°C

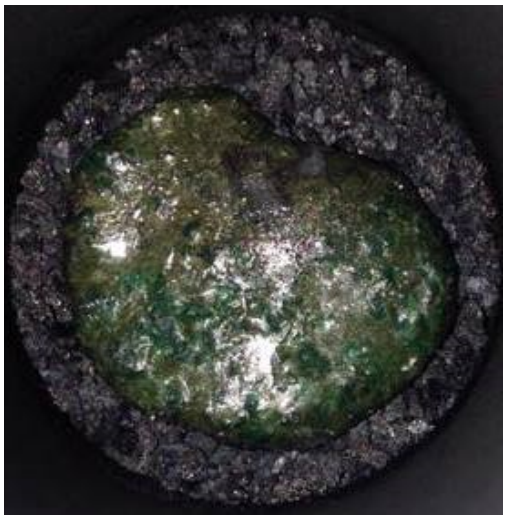

(b) Layered at 1250°C

(c) Layered at 1250°C (bottom surface)

(d) Layered at 1300°C

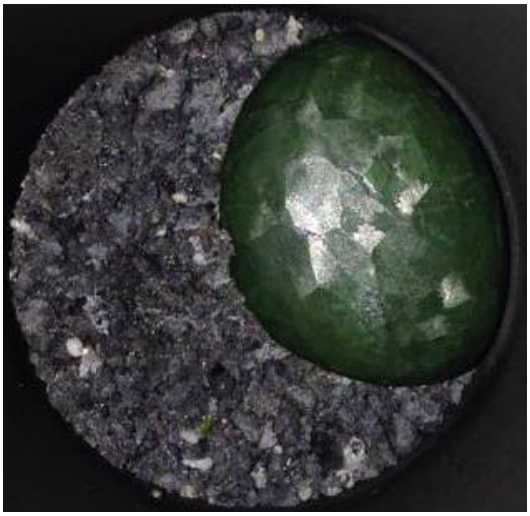

(e) Layered at 1400°C

Figure 4.15: Crucible contents after finished experiments. Image shows coke and large green lump of slag, in addition to a few small quartz particles.

The cross section of the slags were analysed by EPMA in order to investigate the structure. The sample heated to 1200°C was not analysed, as the raw materials had not melted. Figure 4.16 shows the slag structure found in the cross section of sample heated to 1250°C. The matrix of the slag is a two-phase lamellar structure. The bright grey areas are clusters of MnO spheres as observed previously and the dark grey particles in b) are undissolved quartz particles.

The composition of the different phases are presented in table 4.13 according to respective numbering in figure 4.16b. The analyses show that the spherical particles are approximately 100% MnO. The bright matrix phase(phase 2) has 70% MnO and the remaining SiO_2, which correlates to the compound Mn_2SiO_4. Phase 3, the dark matrix phase, is a compound of components MnO-SiO_2-Al_2O_3. Composition 4 is a defocused area analysis that gives the average composition of the fine crystalline structure observed below the undissolved quartz particles.

Small metal particles were observed in the exposed slag structure, of which a few were analysed by EPMA. Table 4.14 presents the composition of two different metal particles found at this temperature. Negligible content of manganese and silicon in both particles, whereas up to 7% phosphorous is reported.

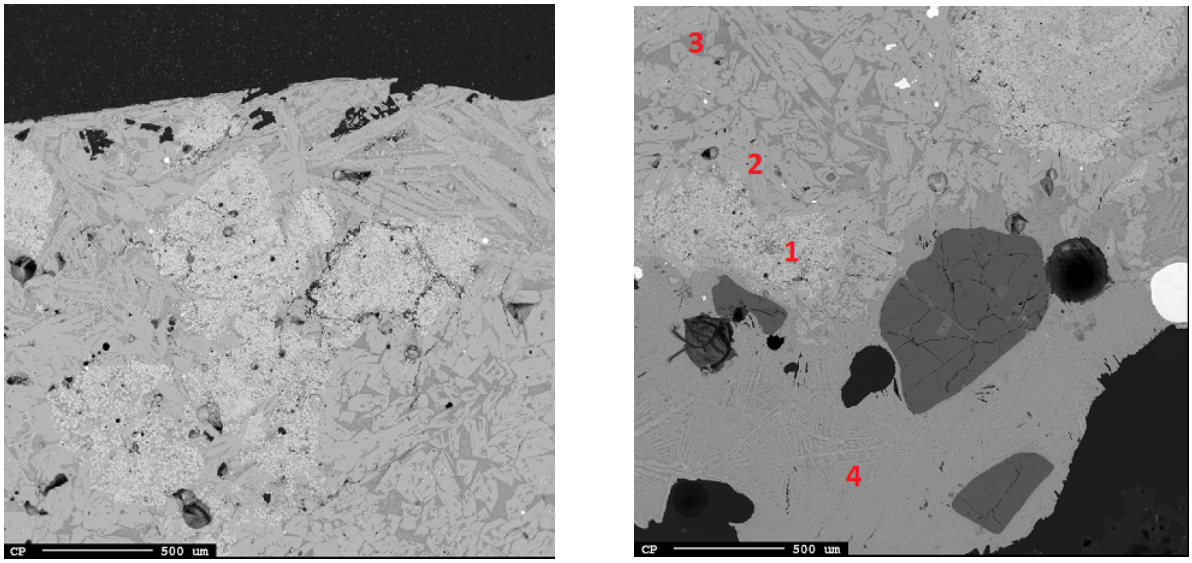

(a) (b)

Figure 4.16: Structure of layered charge based on Comilog ore heated to 1250°C. Scalebar reads 500 um.

Table 4.13: Analysed composition of slag phase for charge with layered raw materials at 1250°C.

Phase	MnO	SiO_2	Al_2O_3	CaO	MgO	K_2O	Total	R-ratio
1	99.34	0.31	0.15	0	0.06	0.01	99.88	0.41
2	70.56	30.18	0.62	0.18	0.18	0.05	101.77	0.60
3	43.70	21.96	27.58	0.41	0	5.53	99.18	0.015
4	52.94	42.20	4.66	0.32	0.26	0.54	100.92	0.13

Table 4.14: Analysed metal composition in layered charge at 1250°C.

Particle	Mn	Si	Fe	C	P	Total
1	1.80	0.01	85.51	3.28	6.69	97.29
2	0.55	0	91.96	2.50	1.40	96.41

Slag structure observed in cross section of sample heated to 1300 and 1400°C is seen in figure 4.17a and 4.17b, respectively. A few clusters of MnO spheres were observed throughout the slag at 1300°C, which can be seen in the lower parts of the structure. A few small metal particles can

also be observed. The matrix is a two-phase lamellar structure. No MnO clusters were observed at 1400°C and the structure was relatively homogeneous.

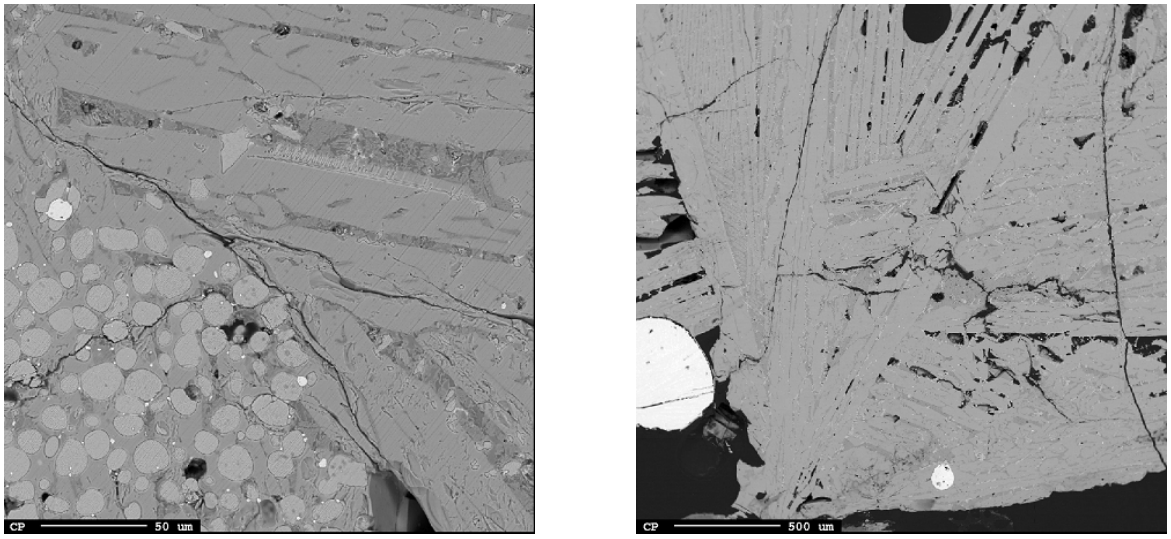

(a) 1300°C (scalebar reads 50 um) (b) 1400°C (scalebar reads 500 um)

Figure 4.17: Structure of layered charge based on Comilog ore heated to 1300 and 1400°C.

The composition of the different phases is presented in table 4.15. It can be seen that the composition of the bright phases versus the dark phases are highly similar at 1300 and 1400°C, i.e high MnO content in bright phase and alumina rich dark phase. The bright phase contains approximately 70% MnO, where the remaining is SiO_2. This fits well with the compound Mn_2SiO_4. The composition of the dark phase was reported to 58% MnO, 19% SiO_2 and 21% Al_2O_3, however it can be seen that the dark phase is not completely homogeneous as some darker fields are observed. This indicates that two different phases are coexisting in the dark matrix phase.

Table 4.15: Analysed composition of slag phase for charge with layered raw materials at 1300 and 1400°C.

Temperature	Phase	MnO	SiO_2	Al_2O_3	CaO	MgO	Total	R-ratio
1300°C	Spheres	99.66	0.67	0.25	0.05	0.14	100.76	0.75
	Bright grey	70.93	31.07	0.53	0.19	0.22	102.93	0.76
	Dark grey	58.26	19.31	21.07	0.36	0.04	99.04	0.02
1400°C	Bright grey	69.65	30.78	0.60	0.27	0.26	101.55	0.88
	Dark grey	58.85	20.34	21.32	0.58	0.06	101.14	0.03

Crucible contents of mixed Comilog and quartz charges are presented in figure 4.18. It is seen that the raw materials are still in their initial form (unmelted) at 1200°C, whereas a slag phase is observed at 1250°C. The structure found in the cross section of the slag at 1250°C is presented in figure 4.19. The structure shows clusters of MnO spheres are observed throughout the slag and the matrix is a two-phase structure of varying coarseness.

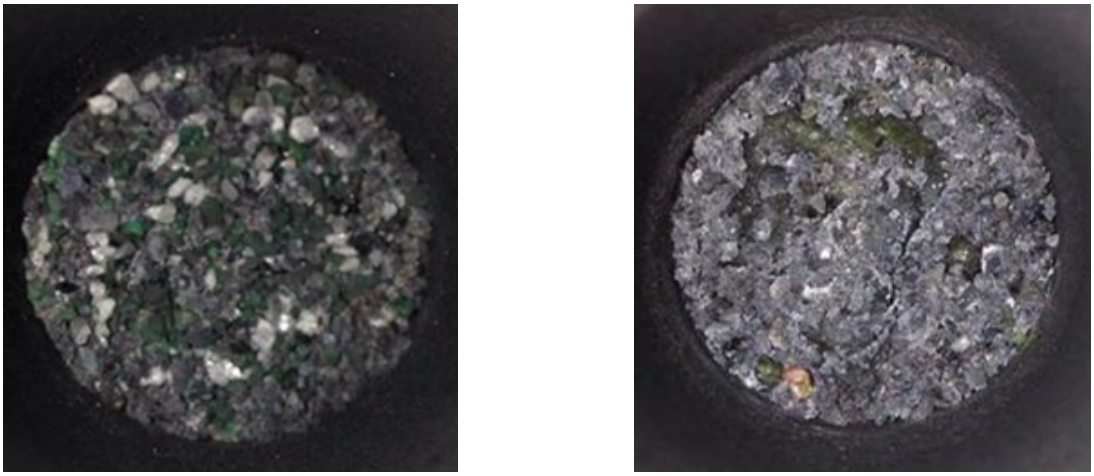

(a) Mixed at 1200°C

(b) Mixed at 1250°C

Figure 4.18: Crucible contents after finished experiments with mixed charge containing Comilog and quartz.

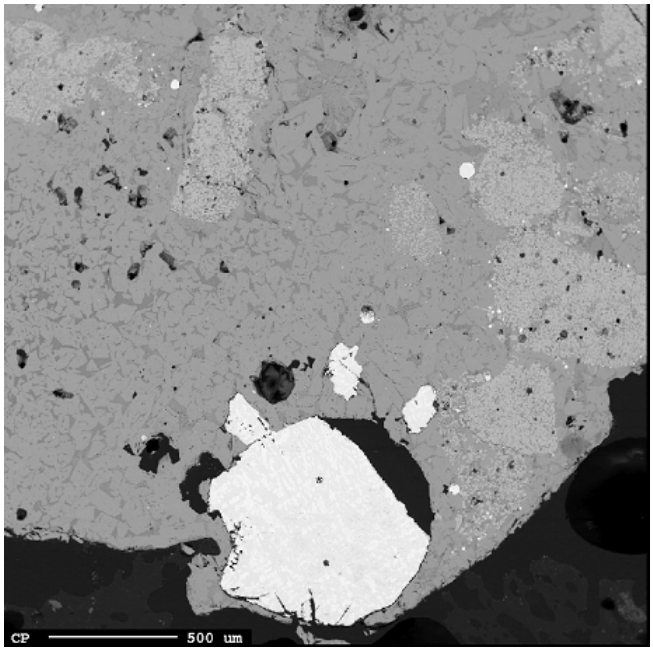

Figure 4.19: Slag structure of mixed charge containing Comilog and quartz at 1250°C

The composition of the two phases in the matrix is presented in table 4.16 where similar composition as for the layered charges are observed, i.e a MnO rich phase that correlates to Mn_2SiO_4 and an alumina rich phase. The large metal particle observed in figure 4.19 was analysed, revealing that the composition consists mainly of iron, however 12% of manganese is recorded.

Table 4.16: Average analysed composition of slag phase for charge with mixed raw materials. All spot analyses are presented in table in appendix A.

Area	MnO	SiO_2	Al_2O_3	CaO	MgO	K_2O	Total	R-ratio
Bright	71.17	30.48	0.27	0.24	0.18	0.01	102.38	1.47
Dark	39.93	19.96	30.20	3.91	0	4.32	98.31	0.13

Table 4.17: Analysed metal composition in layered charge at 1250°C.

Mn	Si	Fe	C	P	Total
12.19	0.01	83.15	4.64	1.74	101.73

4.3 Assmang based charges

Five experiments were conducted with the specific charge composition based on Assmang ore, HC FeMn slag, quartz and coke. The R-value for all experiments in this section is 2.29. The temperature range was 1530-1650°C. The raw materials were added in a specific order of layers according to melting temperature, as mentioned in experimental.

Table 4.18: Obtained weight loss at maximum temperature for the five different experiments with the same charge composition

	Weight loss [g]	% mass loss
1530°C	1.23	10.45
1550°C	1.59	13.06
1570°C	2.34	19.60
1600°C	3.26	27.04
1650°C	4.18	34.36

The obtained weight loss for the charges at maximum temperature is presented in table 4.18, in both grams and mass percent. The values show an increasing weight loss at increasing temperature. Note that the calculated weight loss at 18% Si in alloy and 6% MnO in slag was 4.00 grams, equal to 32.88 mass%. This weight loss was reached at approximately 1650°C.

4.3.1 Temperature profiles and mass loss curves

The furnace used for the experiments logs temperature, time and weight at a five second interval. The temperature as a function of time is presented in figure 4.20, where the fluctuations at temperature interval 850-1200°C and dwell period are fitted to linearity at average. The program starts heating from room temperature, however it is seen that the software records approximately 95-100°C as starting point. The temperature profile shows an approximate heating rate of 25°C/min from room temperature up to 1200°C, where the temperature is dwelled for 30 minutes to ensure a complete prereduction. Further, from 1200°C to maximum temperature a heating rate of 4.5°C/min was executed.

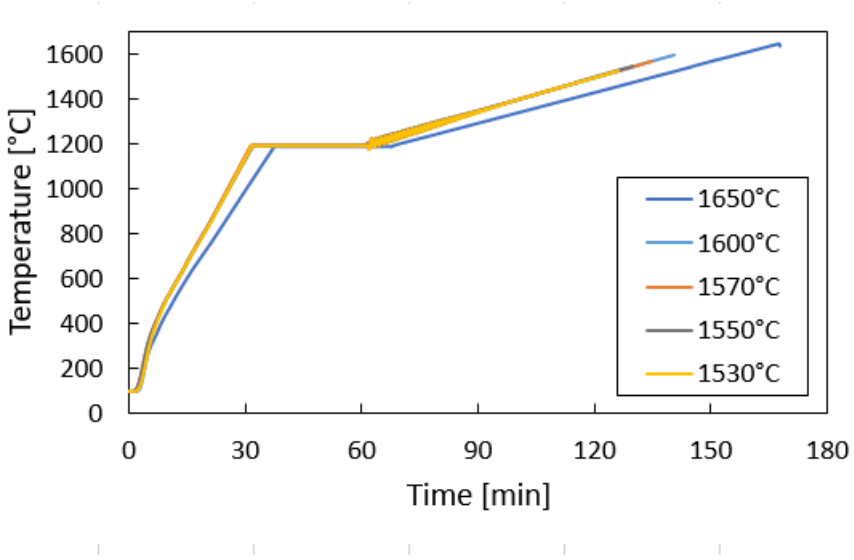

Figure 4.20: Temperature as a function of time when the fluctuations at 900-1200°C has been fitted to linearity at average.

It is seen that the temperature profile for the charge heated to 1650°C deviates from the other temperature profiles. This is most likely due to that the heating element in the furnace was re-

placed prior to this experiment, causing a slightly slower temperature rate at the specific furnace program. This charge reach the dwell period approximately 5.5 minutes after the other charges, whereas the deviation in the high temperature zone is approximately 12 minutes process time. This should however not have an effect on the results, as the charge will have experienced the same temperature as the remaining, only at delayed process time.

Figure 4.21 shows the weight recorded by the thermobalance as a function of time. The dotted lines represents the calculated weight losses after complete prereduction, i.e. 1200°C, and at 1600°C assuming equilibrium amounts of 18% Si, 6% MnO and 40% SiO_2. The weight change of the crucible after the experiments is also noted in the figure, where it is seen that the measured physical mass loss is consistent with the recorded weight from the thermobalance. The deviation from the temperature profile for charge at 1650°C is well observed in figure 4.21. Nonetheless, the shape of the weight loss curve is highly similar for all charges. From figure 4.22, which shows the recorded weight as a function of the recorded temperature, it is confirmed that the deviation is only within the temperature rate, and not the weight loss behaviour itself.

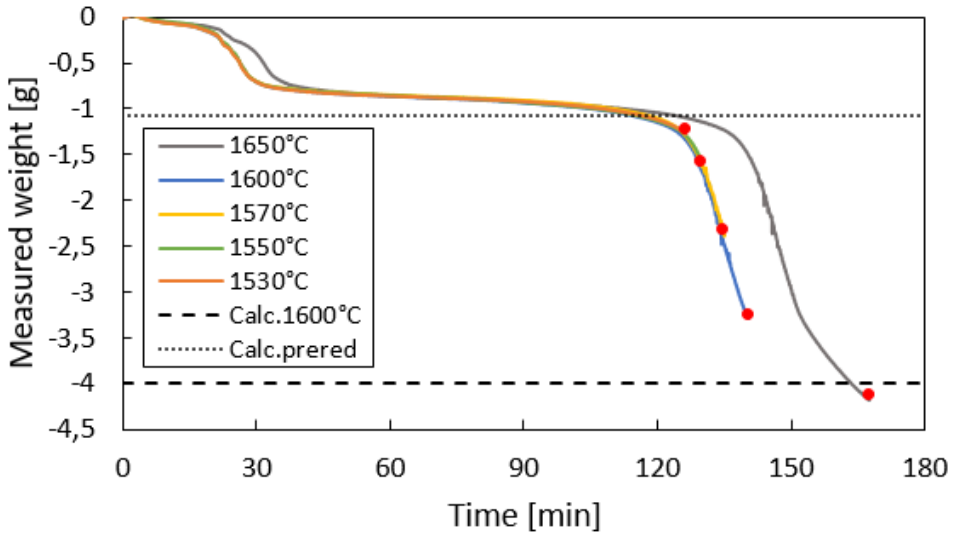

Figure 4.21: Mass loss [g] as a function of time [min] for Assmang based charges.

The curves can be divided into three different intervals at increasing time/temperature: prereduction zone, 30 minute dwell at 1200°C and high temperature zone. It is seen that the weight loss remains insignificant at temperatures below 600°C, where the recorded weight is -0.075 g.

Theoretical weight loss from evaporation of moisture from all raw materials gives a total theoretical weight loss of 0.49 g and 0.29 g when excluding coke. This could imply that the water content from the analyses are inaccurate. From 600°C up to 1200°C, the recorded weight loss is 0.68 g. Theoretical weight loss for reduction of MnO_2 to Mn_2O_3, further to Mn_3O_4 and lastly to MnO is 0.26 g. After completed dwell at 1200°C the charges have obtained a total weight loss of 0.85-0.86 g, which is 0.2 g off the calculated value of 1.07 g. The curve reaches the calculated weight loss at complete prereduction at 1460°C.

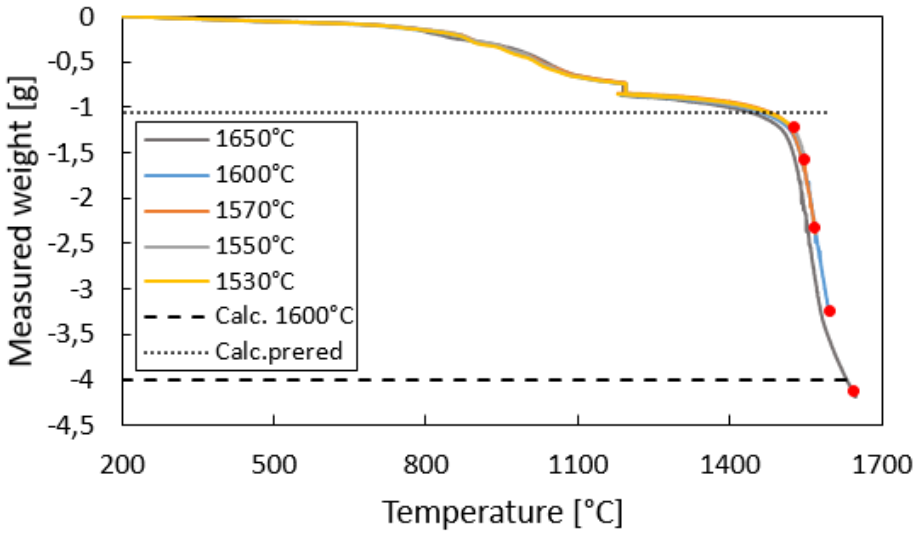

Figure 4.22: Mass loss [g] as a function of temperature [°C] for Assmang based charges.

The calculated weight loss for the charges during the high temperature zone (after 30 minute dwell at 1200°C) to obtain 18% Si in alloy at 1600°C is 2.93 g. This weight loss is obtained at a temperature slightly lower than 1650°C.

4.3.2 Analysis of end product

Visual inspection of the crucibles after finished experiments revealed that foaming had occurred in charges heated to temperatures including and exceeding 1550°C. Figure 4.23a shows the interior of crucible heated to 1600°C, where the lower parts of the crucible shows coke(grey) and slag(pale green). The inner surface of the crucible wall is covered in small metal particles as a result of foaming, ranging approximately 2 cm from bottom and up. The samples were mounted

in epoxy and ground to expose the bottom surface of the slag. Images of the exposed area are shown in figures 4.23b-4.23f.

All slag phases were of amorphous/glassy structure, except for sample A.1 which had a fine crystalline structure. Hence, the only sample with a crystalline structure is the only sample that did not experience foaming. The structure of A.1 is seen in figure 4.24a, whereas 4.24b shows a homogeneous glassy structure. Composition for slags of amorphous structure was determined by defocused area analysis, while the composition for the crystalline sample was determined by analyzing the two phases separately and estimating the distribution of the phases, which was determined to a 1:1 ratio in this case. Resulting slag compositions are presented in table 4.19. Only the five main oxides represented in the slag are included, hence the a total is less than 100% for the samples. The elements making up the remaining amount of the composition can be seen in the raw data presented in appendix B.

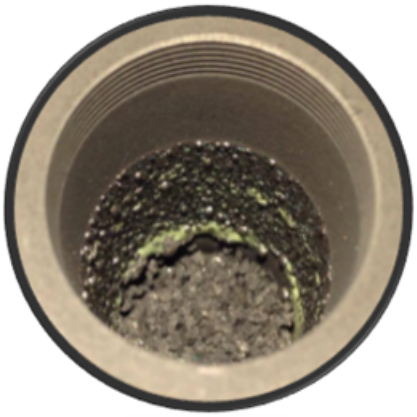

(a) 1650°C

(b) 1530°C

(c) 1550°C

(d) 1570°C

(e) 1600°C

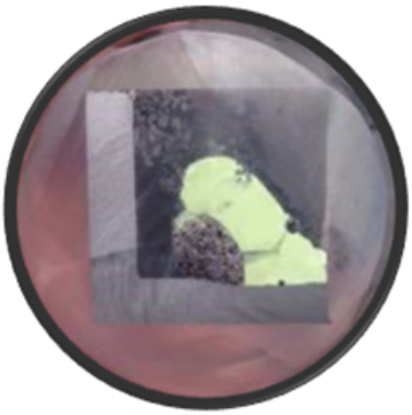

(f) 1650°C

Figure 4.23: Image a) shows the interior of crucible heated to 1650°C where foaming can be confirmed by the small metal particles covering the inside of the crucible surface. Image b)-f) shows samples after mounting in epoxy displaying bottom surface of the slag.

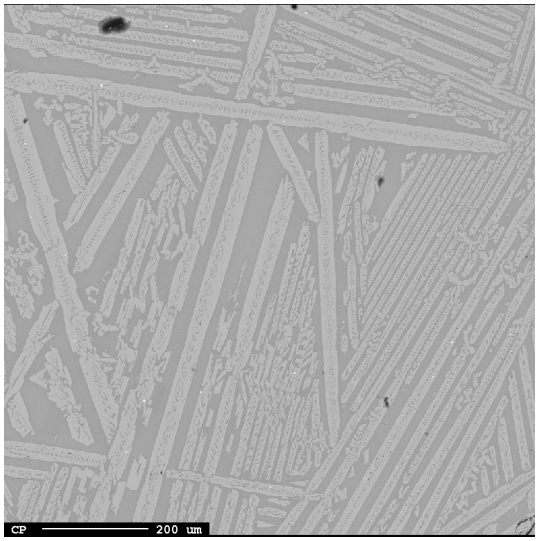

(a)

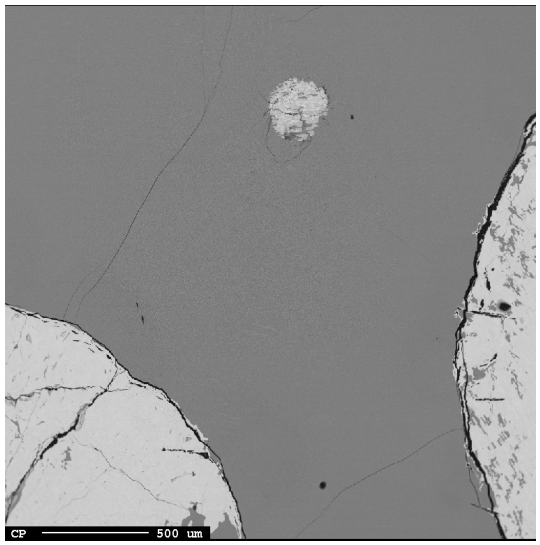

(b)

Figure 4.24: Crystalline structure for sample heated to 1530°C in a) and glassy structure found at all other temperatures in b). Scale bar reads 200 um.

As the oxides CaO, MgO and Al_2O_3 are considered unreducable, their respective amounts should stay constant throughout the process, giving a constant R-ratio. Table 4.20 shows the slag composition where the amounts of MnO and SiO_2 are from the EPMA analyses and the initial amounts were used for the remaining oxides. The composition is hence calculated under the assumption that the slag consists only of these five oxides, which can be considered a fair approximation.

Table 4.19: Average analysed composition of slag phases from EPMA for charges based on Assmang ore. All spot analyses are presented in table in appendix A.

Experiment	Temperature	MnO	SiO_2	Al_2O_3	CaO	MgO	Total	R-ratio
A.1	1530°C	39.25	35.25	5.67	11.03	4.01	95.21	2.65
A.2	1550°C	34.29	38.05	6.70	12.57	4.05	95.65	2.48
A.3	1570°C	24.75	44.97	8.31	15.92	4.82	98.77	2.50
A.4	1600°C	12.25	44.22	11.67	20.79	6.82	95.75	2.37
A.5	1650°C	3.52	40.80	14.97	26.96	8.28	94.53	2.35

Table 4.20: Average analysed composition of slag phases for Assmang based charges where amount of MnO and SiO_2 are from EPMA. CaO, MgO and Al_2O_3 are from initial amounts in raw materials.

Experiment	Temperature	MnO	SiO_2	Al_2O_3	CaO	MgO	R-ratio
A.1	1530°C	39.25	35.25	7.76	13.15	4.58	2.29
A.2	1550°C	34.29	38.05	8.42	14.27	4.97	2.29
A.3	1570°C	24.75	44.97	9.22	15.62	5.44	2.29
A.4	1600°C	12.25	44.22	13.25	22.46	7.83	2.29
A.5	1650°C	3.52	40.80	16.94	28.73	10.01	2.29

The metal composition will vary according to particle size, implying that metal analyses will not be representative for the amount of metal produced. From the calibrated slag composition, the metal composition can be calculated under the assumption that all MnO/SiO_2 that is not recorded in the slag phase has been reduced to the metal phase. Resulting metal compositions are presented in table 4.21.

It is seen that the manganese content increases at increasing process temperature. As for silicon, a negligible increase is seen between 1530 and 1550°C, whereas the reported silicon content at 1570°C is approximately zero. The amounts of MnO/Mn and SiO_2/Si at increasing process time and temperature is graphically presented in figure 4.25. The process time for charge heated to 1650°C was corrected for the observed deviation in the temperature profile. A second order polynomial regression is included for each respective specie.

Table 4.21: Metal composition calculated from analysed slag composition. The initial amounts of the unreducable oxides were used to determine the amounts of MnO and SiO_2 in grams.

Temperature	Mn [g]	Si [g]	Fe [g]	C [g]	Mn [wt%]	Si [wt%]	Fe [wt%]	C [wt%]
1530°C	0.65	0.16	0.44	0.04	50.60	12.42	34.17	2.81
1550°C	1.09	0.17	0.44	0.05	62.65	9.48	25.07	2.80
1570°C	1.72	0.07	0.44	0.15	72.50	2.83	18.44	6.22
1600°C	2.51	0.49	0.44	0.10	70.94	13.75	12.34	2.97
1650°C	2.83	0.74	0.44	0.11	68.84	17.97	10.61	2.58

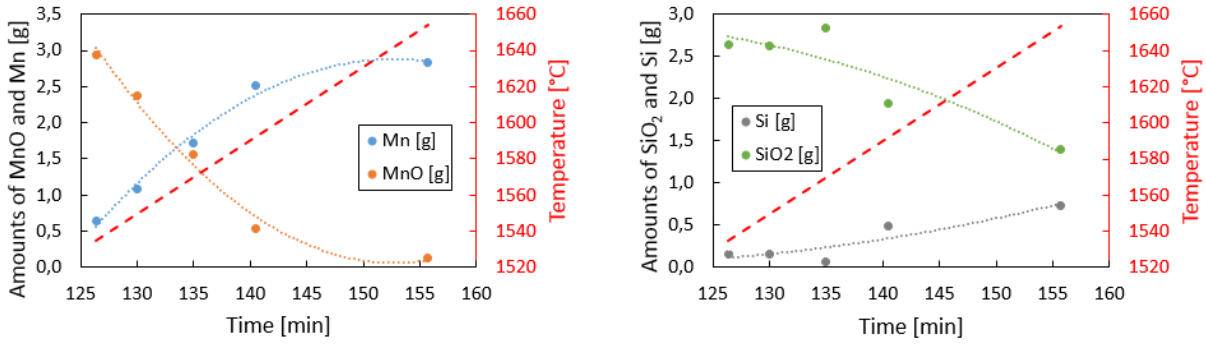

(a) (b)

Figure 4.25: The amounts of MnO/Mn and SiO_2/Si at increasing process time in figure a and b, respectively.

The amount of produced manganese (g) divided by the amount of produced silicon (g) at increasing process time and temperature is presented in figure 4.26. Ratio at 1570°C was excluded, as the silicon content was approximately zero. It is seen that the reduction of MnO is dominating at lower temperatures as the ratio increases. The rapid increase in the ratio indicates that this is the main reduction area of MnO, whereas the reduction of SiO_2 is insignificant in comparison. At higher temperatures, i.e including and exceeding 1600°C, the ratio decreases, implying that the reduction of SiO_2 is more dominant than the reduction of MnO.

As was shown in experimental section 3.3.5, the reaction area is estimated according to the produced amount of manganese and silicon. Table 4.22 shows the resulting reaction area at increasing temperature for the Assmang, HC FeMn slag and quartz charge. Right column shows

the area as percent of initial reaction area (prior to any reduction). The reaction area is reduced by 37% at 1650°C.

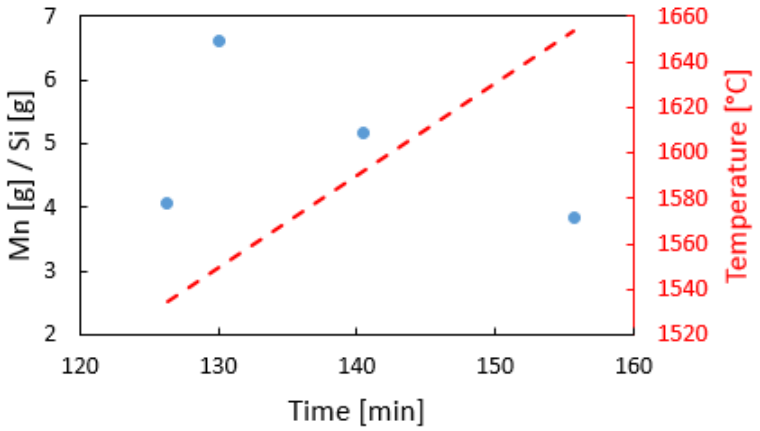

Figure 4.26: Ratio of produced amount of manganese and silicon at increasing process time and temperature for Assmang charges.

Table 4.22: Reaction area calculated according to procedure described in section 3.3.5. Right column shows area as percent of initial reaction area(prior to reduction).

Temperature [°C]	Reaction area [cm^2]	Reaction area [%]
1400	136.36	100
1530	126.10	92.47
1550	122.18	89.60
1570	120.15	88.11
1600	98.54	72.27
1650	85.86	62.96

The models presented by Olsen (2016)[16] that were reprinted in equations 2.9 - 2.12 and thermodynamic equilibrium data from HSC Chemistry[28] were used to estimate the driving forces for MnO and SiO_2 reduction at different temperatures. These are presented in table 4.23 and it is seen that the driving force for MnO decreases at increasing temperature as MnO is being reduced. The driving force for reduction of SiO_2 was negative at 1530°C and 1650°C, which could indicate that the composition is close to equilibrium at this specific temperature. The driving

force at 1570°C is relatively high as a consequence of that the reported amount of SiO_2 in the slag was close to initial value.

Table 4.23: Calculated activities and driving forces at different process times/temperatures.

Temperature [°C]	a(MnO)	a(SiO_2)	a(Mn)/K_T	a(Si)/K_T	DF(MnO)	DF(SiO_2)
1530	0.204	0.109	0.002	0.437	0.201	-
1550	0.151	0.150	0.003	0.146	0.148	0.004
1570	0.071	0.304	0.003	0.011	0.069	0.294
1600	0.034	0.188	0.002	0.108	0.033	0.081
1650	0.010	0.085	0.001	0.090	0.010	-

5 | Discussion

5.1 Comilog charges

Figure 5.1 shows the recorded weight as a function of process time and temperature during the high-temperature zone. The charges were given a new starting point after completed dwell at 1200°C. The theoretical weight loss at 18% Si in alloy and 6% MnO and 40% SiO_2 in slag at 1600°C is included. It is seen that the desired composition is reached at a temperature in the range of 1630-1650°C, which was also confirmed by the analyses presented under results. The reproducibility of the experiments is high, as it can be seen that the curves overlap.

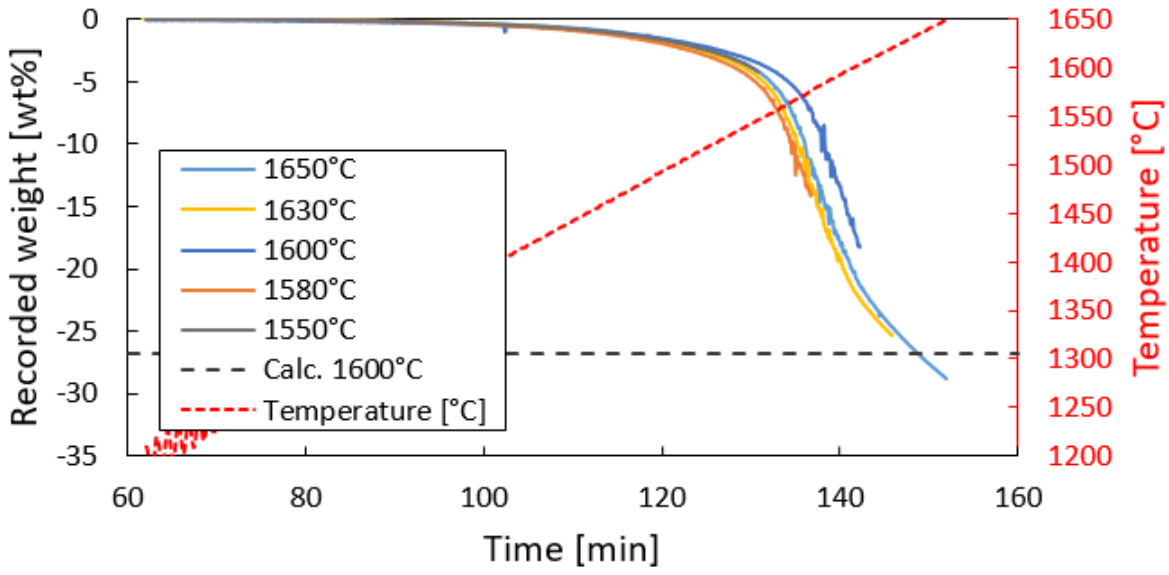

Figure 5.1: Recorded weight with completed dwell at 1200°C as new starting point as a function of process time and temperature.

The charge heated to 1600°C deviates slightly (<5%) from the other charges when presented as a function of time, however the deviation originates from the slower temperature increase directly after the completed dwell in this specific charge. The weight curves are not completely smooth during the reduction stage, which could be an indication of foaming. This will be discussed later on.

The weight loss resulting from the metal producing reactions at high temperatures can be calculated according to the amount of CO-gas formed correlating to the reduced amount of MnO and SiO_2. The weight loss recorded by the TGA furnace at high temperatures, i.e after complete pre-reduction, should be equal to the calculated weight loss, given that the reduction of MnO and SiO_2 by solid carbon are the only reactions occurring. Table 5.1 shows the deviation between weight loss from TGA and EPMA for the different experiments, where the weight loss from TGA is after completed dwell at 1200°C. It can be seen that the TGA has recorded a higher weight loss compared to calculated for all temperatures with a deviation ranging from 0.11 g to 0.33 g. Three out of five charges have a deviation of approximately 0.3 g, whereas charge evaluated at 1550 and 1600°C have a deviation of 0.15 g and 0.11 g, respectively.

Table 5.1: Deviation between weight loss calculated from EPMA analyses and weight loss recorded by TGA furnace. Weight loss from TGA is recorded weight after completed dwell at 1200°C.

Temperature	Weight loss EPMA	Weight loss TGA	Diff. [g]
1550°C	0.31	0.46	0.15
1580°C	1.43	1.76	0.33
1600°C	1.89	2.00	0.11
1630°C	2.42	2.74	0.32
1650°C	2.79	3.10	0.31

According to the values, the specific deviation (g) is not dependent on temperature, implying that the relative deviation (%) decrease at increasing temperature. Deviations will always be observed to an extent as several sources of error are available. The EPMA weight loss is calculated from the raw material analyses, which are given as the average composition of the ores, implying that small differences within the amounts used during experiments will occur. The theoretical

weight loss was calculated by assuming that all off-gas was CO, however it is possible that small amounts of CO_2 was produced. Tangstad also reported a better fit between observed and theoretical weight loss in Comilog charges when assuming that the off gas contained CO_2[17].

Larssen[19] investigated different types of charges based on Comilog ore. All experimental conditions, except for charge composition, were identical to this work. Four different charges were evaluated, where one based on Comilog ore and quartz, one added limestone and two where 0.15-0.2% sulphur was added to the two former charges. Factors that may favour a fast and high reduction are high content of MnO(to give a high driving force) and a high basicity[29]. In addition, a high sulphur content is favourable, as proved by both Larssen[19] and Skjervheim[12]. The wt% sulphur, basicity and initial content of MnO for the different charges are presented in table 5.2. The charges' weight loss curves are presented in figure 5.2 together with the charge investigated in this work. All charges were given a new starting point after completed dwell at 1200°C and are presented for temperatures higher than 1500°C. The rate (dg/dt) at increasing temperature for the same charges is presented in figure 5.3, where the weight change at every minute interval was evaluated.

Table 5.2: Specifications for the different charges presented in figure 5.2. Charge Com+Q+HC is the only charge not retrieved from Larssen's work[19]. Values are valid at 1200°C. (Q = quartz, S = sulphur, HC = HC FeMn slag)

Charge	wt% sulphur	R-ratio	wt% MnO
Com.+Q+Lime	0.008	2.09	49.8
Com.+Q	0.005	0.05	63.6
Com.+Q+Lime+S	0.252	2.09	49.8
Com.+Q+S	0.316	0.05	63.6
Com.+Q+HC	0.214	1.31	45.5

The charge based on Comilog ore and quartz, with or without addition of lime, has a very low reduction and it can be seen from figure 5.3 that the rate is constant and low at all temperatures. There is no observed correlation between the basicity (R-ratio) and the reduction rate as both the highest and lowest rate are observed in charges that have the same basicity. The most substantial factor is observed to be the sulphur content.

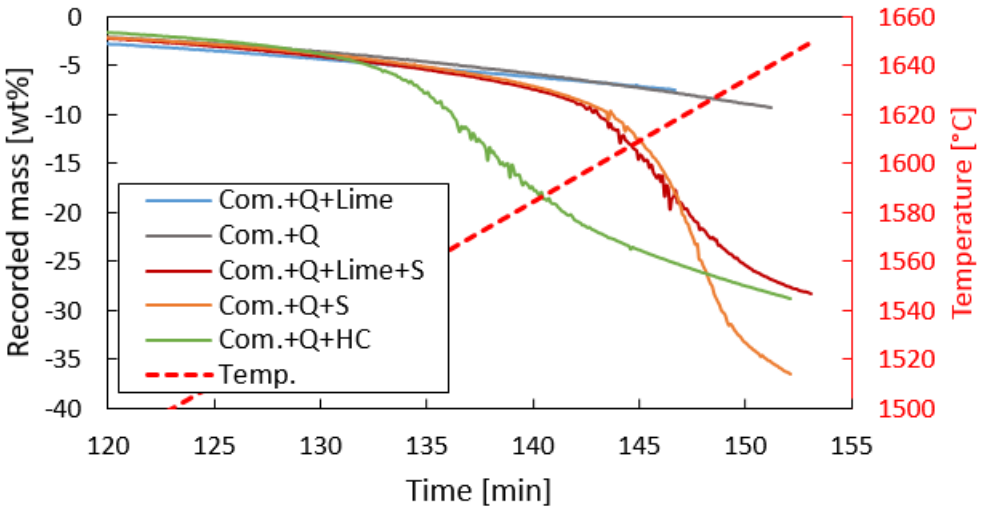

Figure 5.2: Recorded weight as a function of time for Comilog based charges, including charges presented by Larssen[19]

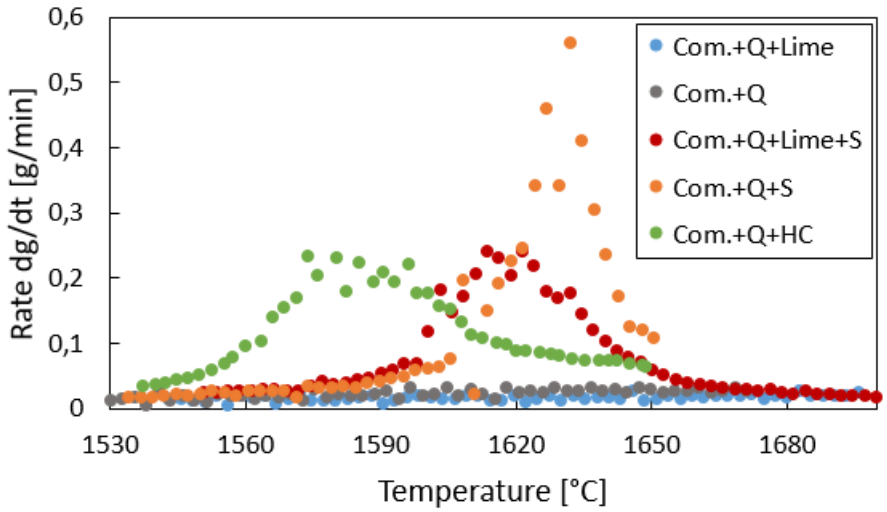

Figure 5.3: Weight loss rate as a function of time for Comilog based charges, including charges presented by Larssen[19]. All charges contain quartz.

Nevertheless, it is seen that the charge investigated in this work, containing both Mn-ore and slag from the HC FeMn process (charge C.HC), reduces at a lower temperature compared to the other charges in spite of not having the highest sulphur content. It is also seen that this charge would have the lowest driving force, as the MnO content is higher in all other charges. The lower reduction temperature in charge containing HC FeMn slag could however be due to that the

FeMn slag reduces at a lower temperature compared to the ore. If so, a potential explanation is that the slag phase is not homogeneous and as such the sulphur content would be constrained within the HC FeMn slag, causing it to reduce first. Consequently, the ore would reduce at a higher temperature at which the sulphur content is distributed throughout the slag. Another potential reason is that the HC FeMn slag has a lower melting temperature and hence reduces at a lower temperature, in correlation with the results presented by Brynjulfsen[22]. Difference in melting temperature for different charges based on Comilog ore and quartz is further discussed in section 5.1.1.

5.1.1 Melting temperature of slag

The slag formation temperature and melting behaviour were investigated in two different charges based on Comilog ore. Both contained ore and quartz, whereas HC FeMn slag was added to one in a 1:1 ratio respective to the ore. The two charges will be discussed separately in relation with existing thermodynamics. If not other specified, similar behaviour is observed for mixed and layered charges.

Comilog, HC FeMn slag and quartz

The experiments showed that the raw materials were still in their initial form at 1200°C and had not started to melt. The ore and HC FeMn slag had melted at 1250°C and formed a slag phase, however the quartz particles remained undissolved for the layered charge. The microstructure showed clusters of MnO-spheres distributed throughout the slag where the matrix was a two-phase structure. Previous studies on FeMn and SiMn slags have shown that the spherical MnO phase has been in solid form at these temperatures, whereas other observed MnO phases have been precipitated during solidification[17, 21]. All raw materials, excluding coke, had formed a homogeneous liquid slag at 1300°C. The analysed composition was highly consistent with composition observed at 1400°C. Two different phases co-existed throughout the slag in a lamellar structure, in addition to a few clusters of MnO-spheres. The decreasing amount of MnO-spheres at increasing temperature supports the assumption that recorded spheres have been in solid form at maximum temperature. The bright phase in the matrix contained 58-59 wt% MnO, 31-

32 wt% SiO_2, 5 wt% CaO and 5 wt% MgO. The dark phase contained 28-33 wt% MnO, 29% SiO_2, 20-25 wt% Al_2O_3 and 11-12 wt% CaO. The five main slag oxides constitutes approximately a total of 95% of the dark phase, whereas the remainder is K_2O, SO_3 and BaO.

The charge based on Comilog, quartz and HC FeMn slag has primary slag composition of 46% MnO, 33% SiO_2, 9% CaO, 9% Al_2O_3 and 4% MgO. There is no available phase diagram covering this specific combination of oxides, however the system may be approximated by combining oxides that have are show miscibility. CaO, MnO and MgO are miscible both in solid and liquid state, implying that the cooling path can be evaluated from the system MnO-SiO_2-Al_2O_3 that was presented in figure 2.6 by adding the amounts of CaO and MgO to the MnO-axis as shown in figure 5.4. The distribution between the precipitated phases will not be accurate, however it will provide an indication.

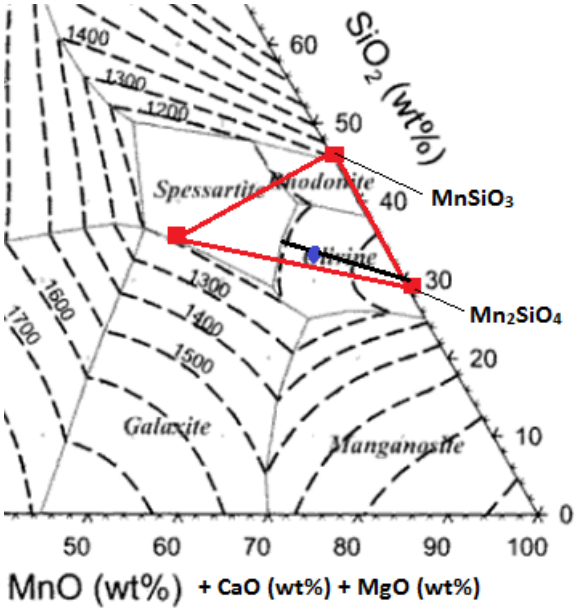

Figure 5.4: Phase and liquidus relations for the MnO-SiO_2-Al_2O_3 system. Modified from Olsen et. al[1]. Red lines represent the Alkemade triangle and solid black line the cooling path.

The primary slag composition is located in the Olivine area, and is marked with a blue circle. The composition is within the alkemade triangle composed of Spessartite, Olivine and Rhodonite, which means that the composition will move towards the eutectic point where the three phase boundaries meet. The primary slag composition is fully liquid at approximately 1240°C and will move towards the phase boundary of Olivine when the temperature decreases. Approximately

25% Mn_2SiO_4 (calculated by the lever rule) will be precipitated before it reach the phase boundary. The remaining 75% is still liquid and will move down the phase boundary between Spessartite and Olivine until the eutectic composition is reached. The theoretical eutectic composition is 48.3% $MnSiO_3$, 33% $Mn_3Al_2Si_3O_{12}$ and 19.9% Mn_2SiO_4.

This shows that the majority is precipitated as $(Ca, Mg, Mn)_2SiO_4$, which is in good accordance with the observed microstructure and analyses. Two phases are co-existing in the dark matrix phase, where the majority is $Mn_3Al_2Si_3O_{12}$ and the remainder is $(Mn, Mg, Ca, Al)SiO_3$.

Comilog and quartz

It was shown that neither the mixed nor the layered charge had melted and fused into a liquid slag at 1200°C, however the ore was partially melted at this temperature when the materials were mixed in the crucible. A liquid slag was seen at 1250°C, whereas most of the quartz particles remained undissolved in layered charge. The structure showed several clusters of MnO-spheres throughout a two-phase matrix. As mentioned in previous section, this phase has been found to be in solid form at these temperatures, while other observed MnO-phases have been precipitated during solidification[17, 21]. All materials had dissolved into the slag phase at 1300°C and the composition was highly similar to the one obtained at 1400°C. Two different phases co-existed throughout the slag in addition to a few clusters of MnO-spheres, where the number of clusters decreased at increasing temperature. The bright phase of the matrix was composed of 70% MnO and 30% SiO_2, correlating to the compound Mn_2SiO_4. The dark phase was seen to be non-homogenous, implying that several different phases may have been analysed and reported as one single phase. The analysed composition was 58% MnO, 20%SiO_2 and 19% Al_2O_3. The precipitated phases can be determined from evaluation of the cooling path in a representative phase diagram.

The Comilog based charge has a negligible content of both CaO and MgO, which means that the system can be approximated by the ternary phase diagram MnO-SiO_2-Al_2O_3 presented in figure 2.6 in the theory section covering thermodynamics. A modified version of the same phase diagram is reprinted here in figure 5.5 where the primary slag composition of the charge is marked by the blue circle. The primary slag composition of 64% MnO, 29% SiO_2 and 7% Al_2O_3 is inside

the Olivine area (Mn_2SiO_4), and is seen to be liquid at a temperature between 1270 and 1300°C. In order to evaluate the different phases that will theoretically precipitate during cooling and their respective distribution, the alkemade triangle has been added.

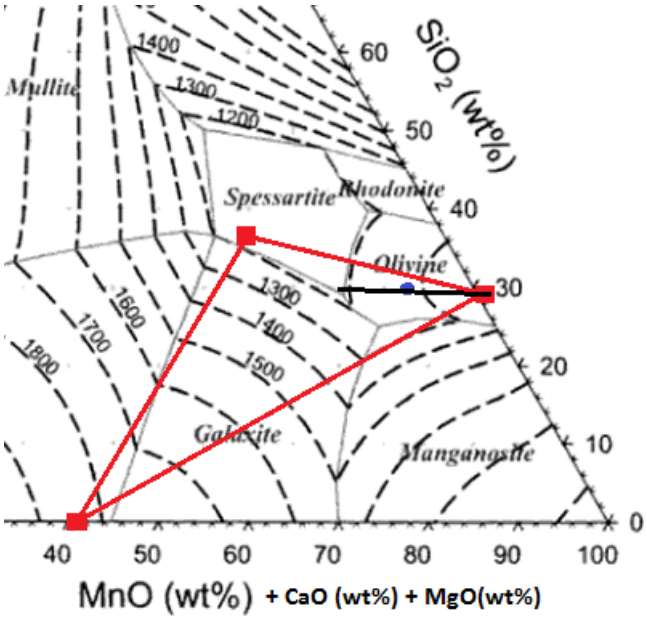

Figure 5.5: Phase and liquidus relations for the MnO-SiO_2-Al_2O_3 system. Modified from Olsen et. al[1]. Red line represents Alkemade triangle, whereas black solid line represents cooling path for the Comilog and quartz charge.

The charge lies within the triangle made up from the three phases $MnAl_2O_4$ (Galaxite), Mn_2SiO_4 (Olivine) and $Mn_3Al_2Si_3O_{12}$ (Spessartite). During cooling, the composition will move towards the boundary line between the Olivine and Spessartite area, away from the Mn_2SiO_4 compound. By applying the lever rule, one can estimate that the amount of Mn_2SiO_4 being precipitated during the first part of the crystallization path is approximately 47%:

$$\%Mn_2SiO_4 = \frac{0.75cm}{1.60cm} \cdot 100\% = 46.88 \tag{5.1}$$

This implies that there is 53.13% liquid remaining when the composition reach the boundary line. This liquid will solidify at the eutectic temperature, which can be seen to be at approximately 1190°C. The eutectic composition is roughly estimated to 49% Mn_2SiO_4, 41% $Mn_3Al_2Si_3O_{12}$ and 10% $MnAlO_4$. Table 5.3 shows the estimated distribution of phases after complete solidifi-

cation. This composition applies both for the layered and mixed charge. Approximately 73% of the structure should theoretically be Mn_2SiO_4. This is consistent with structure observed in image 4.15d which shows a majority of bright phase. The dark phase should theoretically consist of $Mn_3Al_2Si_3O_{12}$ and $MnAl_2O_4$ where the former has a distinct majority. This correlates with the observed structure and analyses.

Table 5.3: Estimated distribution of phases after solidification.

Mn_2SiO_4	$Mn_3Al_2Si_3O_{12}$	$MnAl_2O_4$
72.99%	22.03%	5.25%

Difference in melting behaviour

The two evaluated charges displayed highly similar behaviour in terms of slag formation; ore and HC FeMn slag liquid at 1250°C, whereas quartz particles remained undissolved when charges were prepared by layering of raw materials. At temperatures including and exceeding 1300°C, all raw materials had fused into the slag phase for all charges. No observations were made indicating that difference in slag formation temperature/melting temperature could give the earlier reduction in charge containing HC FeMn slag.

5.2 Assmang charges

Figure 5.6 shows the recorded weight as a function of time and temperature, where the charges have been given a new starting point at completed dwell at 1200°C. The time and temperature values for the experiment with maximum temperature 1650°C have been corrected for the deviation that was observed in the original weight loss curve presented in section 4.3.1. The weight loss behaviour is highly similar in all charges, confirming that the experiments were successfully reproduced. The original curves presented under results showed that the theoretical weight loss at complete prereduction was slightly higher compared to experimental results. The charges had a total weight loss of 0.85-0.86 g after dwell at 1200°C, which correlates to a deviation of 0.2 g compared to calculated value. The dotted line added to figure 5.6 is the theoretical weightloss

at 1600°C, where the deviation after complete prereduction has been taken into account.

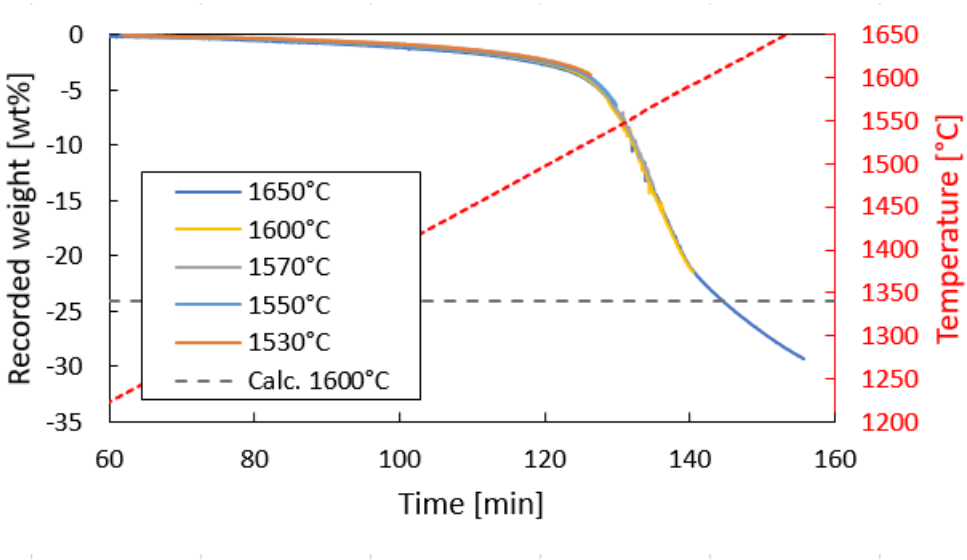

Figure 5.6: Recorded weight (wt%) as a function of time and temperature. Charges were given a new starting point at completed prereduction.

Table 5.4 shows the weight loss calculated from the EPMA analyses and the weight loss recorded by the TGA furnace mass balance during the high temperature zone. The weight loss from EPMA was determined by assuming that the reduction gas product was 100% CO(g) and calculating the amount of CO(g)-formation correlating to the reduced amount of MnO and SiO_2. The furnace has recorded a lower weight loss compared to the calculated for temperatures 1530 and 1550°C, whereas a higher weight loss is recorded by the furnace at remaining temperatures. As mentioned for Comilog charges, a certain deviation between calculated and recorded weight loss is expected due to several available sources of error, e.g from inaccurate ore composition. In the case of Comilog, the deviation was positive at all temperatures, which could indicate that a certain amount of the furnace gas was CO_2. The deviations observed for Assmang charges are alternating positive and negative, meaning that it is not probable that the off gas contained any CO_2. The weight loss at 1570°C has the highest deviation, and it was seen from the analysed composition that the amount of reduced SiO_2 was negligible and not consistent with the other analyses. This gives a lower calculated weight loss compared to if the SiO_2 amount was in accordance with lower an higher temperatures. If this deviation is not considered, it can be observed that the calculated weight loss is increasing at a higher rate compared to the TGA weight loss.

Table 5.4: Deviation between weight loss calculated from EPMA analyses and weight loss recorded by TGA furnace.

Temperature	Weight loss EPMA [g]	Weight loss TGA [g]	Diff. (EPMA - TGA)
1530°C	0.65	0.42	0.23
1550°C	0.86	0.73	0.16
1570°C	1.01	1.54	-0.53
1600°C	2.25	2.43	-0.18
1650°C	2.92	3.32	-0.40

Kim investigated kinetics in Assmang based charges using the same experimental conditions as to this study, including charge composition[30]. The weight loss behaviour in charge evaluated at 1650°C is presented in figure 5.7 (blue curve). The obtained results from this study at the same temperature are included in the figure (grey curve).The charges were given a new starting point at completed dwell at 1200°C. The curves show approximately a complete overlap, confirming that the experiments were a successful reproduction of Kim's work.

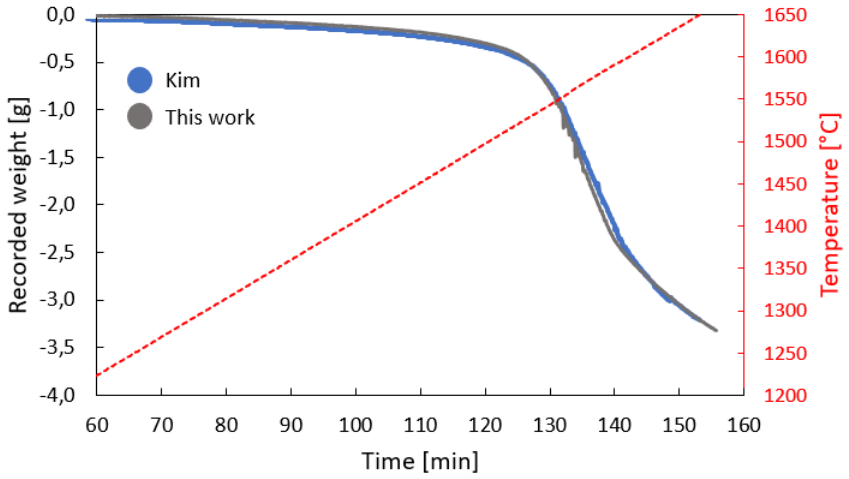

Figure 5.7: Recorded weight as a function of time for Assmang based charges, including results from Kim[30]

The produced amounts of manganese and silicon at increasing process temperature are presented separately in figure 5.7 together with the results reported by Kim[18]. A steady increase in

produced amount of manganese is observed at increasing process temperatures and the trend is highly consistent with Kim's. As for silicon, the amount was relatively stable and insignificant at temperatures 1530-1570°C, whereas an increase was observed at 1600 and 1650°C. The same trend is observed in Kim's results, i.e negligible amount at temperatures lower than 1560°C. The reduction of SiO_2 to Si requires a higher process temperature compared to the reduction of MnO and these results indicate that the reduction of SiO_2 becomes significant at temperatures exceeding 1560-1570°C.

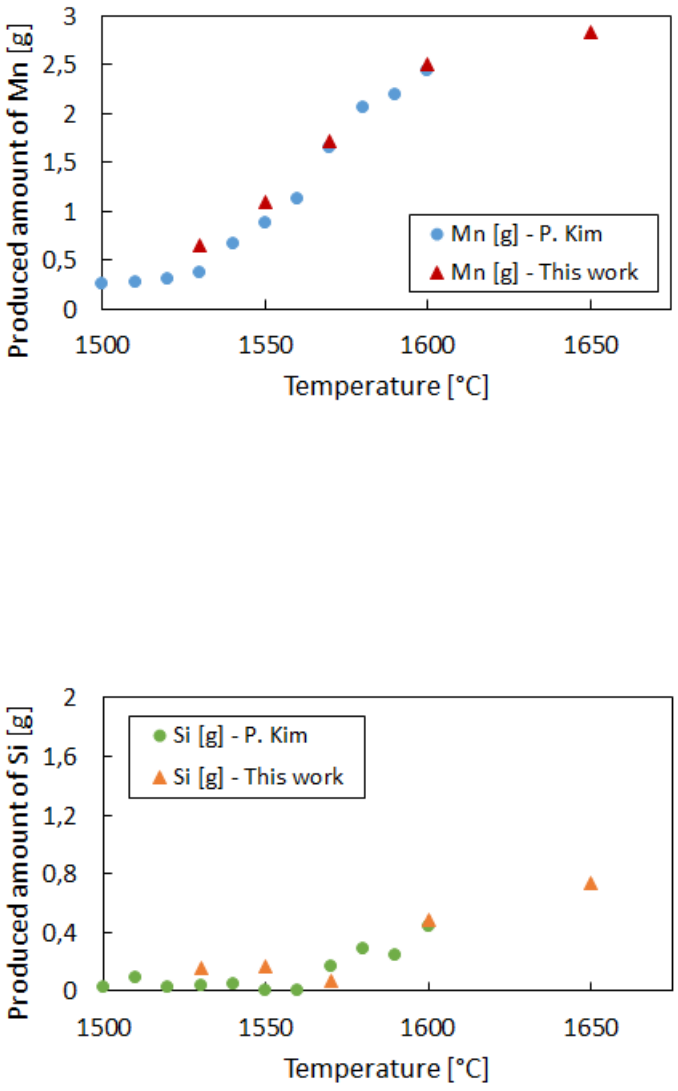

Figure 5.7: Produced amount of Mn and Si at increasing temperature. Values from experiments conducted by Kim[18] are included.

5.3 Choice of ore

Several factors should be taken into consideration when choosing the optimal ore for the production process, including availability, energy consumption at lower temperatures and manganese content. The focus of this work is the kinetics at higher temperatures, hence the ores will therefore be discussed in these terms. The evaluated charges are Assmang or Comilog ore in combination with HC FeMn slag, quartz and coke.

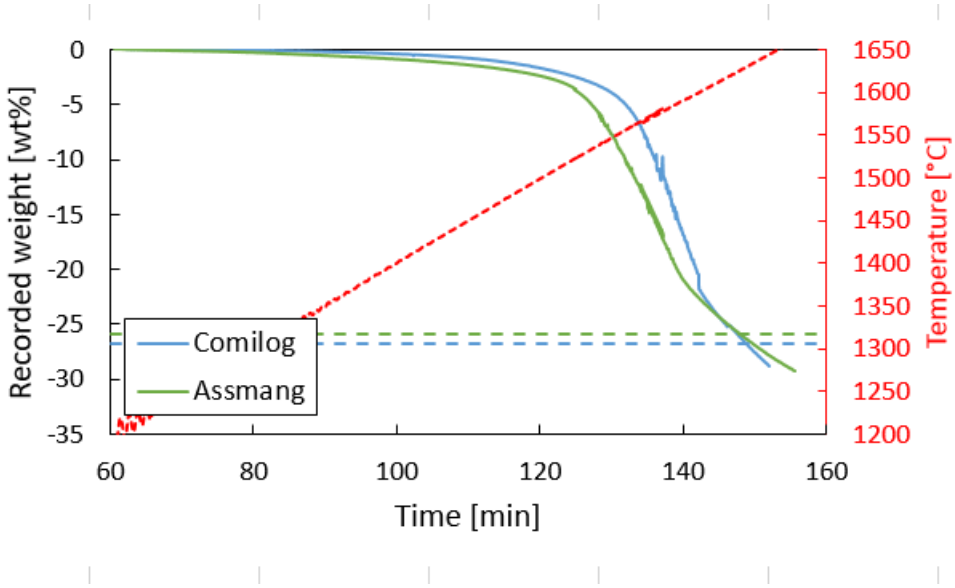

Figure 5.8: Weight loss as a function of temperature for Assmang and Comilog charges, where both charges contain HC FeMn slag and quartz. The charges were given a new starting point at complete prereduction.

Figure 5.8 shows the weight loss curves retrieved from the TGA mass log for both Comilog and Assmang charges with a complete prereduction as starting point. The curves represent the average recorded weight at average time and temperature. The Assmang charge reduces at a slightly lower temperature (<10°C) where the difference decreases with increasing temperature. The weight loss is highly similar for both charges at 1650°C and it can be seen that the two charges reach the desired composition approximately at the same process time. The reduction degree can be evaluated by examining the ratio between amount of produced manganese or silicon and initial amounts of MnO and SiO_2, respectively. The produced amount of metal components were calculated from the slag analyses as was presented in table 4.4 and 4.21 for Comilog and

Assmang, respectively. The obtained reduction degrees are presented in table 5.5.

$$RD_{MnO} = \frac{m_{Mn}}{m_{MnO}} \cdot \frac{M_{MnO}}{M_{Mn}} \tag{5.2}$$

$$RD_{SiO2} = \frac{m_{Si}}{m_{SiO2}} \cdot \frac{M_{SiO2}}{M_{Si}} \tag{5.3}$$

Where m_{Mn} and m_{Si} is the produced amount of Mn (g) and Si (g), respectively, m_{MnO} and m_{SiO_2} is the initial amount of MnO and SiO_2 (g), M_{MnO} and M_{SiO_2} is the molar mass of MnO and SiO_2 (g/mol) and M_{Mn} and M_{Si} is the molar mass of Mn and Si (g/mol).

Table 5.5: Reduction of MnO and SiO_2 in charges based on Assmang ore and charge based on Comilog ore

	Temperature [°C]	RD_{MnO}	RD_{SiO_2}
A.1	1530	0.22	0.11
A.2	1550	0.37	0.12
A.3	1570	0.59	0.05
A.4	1600	0.86	0.35
A.5	1650	0.97	0.53
C.1	1550	0.12	0.05
C.2	1580	0.62	0.18
C.3	1600	0.77	0.27
C.4	1630	0.89	0.40
C.5	1650	0.95	0.51

The calculated reduction degrees shows that MnO is reduced at a slightly lower temperature in the Assmang charge compared to Comilog. At 1550°C, a reduction degree of 0.37 is obtained for Assmang, whereas 0.12 is obtained for Comilog charges. Similarly, 0.86 vs 0.77 is observed at 1600°C. Similar behaviour can be seen for the reduction of SiO_2, i.e reduction at lower temperatures in Assmang charge. Nonetheless, the reduction degrees for both MnO and SiO_2 at 1650°C are similar for the two charges. The faster reduction in Assmang can not be explained in terms

of driving forces, as they are highly similar to the Comilog charge. However, it was observed that the Assmang charge experienced foaming at a lower temperature, which may lead to an increasing reduction rate.

Figure 5.9 shows the ratio between produced manganese and produced silicon at increasing process temperature. Value at 1570°C for Assmang is excluded as the ratio was significantly larger compared to others, due to a considerable reduction of MnO and an insignificant reduction of SiO_2. It is seen that the ratio increases for temperatures 1530 to 1580°C, which implies that the reduction of MnO to Mn is more significant than the reduction of SiO_2 at this temperature range. The ratio decreases for temperatures exceeding and including 1600°C, implying that the reduction of SiO_2 to Si is more significant than the reduction of MnO. The ratios are highly similar for both charges.

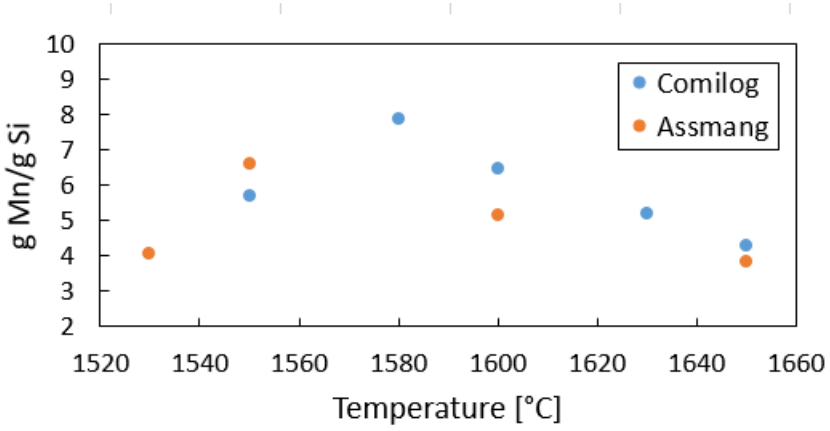

Figure 5.9: Ratio between produced Mn (g) and produced Si (g) for Assmang and Comilog, respectively.

5.3.1 Kinetics

As presented previously, the rate is given by the rate constant, the interfacial reaction area and a driving force. The rate constant is given by the Arrhenius equation and the driving force is given by distance towards equilibrium in terms of activity. In terms of reduction of MnO, the equation takes the form of 5.10.

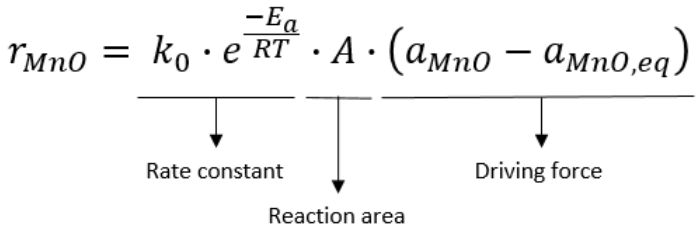

Figure 5.10: Components describing the reduction rate of MnO.

The driving forces were calculated from the models presented by Olsen[16] and presented in table 4.6 and 4.23 for Comilog and Assmang charges, respectively. Similarly, the reaction area was presented in table 4.5 and 4.22 for Comilog and Assmang, respectively. The factors of interest are the activation energy and the mass transfer coefficient (pre-exponential factor) in the rate constant. There will be two different approaches available to estimate these kinetic values:

- Arrhenius plot
- Computational modeling

Arrhenius plot

Second order polynomial regression was performed on the decreasing amounts MnO and SiO_2 in order to find an expression describing the reduction as a function of time. These curves were shown in figure 4.6 and 4.25 for Comilog and Assmang, respectively. Differentiating the polynomial gives an equation describing the reduction rate (g/min). The rate of reduction of MnO and SiO_2 for the two different charges are presented in figure 5.11.

From 5.11a it is seen that the rate is relatively high for MnO in Comilog charges at 1550°C and decreases at increasing process time. At 1650°C, the rate is negative, due to the very low activity of MnO. Similar behaviour, i.e high initial rate that reduces at increasing process time, is observed for Assmang charges, however at a lower initial rate. The rate is negative at 1650°C due to a low activity of MnO. As for the rate of SiO_2 reduction, the rate is fairly constant at 0.06 g/min for Comilog charges at all temperatures. For Assmang charges a consistent increasing rate is observed, from 0.01 g/min at 1530°C to 0.09 g/min at 1650°C.

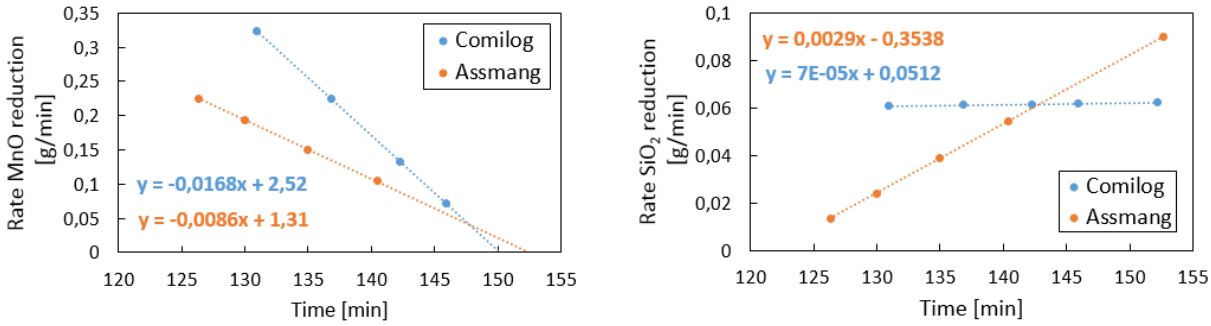

(a) MnO reduction

(b) SiO_2 reduction

Figure 5.11: The rate (g/min) of reduction of MnO and SiO_2 as a function of time (min).

Equation 5.4 is a rearrangement of the original equation shown in figure 5.10, where DF notes the driving force. The specific arrangement gives a constant C equal to $\ln(k_0)$. A graphical representation of ln(r/DF) as a function of the inverse temperature gives a linear relationship where the slope is given by (-Ea/R), i.e the negative activation energy divided by the ideal gas constant.

$$ln(\frac{r}{A \cdot DF}) = ln(k) = \frac{-Ea}{RT} + C \tag{5.4}$$

Only data points with an existing driving force (non-negative) can be used for regression, implying that data points for SiO_2 reduction at 1530°C and 1650°C are excluded for Assmang, whereas data point at 1550°C for SiO_2 reduction is omitted for Comilog. In addition, data point at 1650°C is omitted for MnO for both charges as the rates were found to be negative.

Figure 5.12a shows the Arrhenius plot for MnO reduction for Comilog and Assmang charges, whereas figure 5.12b shows for SiO_2 reduction. For MnO reduction it is seen that the relationship is fairly linear for both Comilog and Assmang based charges in 5.12a. The empirical acitvation energy of MnO for Comilog was found to be 498 kJ/mol, whereas 550 kJ/mol was found for Assmang. Figure 5.12b shows the estimated activation energy of SiO_2 reduction in Comilog charges at 447 kJ/mol. As for Assmang charges, a linear trend within the data points was not observed, hence an activation energy could not be estimated.

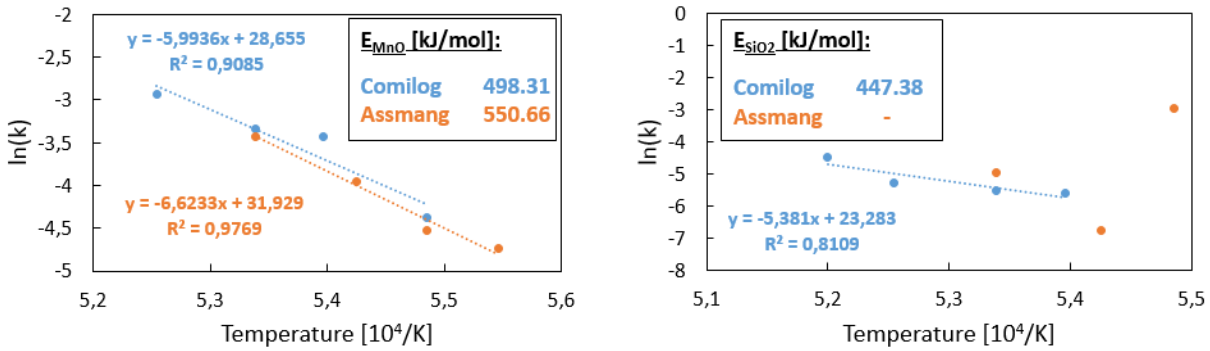

(a) MnO reduction

(b) SiO_2 reduction

Figure 5.12: Arrhenius plot for MnO and SiO_2 where all datapoints with existing driving force are included.

The empirical rate constants at increasing temperature for the two charges are presented in table 5.6. The charges only have two temperatures in common, however it is seen that the rate constants at these temperatures, i.e 1550 and 1600°C, are highly similar, however approximately 10% larger for Comilog. This is expected, as the charges showed similar weight loss behaviour. The rate constants are presented graphically in figure 5.13. The values indicate that the rapid reduction stage of MnO is initiated at approximately 1550°C.

Table 5.6: Rate constants, k [10^{-3} g/min·cm^2], for MnO and SiO_2 in Comilog and Assmang charges, respectively.

	Comilog		Assmang	
	k_{MnO}	k_{SiO_2}	k_{MnO}	k_{SiO_2}
1530°C	-	-	8.78	-
1550°C	12.53	-	10.79	-
1570°C	-	-	19.27	-
1580°C	32.36	3.64	-	-
1600°C	35.52	3.97	32.54	-
1630°C	52.85	5.15	-	-
1650°C	-	11.43	-	-

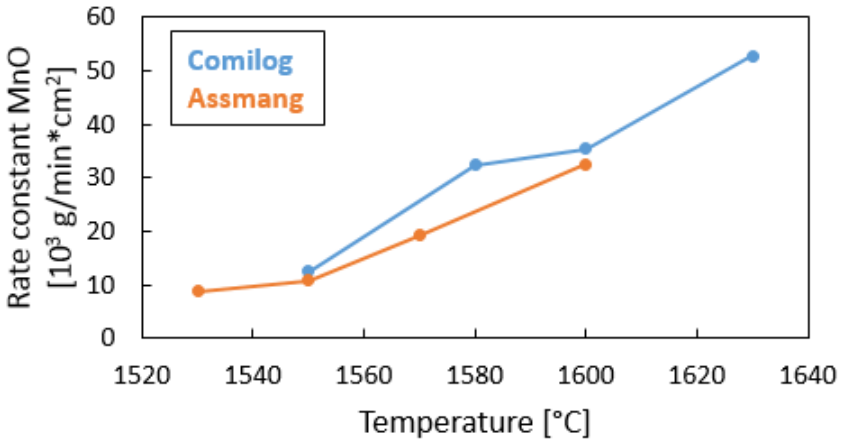

Figure 5.13: Empirical rate constants calculated from estimated rate and driving force for Comilog and Assmang charge, respectively.

Figure 5.14 shows the estimated rate constants for reduction of SiO_2 in the charge containing Comilog, quartz and HC FeMn slag. It can be seen that the rate constant is relatively stable and non-increasing between 1580 and 1630°C, which implies that the rate is relatively constant at these temperatures. This indicates that the rapid reduction stage of SiO_2 is at temperatures exceeding 1630°C, however it was seen in figure 5.11b that the rate was relatively constant at all temperatures as a result of the decreasing driving force.

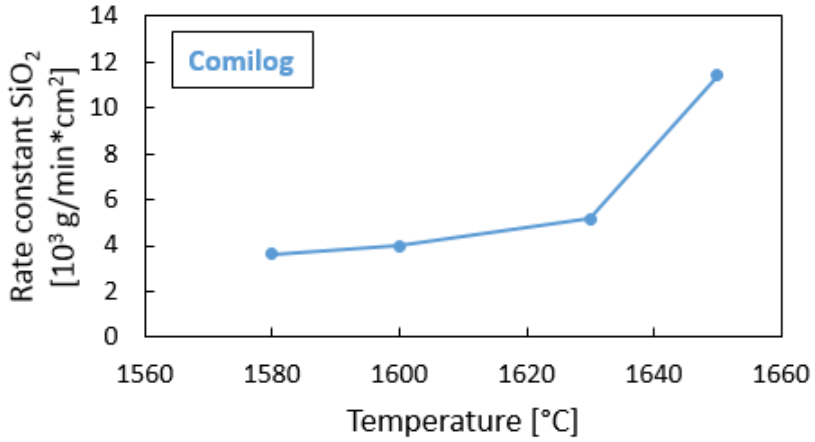

Figure 5.14: Empirical rate constant for SiO_2 calculated from estimated rate and driving force for Comilog charge.

Computational model

The amounts of MnO and SiO_2 in wt% were modeled by using the mass transfer coefficient, k_0, as the only fitting value. Specifics for the setup of the model was presented in the chapter covering experimental work, section 3.3.5. When evaluating an Arrhenius plot, both the activation energy and the mass transfer coefficient can be extracted, whereas the model requires a predetermined activation energy.

Three different combinations of activation energies were modeled for each charge:

- The activation energies estimated from the Arrhenius plots for the respective charges. As an activation energy of SiO_2 was not found for Assmang, the one obtained for Comilog is used for both charges. This is considered a fair approximation as it was shown that the two charges have highly similar reduction behaviour.
- Previously reported activation energy of MnO from ferromanganese slags by Tangstad at 360 kJ/mol[17]. Ea(SiO_2) = 850 kJ/mol were chosen, as this combination was used in the models presented by Olsen[16].
- Reported activation energies from Kim for Assmang charges[18]: Ea(MnO) = 920 kJ/mol and E(SiO_2) = 870 kJ/mol.

The different parameters evaluated by the model are presented in table 5.7. The deviation between the model and the experimental values were calculated according to the standard error of estimate and is also added for the different models.

Table 5.7: Modelling parameters presented together with the estimated pre-exponential factors in the rate constant for Assmang and Comilog charge, respectively. Error value is calculated according to the standard error of estimate.

	$E_{a,MnO}$ [kJ/mol]	E_{a,SiO_2} [kJ/mol]	$k_{0,MnO}$ [g/min·cm^2]	k_{0,SiO_2} [g/min·cm^2]	Error
Comilog 1	498	447	$1.61 \cdot 10^{12}$	$1.14 \cdot 10^{10}$	6.71
Comilog 2	360	850	$2.09 \cdot 10^{8}$	$1.12 \cdot 10^{20}$	9.13
Comilog 3	920	870	$1.99 \cdot 10^{24}$	$7.13 \cdot 10^{21}$	5.23
Assmang 1	550	447	$4.93 \cdot 10^{13}$	$2.83 \cdot 10^{10}$	5.18
Assmang 2	360	850	$1.57 \cdot 10^{8}$	$1.40 \cdot 10^{22}$	7.31
Assmang 3	920	870	$2.72 \cdot 10^{24}$	$2.93 \cdot 10^{21}$	5.73

According to the standard deviation of estimate, it can be seen that the activation energies estimated from the Arrhenius plots(combination 1) and the ones reported by Kim(combination 3) give a relatively similar fit for the both charges, whereas the values reported by Tangstad[17] gives the highest inaccuracy. However, it is necessary to investigate the produced curves in order to see the source of deviation.

Arrhenius activation energies

Figure 5.15a shows the produced curve from the model at the activation energies estimated from the Arrhenius plots for charge containing Comilog, HC FeMn slag and quartz. Figure 5.15b shows the deviation between the calculated and experimental values. It can be seen that the model fits the experimental values well, however the deviation for the first data point at 1550°C is high, giving approximately 84% of the total deviation. The distribution of the phases and thereby the composition in the Comilog charge heated to 1550°C was determined by estimation by visual observation. These results could be an indication that the content of bright phase was estimated to be higher than the real distribution, hence giving a higher MnO content. The distribution was estimated to 55% bright phase and 45% dark phase. In order for the experimental value to fit the calculated curve, the distribution required is 70% dark phase, which is not consistent with the observed microstructure that showed a majority of bright phase.

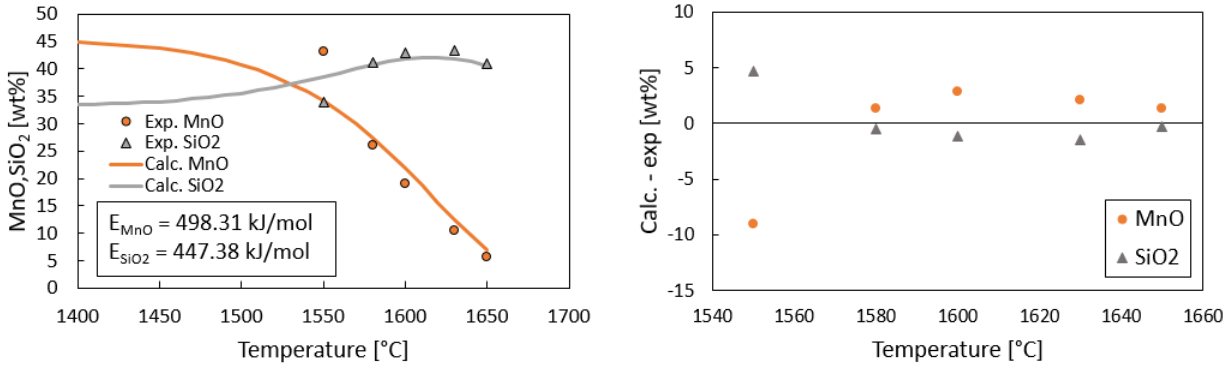

(a) Comilog 1

(b) Deviation Comilog 1

Figure 5.15: Curves fitted for Comilog, HC FeMn slag and quartz charge to the activation energies from Arrhenius plots and the corresponding deviation.

Figure 5.16 shows the modeled curve and the corresponding deviation for the Assmang, HC FeMn slag and quartz charge fitted to the Arrhenius activation energies. The SiO_2 content at

1570°C was inconsistent with the remaining charges, indicating that the analysis may be inaccurate. Deviation for this data point is thereby expected. It is seen that the deviation is fluctuating positive and negative at a fairly acceptable size.

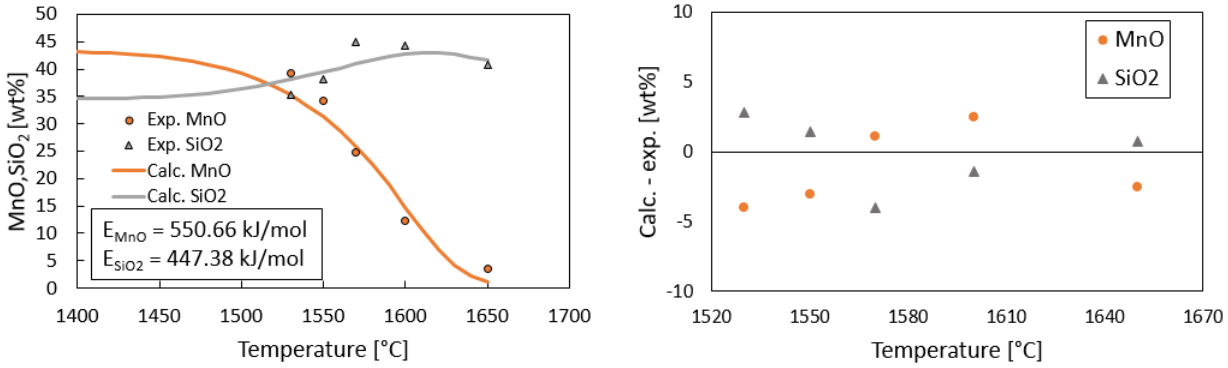

(a) Assmang 1

(b) Deviation Assmang 1

Figure 5.16: Curves fitted Assmang, HC FeMn slag and quartz charge to the activation energies from Arrhenius plots. b) shows the deviation between calculated and expeirmental values.

Activation energies presented by Tangstad

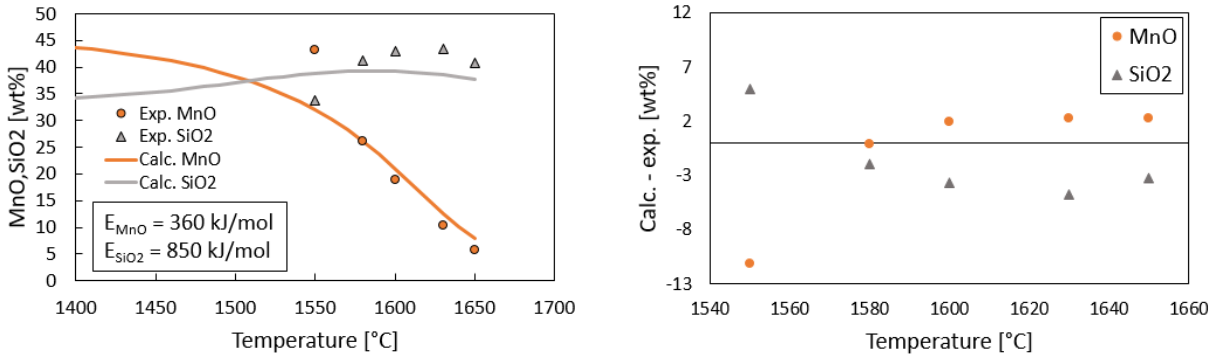

(a) Comilog 2

(b) Deviation Comilog 2

Figure 5.17: Curves fitted for Comilog to activation energies from Tangstad[17] and the corresponding deviation.

Figure 5.17 shows the produced curves utilizing the activation energies presented by Tangstad for charge containing Comilog, HC FeMn slag and quartz. Figure 5.17b shows the corresponding deviation betweeen calculated and experimental values. It is seen that the fit for MnO is fairly acceptable, however deviation at 1550°C is high. As for the SiO_2 curve, it does not correlate with

the experimental values, implying that the specific combination of activation energies does not describe the system.

Figure 5.18 shows the modeled system for charge containing Assmang, HC FeMn slag and quartz at the activation energies presented by Tangstad[17]. The curve shows that the model does not describe the SiO_2 amounts and that the deviation is generally high.

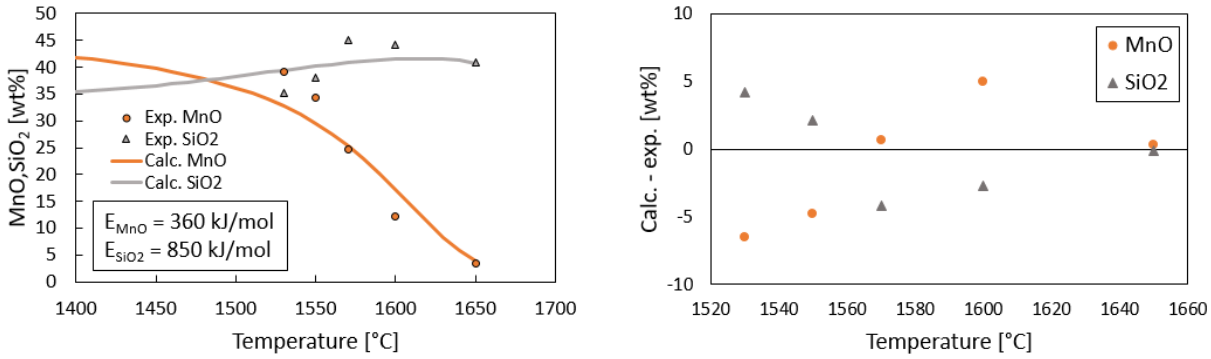

(a) Assmang 2

(b) Deviation Assmang 2

Figure 5.18: Curves fitted for Assmang to activation energies from Tangstad[17] and the corresponding deviation.

Activation energies presented by Kim

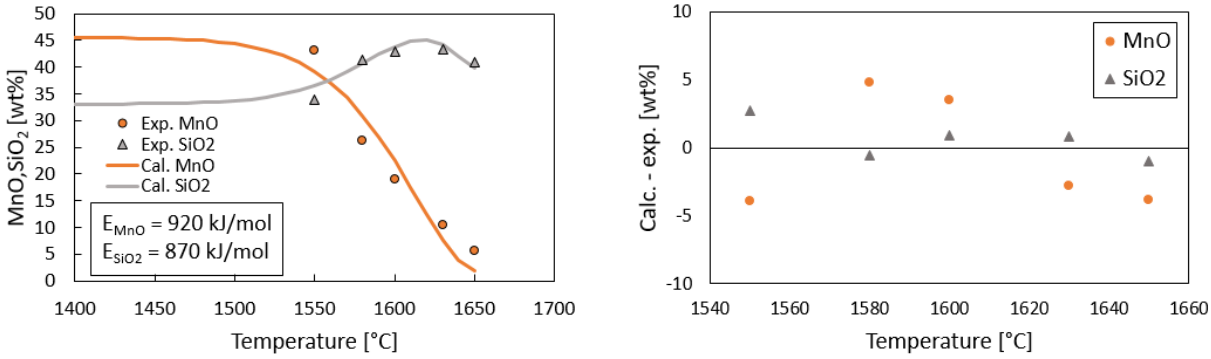

(a) Comilog 3

(b) Deviation Comilog 3

Figure 5.19: Curves fitted for Comilog, HC FeMn slag and quartz charge to activation energies from Kim[18].

Figure 5.19 shows the results when the activation energies presented by Kim[18] were used as parameters for charge containing Comilog, HC FeMn slag and quartz. It can be observed that

the model and the experimental values correlate well, including data point at 1550°C which had the highest deviation for the other models.

Figure 5.20 shows the produced curve for the Assmang, HC FeMn slag and quartz charge at the activation energies presented by Kim[18]. The model and the experimental values correlate for the Assmang charge for the amount of MnO, whereas the SiO_2 reduction is not successfully described by the model. The deviation is largest for values at 1600 and 1650°C.

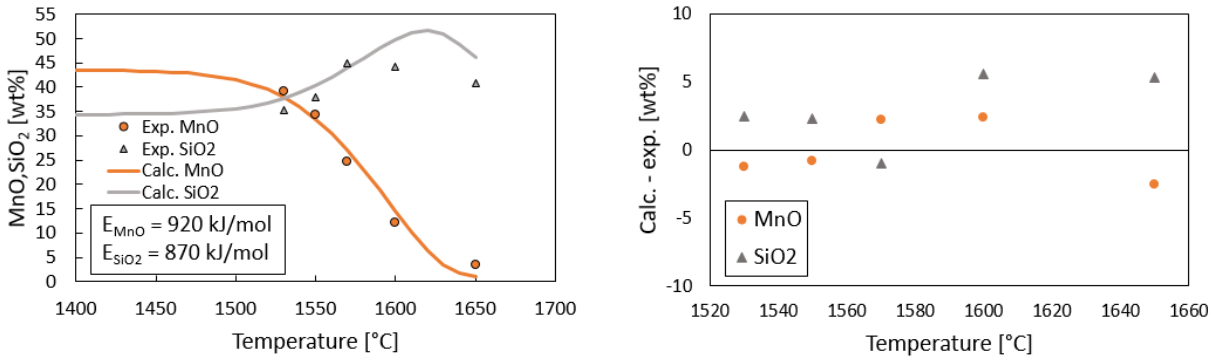

(a) Assmang 3

(b) Assmang 3

Figure 5.20: Curves fitted for Assmang, HC FeMn slag and quartz charge to activation energies from literature[18].

The activation energies presented from Kim gives the best fit for charges containing Comilog, quartz and HC FeMn slag, however the fit by utilizing the Arrhenius activation energies is considered acceptable. In the case of Assmang, the best fit was obtained for the activation energies described from the Arrhenius plot. As such, the activation energies estimated from the Arrhenius plots will be further discussed for both charges.

Values for the pre-exponential factors $k_{0,MnO}$ and k_{0,SiO_2} will depend on the activation energies of MnO and SiO_2, whereas the rate constants k_{MnO} and k_{SiO_2} will describe the rate of the reductions. Table 5.8 shows the rate constants estimated from the Arrhenius plots and the corresponding rate constants determined from the model at the same activation energies. The rate constants for the reduction of MnO are fairly similar in the case of Comilog and Assmang for both the model and the polynomial estimations. At 1530°C, the rate constant for MnO is approximately 3% larger for the Comilog charge according to the computational model. As the rate constant is exponentially dependent on temperature, the deviation becomes more significant at

higher temperatures. On the contrary, the rate constant for SiO_2 reduction is significantly larger for Assmang compared to Comilog. In general, it can be observed that the rate constants from the Arrhenius plot are larger than the calculated, for both MnO and SiO_2. The rate constants are graphically presented in figure 5.21 and 5.22 for MnO and SiO_2 respectively.

Table 5.8: Rate constants determined by the computational model utilizing activation energies estimated from the Arrhenius plots and rate constants extracted directly from the Arrhenius plots [10^{-3} g/min·cm^2].

	Model				2. degree polynomial			
	Comilog		Assmang		Comilog		Assmang	
	k_{MnO}	k_{SiO_2}	k_{MnO}	k_{SiO_2}	k_{MnO}	k_{SiO_2}	k_{MnO}	k_{SiO_2}
1530°C	5.92	1.25	5.74	3.10			8.78	
1550°C	8.52	1.73	8.59	4.30	12.53		10.79	
1570°C	12.17	2.38	12.73	5.92			19.27	
1580°C	14.50	2.79	15.45	6.93	32.36	3.64		
1600°C	20.49	3.81	22.62	9.44	35.52	3.97	32.54	
1630°C	33.93	5.99	39.47	14.86	52.85	5.15		
1650°C	47.08	8.03	56.67	19.94		11.43		

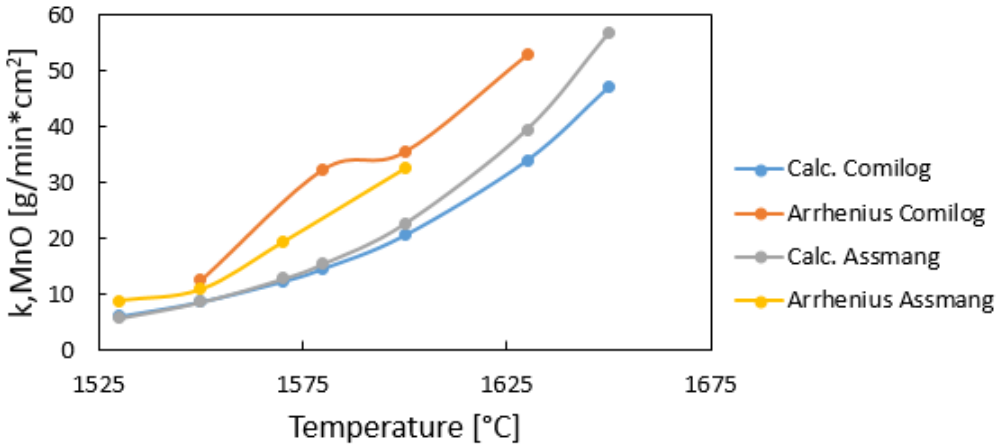

Figure 5.21: Rate constants for MnO for Assmang and Comilog determined from 2. degree polynomial and computational model. Utilized activation energies were determined from Arrhenius plot.

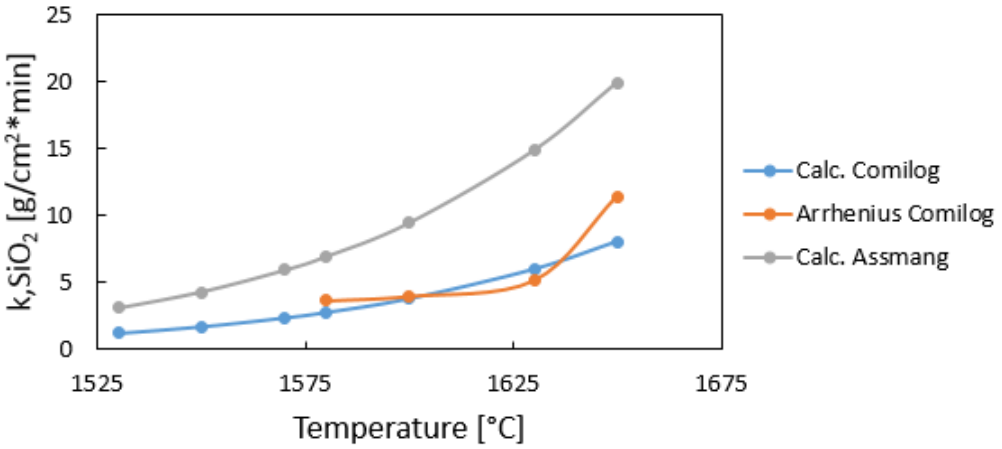

Figure 5.22: Rate constants for SiO_2 for Assmang and Comilog determined from 2. degree polynomial and computational model. Utilized activation energies were determined from Arrhenius plot.

Factors affecting the reduction rate that are not described by the reaction area or the driving force, will give their contribution to the rate constant. Potential factors are viscosity, impact of trace elements or diffusivity. It was shown in section 5.1 that there was no observed correlation between the reduction rate and the lime basicity (R-ratio). The R-ratio is constant throughout the process, whereas the total basicity changes according to the extent of the reduction of MnO and SiO_2. The total bacisity and the viscosity of the charge is hence closely related. To evaluate whether the viscosity (or total basicity) affects the offset of the rapid reduction stage, the temperature at which the initiation of the rapid reduction stage is observed is presented in table 5.9 together with the corresponding viscosities for the different charges, including the charges presented by Larssen[19]. The two charges investigated by Larssen containing additional sulphur were not analysed at 1600°C, however as the reductions are at the initiation of the rapid reduction stage, the new composition can be estimated by assuming that the ratio between reduced MnO and SiO_2 is similar to the ratio obtained by the other charges at the same reduction stage. Two of the charges did not experience a rapid reduction stage at the evaluated temperatures 1500-1725°C. The viscosities at 1650°C are presented for these two charges.

The table shows the charges from lowest to highest temperature at which the rapid reduction stage starts and it can be seen that there is no apparent correlation with the viscosity. The charge with the lowest viscosity did not experience a rapid reduction stage, whereas the charge that

reduces at the lowest temperature has the highest viscosity, larger by a factor 1.8. These results indicate that the viscosity has insignificant or no effect on the reduction rate.

Table 5.9: Temperature at reduction start and the corresponding viscosities for the different charges. (A = Assmang, C = Comilog, Q = quartz, HC = HC FeMn slag, L = Lime, S = sulphur)

Charge	Temperature at reduction start	Viscosity [poise]
A.Q.HC	1530°C	1.286
C.Q.HC	1550°C	0.934
C.Q.S	1600°C	0.818
C.Q.L.S	1600°C	1.115
C.Q	>1650°C	0.936
C.Q.L	>1650°C	0.717

The rate constants at 1600°C, which is within the rapid reduction stage for all charges, were plotted against the sulphur content at the specific temperature to evaluate any potential correlation. The results are presented in figure 5.23. The graph indicates that there is a relationship between the rate constant and the sulphur content, as it can be observed that higher sulphur content correlates to a higher rate constant.

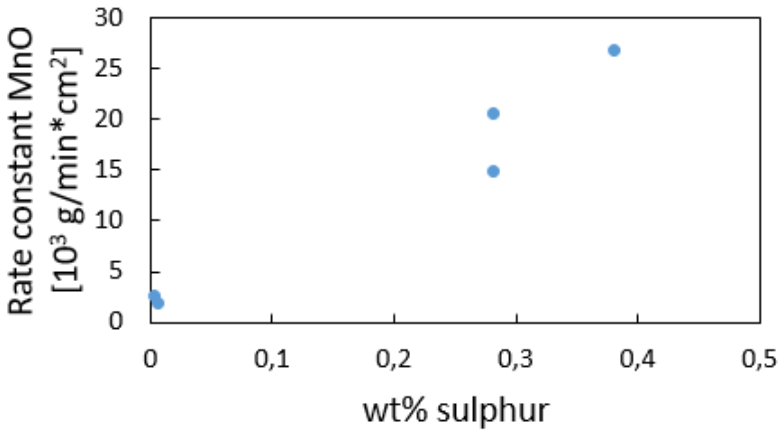

Figure 5.23: Rate constant at 1600°C as a function of the sulphur content at the specific temperature.

5.3.2 Evaluation of kinetic model

This section will evaluate the assumptions, approximations and validity of the computational model that was utilized in the previous section. The model's deviation at each evaluated temperature is presented in figure 5.24 where the activation energies from the Arrhenius plot were utilized, which were determined to have the best fit. These are the same curves as were presented in 5.17 and 5.18. The curves show that the deviation of MnO and SiO_2 are related in terms that a positive deviation for MnO correlates to a negative deviation of SiO_2. The size of the deviation indicates that not all factors that are affecting the reduction rates are described by the model, or that some of the the parameters are inaccurately estimated.

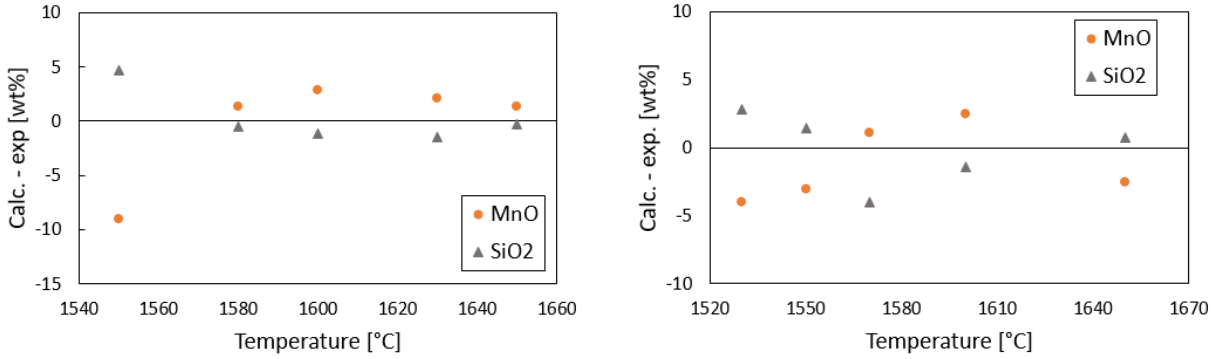

(a) Comilog 1

(b) Assmang 1

Figure 5.24: Deviation between calculated and experimental values for MnO and SiO_2 [wt%] for Comilog and Assmang, respectively, in combination with HC FeMn slag and quartz. Model utilizes activation energies determined from Arrhenius plot for the respective charges.

The only value that was estimated prior to the execution of the calculations was the reaction area. The reaction area was estimated by assuming that coke was the only carbon source utilized during the reductions of MnO and SiO_2. The reaction area was reduced by approximately 35% at 1650°C for both evaluated charge compositions, as was shown in table 4.5 and 4.22 for Comilog and Assmang, respectively, in combination with HC FeMn slag and quartz. Foaming was observed at higher temperatures for both charges, confirmed by metal particles covering the inner crucible wall. This implies that the slag also utilized carbon from the graphite crucible during the reduction course, meaning that the coke consumption is lower than what was calculated. To correct for the amount of carbon that was utilized from the graphite walls, the available

crucible reaction area can be calculated from the dimensions of the graphite crucible. The extent of foaming increased as a function of temperature, implying that the ratio between carbon consumption from coke and crucible is not constant. The surface area of the crucible walls can be given as A = 2·π·1.5 cm·[Height of foaming in cm]. The total depth of the crucible is 61 mm, whereas foaming at maximum temperature was observed at a roughly estimated height of 2-3 cm from the bottom. The extent of foaming at increasing temperature, expressed by the height, can be roughly approximated by a linear relationship from 0 cm foaming at lowest temperature to 2.5 cm foaming at maximum. Combination of the available crucible area to the available coke area, results in the reaction area being reduced by 20% at 1650°C, compared to 35% when only assuming coke consumption. The resulting effect on the estimated activation energy is presented in figure 5.25 in the case of MnO reduction in the Comilog charge. The change of slope appears insignificant, however the estimated activation energy is changed from 498 kJ/mol to 428 kJ/mol. This shows that either the foaming phenomena should be taken into consideration or the experiment should be executed with a considerable excess of carbon.

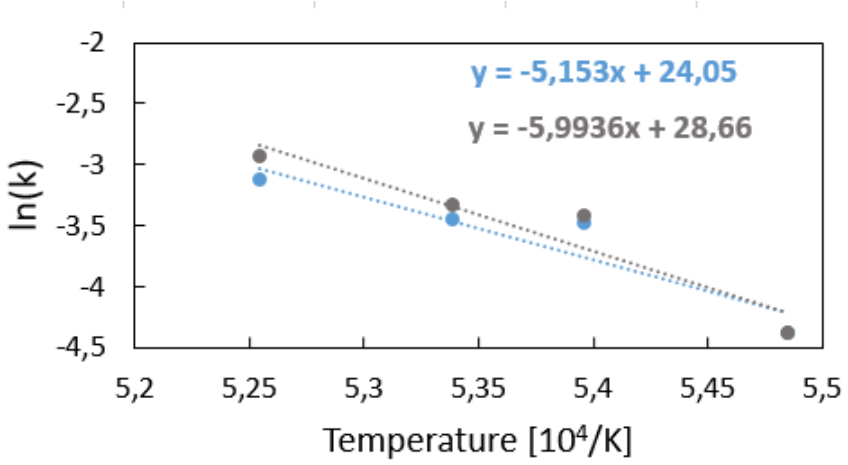

Figure 5.25: Arrhenius plot for MnO reduction in charge based on Comilog, quartz and HC FeMn slag. Blue: reaction area is estimated by assuming coke is the only carbon source utilizied. Orange: the available crucible surface area is included in the reaction area.

The activity of MnO depends on the activity of SiO_2 and vice versa, which means that the fitting of the curves will need to be executed simultaneously. As the model is constructed to minimize the combined deviation for MnO and SiO_2, this could result in an optimal fit for MnO and an inaccurate fit for SiO_2. Similar activation energies for SiO_2 have been used in 5.26a and 5.26b,

whereas significantly different activation energies have been used for MnO. It can be seen that the deviations for MnO is quite similar for both cases, however the fit is very dissimilar in the case of SiO_2, in spite of the similar activation energy being utilized.

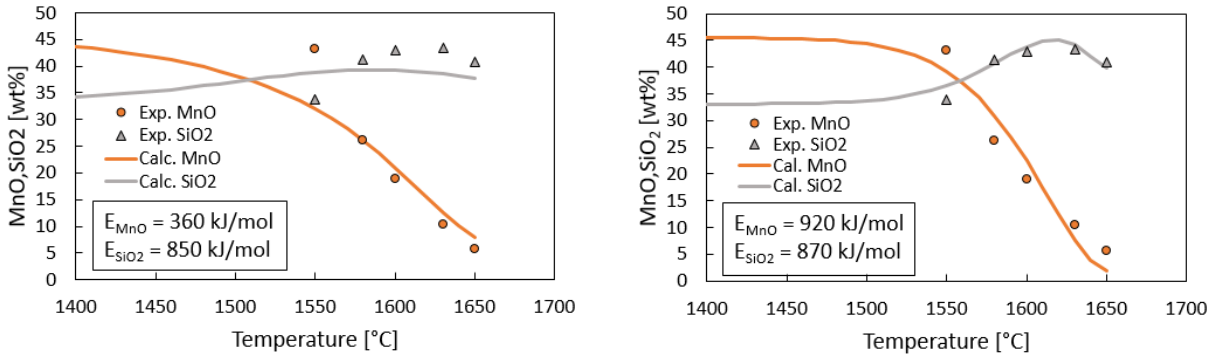

(a) Comilog 2

(b) Comilog 3

Figure 5.26: Curves showing different accuracy for calculated amount of SiO_2 at similar activation energies.

5.3.3 Foaming

Foaming was observed in the charge containing Comilog, quartz and HC FeMn slag at temperatures 1580°C and higher, whereas the Assmang charge experienced foaming for temperatures including and exceeding 1550°C. As presented in theory section 2.2.1, foaming is a result of a viscous slag and the CO-gas production rate. Hence, the viscosity was calculated via FACTSage 7.1 and the results are presented in figure 5.27 as a function of temperature for the charge based on Comilog, quartz and HC FeMn slag. In addition, the total basicity B = (MnO+CaO+MgO)/(SiO_2+Al_2O_3) is presented.

It is seen that the viscosity is approximately 1 poise at 1550°C and shows a steady increase up to 1630°C, where 3.79 poise was calculated by FACTSage. MnO is a network breaking oxide which implies that the viscosity should increase as MnO is being reduced to Mn. The viscosity does also depend on temperature by means that liquid viscosity tends to decrease with increasing temperature. Hence, the effect of the reduced amount of MnO is larger than the temperature effect at this temperature range.

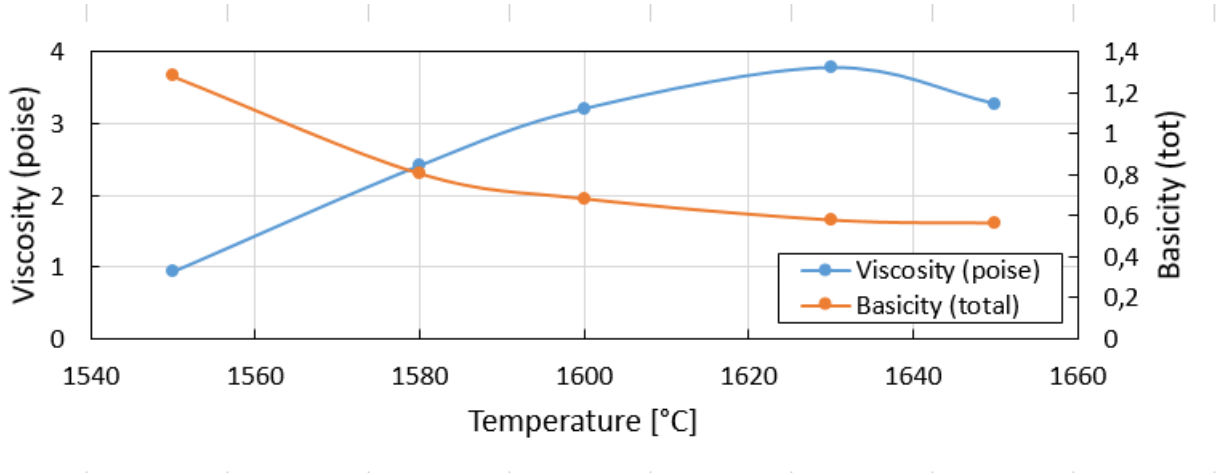

Figure 5.27: Viscosity as a function of temperature for Comilog, HC FeMn slag and quartz charge calculated by FACTSage 7.1.

There is an observed decrease in viscosity at temperature range 1630-1650°C, which could be due to that the amount of the network forming oxide SiO_2 is being reduced to Si, the effect of increased temperature or a combination of both. In addition, the relationship between the total basicity and viscosity is easily observed in the figure. The basicity decreases as the viscosity increases and vice versa. Foaming was observed in the charge at 1580°C, meaning that the first occurrence of foaming is within temperature range 1550-1580°C. The viscosity increases from 0.93 to 2.42 poise during this range and the amount of CO-formation increases from 0.31 g to 1.43 g.

The calculated viscosity for the charge containing Assmang, quartz and HC FeMn slag is presented in figure 5.28. It is seen that the viscosity is approximately 1 poise at 1530°C and appears relatively constant up to 1550°C. The viscosity increases to a large extent between 1530 and 1570°C, implying that the network breaking oxide MnO is being reduced to Mn at this interval. The following decrease between 1570 and 1600°C can be due to the reduction of the network forming oxide SiO_2, the increase in temperature or a combination of both. The relationship between the basicity and the viscosity is easily observed from the figure, where the basicity decreases when the viscosity increases and vice versa. The temperature's effect on the viscosity can be seen for temperatures exceeding 1560°C as the viscosity decreases to a larger extent than the basicity increases. The viscosity has not increased significantly in the Assmang charge from 1530°C to 1550°C, i.e from 1.03 to 1.29 poise, however the foaming phenomena is initiated dur-

ing this temperature range. Approximately 0.64 g of CO-gas was formed at the slag and coke interface at 1530°C, whereas 0.88 g was calculated at 1550°C.

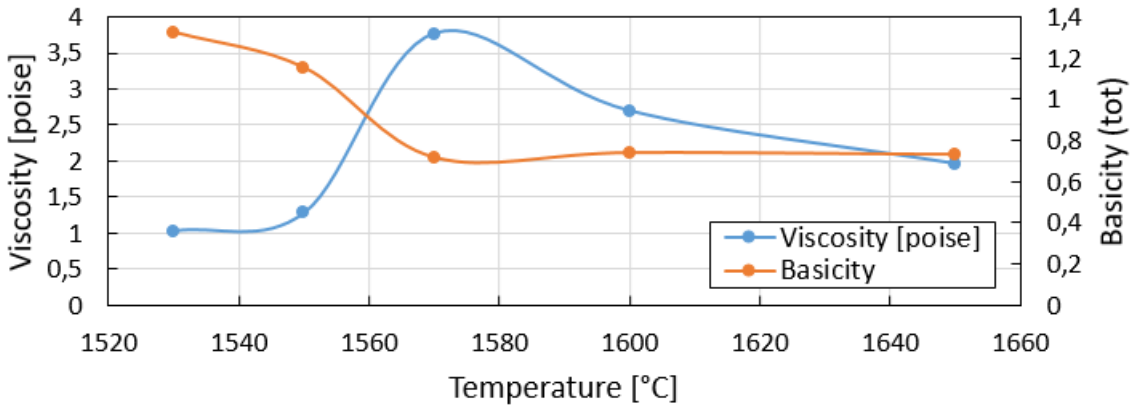

Figure 5.28: Viscosity as a function of temperature for Assmang, HC FeMn slag and quartz based charge calculated by FACTSage 7.1.

The viscosity at increasing temperature will change according to the extent CO(g) formation, implying that the foaming phenomena may be evaluated from the initial viscosity (prior to any reduction) and the reduction rate at relatively low process temperature. The charge investigated by Larssen containing Comilog and quartz (and limestone) did not experience foaming, however a small extent of foaming was observed when 1% sulphur was added to the charges. Figure 5.29 shows the viscosity at increasing temperature for the two charges investigated in this study together with the charges evaluated by Larssen. The temperature at which foaming was first observed has been marked. It is seen that the two charges that did not contain HC FeMn slag have a relatively stable viscosity at all temperatures, implying that the temperature effect balances out the viscosity increase that should be observed by the decreasing amount of MnO. However, the reduction was also significantly lower, causing less changes in composition. The viscosity at low temperatures(prior to reduction of MnO) will be similar for charges with and without sulphur addition in Larssen's charges.

As foaming was observed at 1550°C for the Ass+Q+HC charge, it is reasonable to assume that foaming was initiated at approximately 1560°C for Com+Q+HC. At 1560°C, the Com+Q+HC charge will have approximately the same viscosity and produced amount of CO(g) as Assmang at 1550°C.

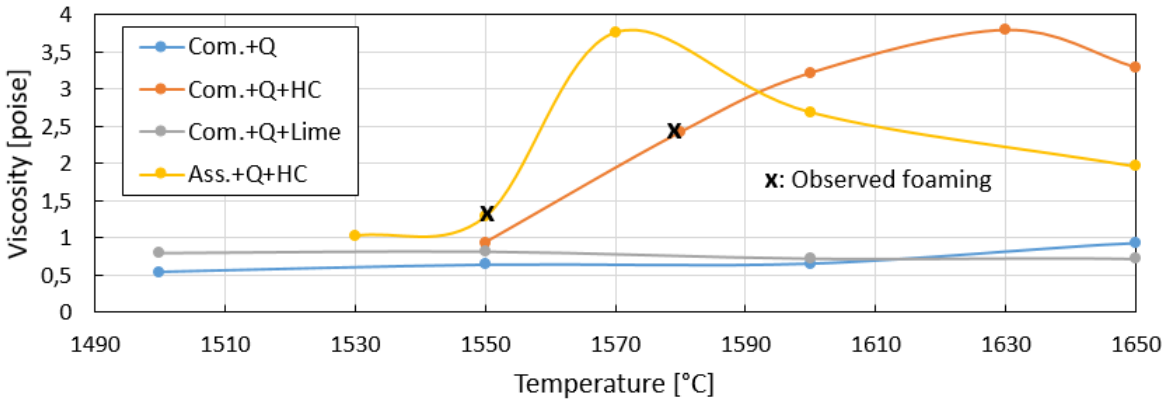

Figure 5.29: Viscosity as a function of temperature charges investigated in this study, as well as charges presented by Larssen[19] calculated by FACTSage 7.1.

The rapid reduction stage was initiated prior to the foaming phenomena in both charges that contained HC FeMn slag. This implies that foaming occurs as a result of high reduction rate, rather than vice versa, i.e foaming causing a high reduction rate. This is supported by the fact that the charges investigated by Larssen containing Comilog and quartz (and limestone) did not experience foaming, whereas foaming was observed when sulphur was added, in spite of having the same initial viscosity.

6 | Conclusions

The effect of different raw materials on the reduction of MnO and SiO_2 in the SiMn process was investigated, where evaluated raw materials included Assmang and Comilog ore, HC FeMn slag and quartz.

The following conclusions were made:

- The slag formation temperature was observed to be in the range of 1250-1300°C for charge containing Comilog and quartz and charge containing Comilog, HC FeMn slag and quartz. All materials had melted into a slag phase at 1250°C when prepared by mixing, whereas the quartz particles remained undissolved until 1300°C when charge was prepared by layering.
- The rapid reduction stage was initiated at a lower temperature in the Assmang charge, i.e 1535°C vs 1545°C for Comilog.
- Charges based on ore(Comilog or Assmang) and HC FeMn slag starts to reduce at approximately 50°C lower than charges based on Comilog, quartz and coke (and limestone), in spite of lower sulphur content, lower basicity and lower driving force.
- No correlation between the basicity, neither total(B) nor lime(R), and the reduction rates were observed, implying that the viscosity has insignificant or no effect.
- The rate constants, and hence reduction rate, increased with sulphur content.
- Foaming was observed at 1550°C for the Assmang charge, whereas the first occurrence was at approximately 1560°C for Comilog. It was concluded that the foaming phenomena is a result of a high reduction rate, rather than vice versa.

Bibliography

[1] S. E. Olsen, M. Tangstad, and T. Lindstad, *Production of Manganese Ferroalloys*. NTNU, Trondheim: Tapir Academic Press, 2007.

[2] "Essential manganese - annual review 2016," manganese.org, February 2017.

[3] S. E. Olsen and M. Tangstad, "Silicomanganese Production - Process Understanding," *Proceedings of the Tenth International Ferroalloys Congress (INFACON X)*, 2004.

[4] J. Steenkamp, J. Sutherland, D. Hayman, and J. Muller, "Tap-hole life cycle design criteria: A case study based on silicomanganese production," *JOM*, vol. 68, no. 6, pp. 1547–1555, 2016.

[5] P. Kim, J. Holtan, and M. Tangstad, "Reduction behaviour of Assmang and Comilog ore in the SiMn Process," *Proceedings of the Tenth International Conference on Molten Slags, Fluxes and Salts*, 2016.

[6] M. Tangstad, "Manganese course: Thermodynamics," Course Lecture at manganese course held by Teknova, Kristiansand, 2016.

[7] M. Eissa, A. Fathy, A. Ahmed, A. El-Mohammady, and K. El-Fawakhary, "Factors affecting silicomanganese production using manganese rich slag in the charge," *Proc. 10th Int. Ferroalloys Cong*, pp. 245–253, 2004.

[8] M. Tangstad, *Handbook of ferroalloys: theory and technology*. Butterworth-Heinemann, 2013.

[9] J. Tuset and J. Sandvik, "Carbon solubility in ferrosilicomanganese at 1330-1650°C," *SINTEF report. no B2268.*, 1970.

[10] K. Xu, G. Jiang, W. Ding, L. Gu, S. Guo, and B. Zhao, "The kinetics of reduction of MnO in molten slag with carbon saturated liquid iron," *ISIJ international*, vol. 33, no. 1, pp. 104–108, 1993.

[11] W. L. Daines and R. D. Pehlke, "Kinetics of manganese oxide reduction from basic slags by carbon dissolved in liquid iron," *Metallurgical Transactions*, vol. 2, no. 4, pp. 1203–1211, 1971.

[12] T.-A. Skjervheim and S. Olsen, "The rate and mechanism for reduction of manganese oxide from silicate slags," *INFACON 7*, pp. 631–639, 1995.

[13] H. Sun, K. Mori, and R. D. Pehlke, "Reduction rate of SiO2 in slag by carbon-saturated iron," *Metallurgical Transactions B*, vol. 24, no. 1, pp. 113–120, 1993.

[14] J. Fulton and J. Chipman, "Kinetic factors in the reduction of silica from blast-furnace type slags," *Transactions of the American Institute of Mining and Metallurgical Engineers*, vol. 215, no. 6, pp. 888–891, 1959.

[15] O. Ostrovski, S. Olsen, M. Tangstad, and M. Yastreboff, "Kinetic modelling of MnO reduction from manganese ore," *Canadian metallurgical quarterly*, vol. 41, no. 3, pp. 309–318, 2002.

[16] H. Olsen, "A Theoretical Study on the Reaction Rates in the SiMn Production Process," Master's thesis, Department of Materials Science and Engineering (DMSE), Norwegian University of Science and Technology (NTNU), 2016.

[17] M. Tangstad, "The high carbon ferromanganese process-coke bed relations," *Dr. Ing. Dissertation, NTH, Trondheim, Norway*, 1996.

[18] P. Kim, T. Larssen, R. Kawamoto, and M. Tangstad, "Empirical Activation Energies of MnO and SiO_2 reduction in SiMn slags between 15000-1650°c," *Applications of Process Engineering Principles in Materials Processing, Energy and Environmental Technologies*, 2016.

[19] T. Larssen, "Reduction of MnO and SiO_2 from Comilog based Charges," 2016, project work, TMT4500, NTNU.

[20] ——, "Kinetics in SiMn production - Comilog," *Report from summer internship at SFI Metal Production*, 2016.

[21] J. Holtan, "Production of Silicomanganese from Comilog ore," Master's thesis, Norwegian University of Science and Technology, NTNU, Trondheim, 2016.

[22] T. Brynjulfsen, "Reduction of manganese ore agglomerates," Ph.D. dissertation, Norwegian University of Science and Technology, 2013.

[23] K. Tang and M. Tangstad, "Modeling Viscosities of Ferromanganese Slags," *INFACON XI*, pp. 344–357, 2007.

[24] T.-A. Skjervheim, "Kinetics and mechanisms for transfer of manganese and silicon from molten oxide to liquid manganese metal," *Dr. Ing. Dissertation, NTH, Trondheim, Norway*, 1994.

[25] S. Hara and K. Ogino, "Slag-foaming phenomenon in pyrometallurgical processes." *ISIJ international*, vol. 32, no. 1, pp. 81–86, 1992.

[26] P. Kozakevitch and T. John, "Foams and emulsions in steelmaking," *JOM*, vol. 21, no. 7, pp. 57–68, 1969.

[27] V. Yavoiskiy, "Theory of steelmaking processes," *Metallurgia, Moscow*, vol. 789, 1967.

[28] "Outotec: HSC Chemistry 7," hsc-chemistry.com, August 2016.

[29] K. Tang and S. E. Olsen, "Computer simulation of equilibrium relations in managanese ferroalloy production," *Metallurgical and Materials Transactions B*, vol. 37, no. 4, pp. 599–606, 2006.

[30] P. Kim, "Kinetics and mechanisms in SiMn production," *Dr. Ing. Dissertation, NTNU, Trondheim, Norway - to be published*, 2018.

[31] W. Lee and S. Zhang, "Direct and indirect slag corrosion of oxide and oxide-c refractories," in *VII International Conference on Molten Slags Fluxes and Salts, Cape Town, South Africa*, 2004, pp. 309–320.

[32] ——, “Melt corrosion of refractories,” in *Ageing Studies and Lifetime Extension of Materials*. Springer, 2001, pp. 215–218.

A | Investigation of static corrosion by SiMn slag on tap-hole clay

This chapter presents the development of a method that aims to investigate static corrosion by SiMn slag and/or alloy on tap-hole clay. The work was performed at Mintek, Johannesburg during the spring semester of 2017.

One of the steps in production of silicomanganese is the tapping of slag and alloy from the furnace. This is an important part of the process regarding yield, energy consumption and safety. The materials used in the tap-hole must properly keep the tap-hole closed in-between tapping and optimally be chemically inert towards the slag and alloy that will pass through during tapping.

The following research questions have been asked:

- Will slag and/or alloy interact with tap-hole clay during tapping?
- And if so, to an extent that specific types of clay should be used in the tap-hole depending on the furnace process?

Information on slag (or alloy) interaction with refractory type materials that are utilized as tap-hole clay is rather scarce, whereas extensive research has been done on refractories used as tap-blocks or lining of the inner surface. The main difference between these types of refractories and tap-hole clay is the strength, as tap-hole clay needs to be sufficiently soft to be pushed by the mudgun into the tap-hole. Nonetheless, the components of the materials are in general similar. Refractory tests have been developed in order to investigate the environment the re-

fractories are exposed to during process operation. Several different tests have been developed, of which both static(sessile, dipping, crucible) and dynamic(rotating finger, rotating slag). The crucible tests, also known as the cup, cavity or brick test[31], will be the focus of this work. A crucible is made out of the refractory material that is to be tested and slag/alloy will be filled in the cavity. The crucible will be exposed to desired temperature and dwell time before being cooled and cut to be investigated. Chemical attack by the slag/alloy can be evaluated from changes in refractory crucible diameter and/or by analysing the composition near the interface. The method is very popular due to its simplicity, and many tests can be conducted in a short amount of time. Drawbacks with the method, as similar for all static tests, are that the temperature gradient experienced in industrial practice is not simulated in the test, rapid saturation of slag composition and lack of slag flow[32]. The test can thereby not be used for thermal spalling investigations, as it has been determined that a temperature gradient is responsible for this type of wear. Nonetheless, chemical wear and structural spalling can be investigated.

A.1 Equipment and materials

Raw materials

The slag that was used in the experiments conducted in this study was retrieved from smelting plant Transalloys in Johannesburg, South-Africa. The chemical composition was determined by electron microprobe analysis and is presented in table A.1. Two different types of clay were utilized: Intocast and Elkem. The Intocast is already utilized as tap-hole clay, whereas Elkem is a newly developed clay that producers hope to be applicable. As this work focus on the validity of the method, the specific chemical interactions between slag and clay are not discussed. Hence, the composition of the clays are not presented.

Table A.1: Chemical composition of slag.

	MnO	CaO	SiO_2	Al_2O_3	Fe_2O_3	MgO	Cr_2O_3	C	Total
Slag [wt%]	18.90	26.95	38.43	3.93	1.01	6.54	0.10	-	95.85

Crucible preparation

Graphite crucibles of dimensions 10 cm outer diameter, 8.5 cm inner diameter and 14 cm height were used as the outer surface of the clay-crucibles. To simulate the industrial practice in best possible manner, the clay was mounted in the graphite crucible by a mud gun. The graphite crucible was placed in a steel cylinder, as shown in figure A.1a, before being bolted to the opening of the mud gun, as shown in figure A.1b. The mud gun utilizes a pressure of approximately 10 bar to fill the graphite crucibles with clay. When the crucible is detached from the mud gun, it is completely filled as shown in A.1c. The crucible is then drilled, giving a diameter of 5 cm. The final result is shown in A.1d.

(a) Graphite crucible inside metal cast

(b) Metal cast connected to mudgun

(c) Graphite crucible filled with clay

(d) Crucible after drilling

Figure A.1: Image a)-d) shows crucible preparation procedure in chronological order.

The crucibles are then baked in a muffle furnace to ensure that all volatiles and moisture has gone off. The specific procedure is described below.

Baking of crucibles in muffle furnace

The crucible is placed inside the furnace before it is tightly sealed. Argon is used at ambient pressure throughout the process. The temperature profile was programmed in the furnace and is presented in figure A.2. The crucible was heated to a rate of 5°C/min up to 950°C, where it was dwelled for 1 hour before the power supply is disconnected, leaving the furnace to cool.

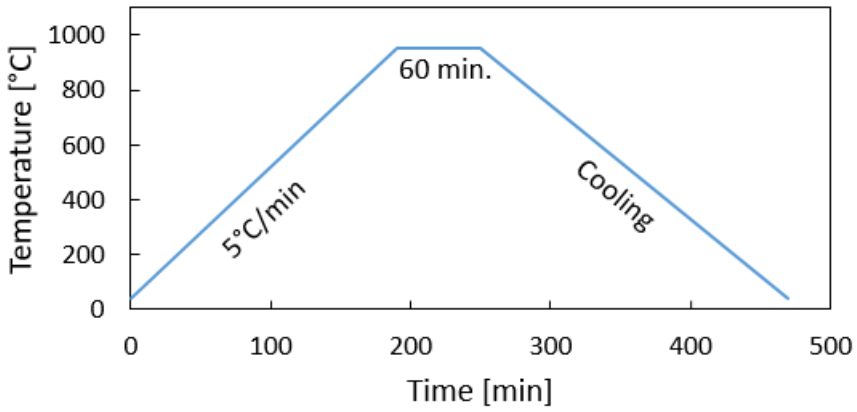

Figure A.2: Temperature profile for baking of crucibles.

A.2 Corrosion experiments

A.2.1 Trial 1

100 grams of slag was added to a Intocast crucible. The crucible lid was drilled to give three centered holes for thermocouple, gas inlet and outlet, respectively. The thermocouple was placed ranging 4 cm from the top of the crucible, 6 cm including the lid. This gave a distance between thermocouple and slag of approximately 1 cm.

A small induction furnace where power input is manually controlled was used for the first trial. The crucible was placed inside the coil and the remaining space between the crucible and the

coil-box walls was filled with alumina bubbles to enhance the heat isolation. Three layers of Fibrofax was placed on top, covering both the coil-box and the crucible.

The power was 2.5% initially and was increased to 5% when the thermocouple read 700°C. Further, the power was increased with 2.5% every 30 minute interval. When the temperature reached 1600°C, the power was manually increased and decreased systematically in order to maintain a dwell of 60 minutes according to the temperature read from the Pt-thermocouple.

Remarks/visual observations

Figure A.3 shows the crucible and lid after finished experiment. The different colours observed at the bottom surface of the lid and also the upper surface of the crucible could imply that the baking of the crucibles did not successfully remove all volatiles from the clay.

(a) Crucible lid.

(b) Crucible.

Figure A.3: Crucible and lid after finished experiment.

As the furnace is relatively small in size, small adjustments in the power supply caused large effects, hence making it extremely hard to dwell the temperature at 1600°C. In fact, the temperature recorded during the dwell ranged from 1560°C to 1680°C. It was also observed that the thermocouple was located in the slag, either due to that the thermocouple had moved from it's initial position or as a result of slag foaming. In spite of this being the most accurate position

of measuring the temperature, i.e in slag, this would imply that the thermocouple itself could interact with slag/clay and compromise the results.

Conclusion: Specific setup can not be used as thermocouple would contaminate the sample and the temperature is too sensitive to be controlled when located in slag.

A.2.2 Trial 2

A second experiment with an Intocast crucible was performed in the small induction furnace. The amount of slag was adjusted to 80 g to ensure that the thermocouple would not be in contact with the thermocouple, as was observed in trial 1. A lid was placed on top of the crucible giving entrance for thermocouple and gas inlet and outlet. Layers of fibrofax was placed to cover the top surface of the furnace to isolate the heat. The thermocouple was placed approximately 1 cm over the slag, to ensure no contact.

The same temperature program as trial 1 was executed by increasing the power with 2.5% every 30 minute interval after 700°C was read by the thermocouple.

Remarks/visual observations

It was observed that slag and thermocouple were not in contact during this trial. The same temperature program as in trial 1 was executed, however the observed temperature increase was highly inconsistent. Trial 1 reached 1600°C after 4 hours and 20 minutes, whereas in trial 2 the temperature was only 1330°C at this point. The power was further increased every 30 minutes and the temperature showed a very slow increase. After 6 hours the power was at 65% giving a temperature of 1540°C. Flames were observed at the lower parts of the furnace. Continued increase caused the furnace to shut down due to malfunction. This could indicate that the temperature in the furnace was significantly higher than measured by the thermocouple.

After cooling, the crucible was impossible to remove from the coil-box seemingly due to melted alumina bubbles. Figure A.4 shows the lid and the crucible after furnace and crucible had cooled to room temperature. No slag could be observed in the crucible and parts of the clay

was eaten away in the lower parts. This also supports the fact that the temperature was higher than recorded by the thermocouple.

(a) Crucible lid

(b) Crucible

Figure A.4: Crucible and lid after finished experiment.

Conclusion: The different temperature readings from trial 1 and trial 2 indicates that the temperature in the slag and the air directly above slag differs by several hundred degrees, making accurate measurements impossible. Another potential explanation is furnace malfunction.

A.2.3 Trial 3

When proven that it was impossible to control the temperature using the small induction furnace without contaminating the sample, the decision was made to try a larger induction furnace.

An Elkem clay crucible containing 100 g of slag was placed inside the furnace. The thermocouple was placed outside the crucible, inside the alumina bubbles, so that the lower parts of the thermocouple was at the same height as the slag in the crucible. The power was initially set to 2.5% and was increased with 1% every 30 minute interval.

Remarks/visual observations

Temperature program was successfully run and the temperature was relatively stable at 1600°C +/- 10°C during the dwell. No detrimental observations were made during this trial, indicating that this setup could be used for investigating static corrosion of tap-hole clay by slag/alloy.

(a) (b)

Figure A.5: Crucible after finished experiment.

A.2.4 Trial 4 and 5

To confirm the repeatibility of previous trial it was decided to run two additional tests of the exact same setup. The power input was changed slightly during dwell to see if the temperature could potentially be more stable compared to trial 3.

Remarks/visual observations

Both trial 4 and 5 were highly consistent with trial 3, indicating that the method can be used with confidence in terms of temperature measurements. As the thermocouple was located outside the crucible within the alumina bubbles, it is necessary to determine the temperature difference between the specific location of the thermocouple and the temperature in the slag.

Validation of temperature

One experiment was done with the Elkem crucible in the large induction furnace, where the only difference from trial 3-5 was the position of the thermocouple, which now was submerged in the slag. Identical heating program as previous trials, i.e increase of 1% every 30 minutes from 2.5% initial power. Figure A.6 shows that the temperature in the slag and in the alumina bubbles show similar behaviour at increasing temperature.

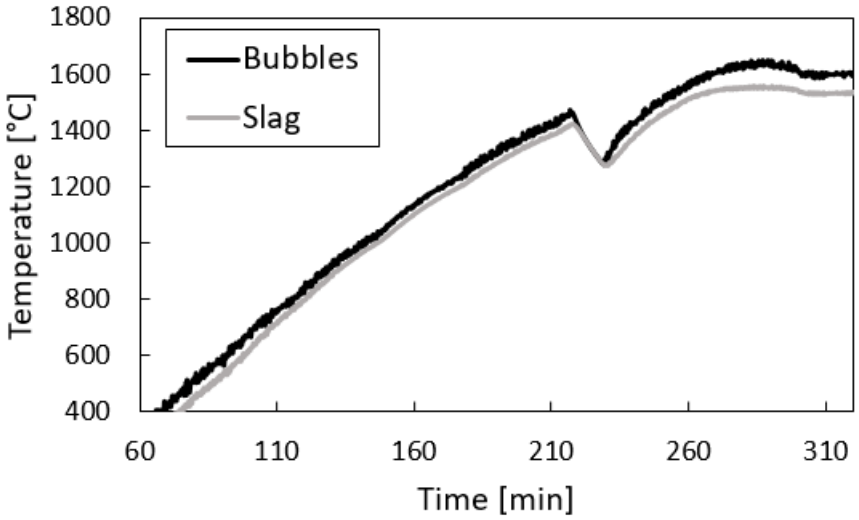

Figure A.6: Temperature measured in slag and alumina bubbbles, respectively, as a function of time.

The specific deviation between the two thermocouples can be seen in figure A.7a for all temperatures. The values are calculated from average deviation within a minute interval, as excessive fluctuation was observed. Although an average is presented, it is still seen that the deviation between the two temperature readings are inconsistent. A deviation of minimum 25°C at lower temperatures is observed and the deviation increases at increasing temperature in the high temperature zone.

Figure A.7b shows the average deviation within a minute interval during the dwell period at 1600°C. The start of the dwell is at the first reading of a temperature at 1600°C by the thermocouple in the alumina bubbles. It can be seen that the deviation at this point is approximately 65°C. The temperature difference increases within the dwell period and a maximum difference of 85°C is recorded.

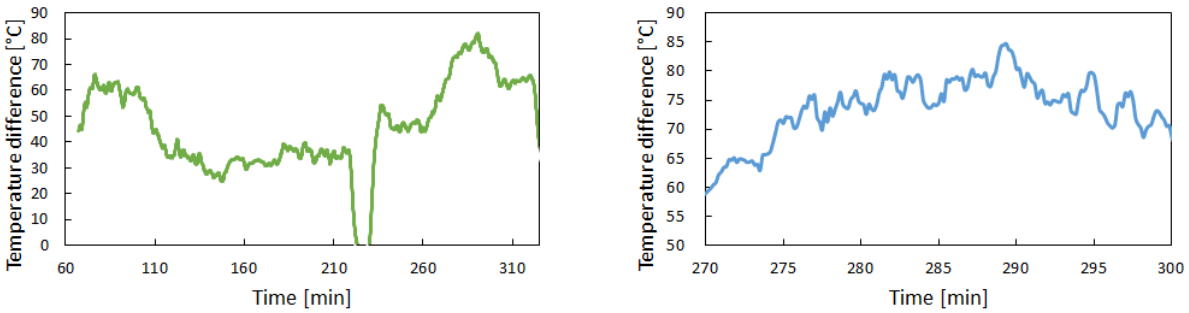

(a) All temperatures

(b) Dwell period at 1600°C

Figure A.7: Temperature difference between thermocouple in slag and alumina bubbles.

A.3 Discussion/conclusion

A method for investigating and evaluating static corrosion of tap-hole clay by SiMn slag was not successfully developed. The temperature control was substantially increased when the larger induction furnace was used, however the deviation in temperature between the slag and alumina bubbles is high and inconsistent during the trials. Hence, temperature control and reproducibility will be low.

Further work needs to be executed in order to obtain a valid method. It is likely that the temperature control would be better if the thermocouple is located within the crucible wall, rather then outside in the alumina bubbles.

B | Raw data from EPMA analyses

B.1 For kinetic investigations

Table B.1 shows the raw data from EPMA for the charges based on Comilog ore, HC FeMn slag and quartz. Similarly, table B.2 shows for charges based on Assmang ore, HC FeMn slag and quartz.

Table B.1: All spot analyses from Comilog based slag phases given by EPMA. Notation x.y corresponds to point x at experiment with maximum temperature y.

Point	MnO	SiO_2	Al_2O_3	CaO	MgO	SO_3	BaO	K_2O	Total	R-ratio
1.1550	28.20	36.29	15.95	14.45	0.86	1.50	1.13	0.79	99.17	0.96
2.1550	28.14	36.15	16.05	14.26	0.84	1.44	1.21	0.75	98.83	0.94
3.1550	28.09	36.48	16.27	14.58	0.76	1.55	1.13	0.81	99.66	0.94
4.1550	55.10	31.85	0.31	4.32	6.39	0.00	0.00	0.01	97.98	34.42
5.1550	55.60	32.07	0.27	4.58	5.79	0.00	0.00	0.02	98.33	38.39
5.1550	55.53	31.73	0.27	4.64	5.51	0.00	0.13	0.03	97.84	37.61
1.1580	26.25	41.35	11.68	12.94	4.39	1.19	0.71	0.00	99.21	1.49
2.1580	26.53	41.03	11.66	13.07	4.36	1.07	0.72	0.70	99.14	1.50
3.1580	25.90	41.18	11.87	13.17	4.44	1.06	0.68	0.65	98.95	1.48
4.1580	25.84	41.35	11.96	13.05	4.40	1.13	0.68	0.63	99.03	1.36
5.1580	26.12	41.50	11.68	13.05	4.35	1.20	0.83	0.69	99.42	1.49
6.1580	26.32	41.34	11.72	12.91	4.31	1.14	0.89	0.66	99.27	1.47

1.1600	19.28	43.10	14.08	14.29	5.09	1.33	0.89	0.81	98.88	1.38
2.1600	18.74	42.87	14.19	14.82	5.08	1.35	0.70	0.76	98.52	1.40
3.1600	18.90	43.11	14.03	14.63	5.11	1.46	0.97	0.79	98.99	1.41
4.1600	18.98	42.86	14.25	14.74	5.04	1.31	0.94	0.78	98.88	1.39
5.1600	18.71	42.91	14.26	14.95	5.17	1.33	0.81	0.79	98.93	1.41
6.1600	19.26	43.02	14.21	14.55	5.02	1.28	0.95	0.75	99.03	1.38
1.1630	11.35	42.70	17.82	18.81	6.46	1.12	1.12	0.91	100.30	1.42
2.1630	10.41	43.37	17.69	19.13	6.58	1.17	1.22	0.87	100.44	1.45
3.1630	10.31	43.59	17.70	18.76	6.55	0.96	1.30	0.92	100.07	1.43
4.1630	10.40	42.99	17.61	18.90	6.44	1.27	0.99	0.92	99.50	1.44
5.1630	9.76	43.62	17.70	19.12	6.58	1.19	1.16	0.95	100.07	1.45
6.1630	10.19	43.73	17.85	19.11	6.50	1.11	1.12	0.97	100.58	1.44
1.1650	5.85	41.10	20.52	22.42	7.72	1.08	1.36	0.69	100.75	1.47
2.1650	5.75	40.74	20.60	22.30	7.57	0.78	1.36	0.80	99.91	1.45
3.1650	5.68	40.65	20.40	22.03	7.66	0.91	1.32	0.81	99.46	1.46
4.1650	5.76	40.77	20.57	22.03	7.62	1.18	1.29	0.79	100.00	1.44
5.1650	5.70	40.96	20.45	22.27	7.68	0.92	1.21	0.75	99.95	1.47
6.1650	5.49	41.09	20.80	22.00	7.51	0.86	1.53	0.77	100.04	1.42

Table B.2: All spot analyses from Assmang based slag phases given by EPMA. Notation x.y corresponds to point x at experiment with maximum temperature y.

Point	MnO	SiO_2	Al_2O_3	CaO	MgO	SO_3	BaO	K_2O	Total	R-ratio
1.1530	23.33	39.07	12.39	16.68	0.83	1.82	1.36	0.42	95.92	1.41
2.1530	25.55	38.84	11.15	16.05	1.09	1.70	1.13	0.39	95.90	1.54
3.1530	28.28	38.62	10.09	16.00	1.30	1.54	1.12	0.30	97.26	1.72
4.1530	52.51	31.51	0.15	5.78	7.16	0.01	0.00	0.00	97.12	86.85
5.1530	53.18	31.68	0.11	5.92	6.60	0.00	0.00	0.01	97.49	114.82
6.1530	52.68	31.77	0.14	5.74	7.08	0.00	0.00	0.00	97.40	94.99

1.1550	33.91	37.94	6.63	12.66	4.08	0.95	0.85	0.36	97.38	2.52
2.1550	34.35	38.24	6.78	12.53	4.06	0.98	0.81	0.29	98.03	2.45
3.1550	34.49	38.27	6.73	12.75	4.11	1.05	0.76	0.29	98.45	2.51
4.1550	34.04	38.14	6.77	12.52	4.06	1.01	0.76	0.24	97.56	2.45
5.1550	34.49	37.98	6.60	12.58	4.04	1.00	0.86	0.30	97.83	2.52
6.1550	34.43	37.72	6.70	12.39	3.96	1.04	0.76	0.27	97.25	2.44
1.1570	17.52	49.95	11.54	14.30	6.13	0.92	1.07	0.96	99.38	1.77
2.1570	17.48	47.39	11.51	14.27	6.22	0.93	1.07	0.95	99.81	1.78
3.1570	17.03	47.30	11.37	14.54	6.19	0.90	0.91	0.92	99.17	1.82
4.1570	17.52	47.28	11.35	13.95	6.33	0.94	0.87	0.89	99.12	1.79
5.1570	15.63	49.00	11.59	14.55	6.08	0.95	0.98	1.07	99.84	1.78
6.1570	17.52	47.09	11.62	14.01	6.24	0.99	0.88	0.91	99.26	1.74
1.1600	12.30	44.15	11.65	21.09	6.82	1.69	1.15	0.42	99.24	2.40
2.1600	12.12	43.96	11.62	20.65	6.89	1.68	1.09	0.49	98.50	2.37
3.1600	12.22	44.09	11.61	20.52	6.77	1.70	1.31	0.40	98.63	2.35
4.1600	12.08	42.20	11.62	20.78	6.80	1.46	1.09	0.50	98.53	2.37
5.1600	12.32	44.45	11.78	20.59	6.77	1.74	1.10	0.46	99.20	2.32
6.1600	12.43	44.47	11.72	21.15	6.86	1.56	1.22	0.47	99.88	2.39
1.1650	3.31	40.24	14.87	26.94	8.35	1.39	1.54	0.19	96.83	2.37
2.1650	3.61	40.20	14.78	26.74	8.19	1.44	1.56	0.18	96.70	2.36
3.1650	3.64	41.95	15.27	27.20	8.31	1.49	1.68	0.17	99.71	2.33

B.2 Investigation of slag formation

Table B.3 shows the EPMA raw data for charge containing Comilog, quartz and HC FeMn slag.

Similarly, table B.4 shows raw data for charge containing Comilog and quartz.

Table B.3: All spot analyses from slag formation investigation for charge containing Comilog, quartz and HC FeMn slag. Notation x.y corresponds to point x at experiment with maximum temperature y.

Point	MnO	SiO_2	Al_2O_3	CaO	MgO	SO_3	BaO	K_2O	FeO	Total	R-ratio
1.1250	7.58	0.31	0.03	0.00	0.00	0.05	0.20	0.00	124.22	132.38	0.00
2.1250	95.45	0.35	0.22	0.33	4.02	0.04	0.01	0.00	0.43	100.87	19.44
3.1250	53.73	31.63	0.41	8.00	6.67	0.02	0.04	0.00	0.26	100.77	35.53
5.1250	27.00	27.24	25.70	12.67	0.51	1.98	1.86	2.85	0.17	99.97	0.51
6.1250	35.15	37.43	9.94	11.41	3.46	0.86	0.59	0.62	0.14	99.59	1.50
7.1250	53.67	32.45	2.26	5.16	8.10	0.09	0.10	0.15	0.19	102.15	5.87
1.1300	47.11	30.73	11.31	8.34	2.36	0.83	0.76	0.85	0.15	102.44	0.95
2.1300	59.28	32.02	0.63	4.96	4.77	0.01	0.00	0.02	0.14	101.82	15.45
3.1300	33.17	28.96	21.40	11.62	0.49	1.79	1.23	1.62	0.08	100.34	0.57
1.1400	58.77	31.58	0.61	4.98	4.45	0.06	0.02	0.02	0.14	100.62	15.42
2.1400	28.65	28.50	24.49	12.57	0.39	2.01	1.41	1.47	0.10	99.60	0.53
1.1250-M	59.70	31.46	0.31	4.86	5.35	0.00	0.05	0.04	0.14	101.91	33.47
2.1250-M	30.94	30.12	21.99	12.32	0.47	1.86	1.41	1.19	0.05	100.34	0.58

* M = Mixed materials

Table B.4: All spot analyses from slag formation investigation for charge containing Comilog and quartz. Notation x.y corresponds to point x at experiment with maximum temperature y.

Point	MnO	SiO_2	Al_2O_3	CaO	MgO	SO_3	BaO	K_2O	FeO	Total	R-ratio
1.1250	1.25	0.10	0.12	0.00	0.00	0.08	0.00	0.01	134.41	135.97	0.00
2.1250	99.34	0.31	0.15	0.00	0.06	0.00	0.00	0.01	2.16	102.03	0.41
3.1250	70.56	30.18	0.62	0.18	0.18	0.00	0.05	0.05	0.80	102.62	0.60
4.1250	43.70	21.96	27.58	0.41	0.00	0.03	1.19	5.53	0.78	101.19	0.02
5.1250	52.94	42.20	4.66	0.32	0.26	0.12	0.07	0.54	0.62	101.74	0.13
1.1300	99.66	0.67	0.25	0.05	0.14	0.02	0.06	0.01	1.17	102.02	0.75
2.1300	70.93	31.07	0.53	0.19	0.22	0.02	0.00	0.00	0.49	103.44	0.76
3.1300	70.66	30.50	0.68	0.17	0.24	0.00	0.00	0.04	0.48	102.78	0.60
4.1300	58.26	19.31	21.07	0.36	0.04	0.03	0.21	0.10	0.68	100.05	0.02
1.1400	99.30	0.33	0.40	0.04	0.03	0.06	0.00	0.08	0.41	100.64	0.19
2.1400	69.65	30.78	0.60	0.27	0.26	0.00	0.03	0.00	0.19	101.77	0.88
3.1400	58.85	20.34	21.32	0.58	0.06	0.10	0.25	0.34	0.23	102.06	0.03
1.1250-M	102.1	0.03	0.24	0.11	0.05	0.00	0.06	0.03	0.68	103.29	0.65
2.1250-M	71.17	30.48	0.29	0.24	0.18	0.00	0.09	0.01	0.26	102.73	1.47
3.1250-M	39.93	19.96	30.20	3.91	0.00	0.50	1.41	4.32	0.16	100.38	0.13
4.1250-M	52.04	16.36	28.83	2.07	0.00	0.09	0.93	2.36	0.18	102.84	0.07

* M = Mixed materials